

71-1498

NICHOLS, Clayton Ralph, 1938-  
THE GEOLOGY AND GEOCHEMISTRY OF THE PATHE  
GEOTHERMAL ZONE, HIDALGO, MEXICO.

The University of Oklahoma, Ph.D., 1970  
Geology

University Microfilms, A XEROX Company, Ann Arbor, Michigan

THE UNIVERSITY OF OKLAHOMA

GRADUATE COLLEGE

THE GEOLOGY AND GEOCHEMISTRY OF THE PATHE GEOTHERMAL  
ZONE, HIDALGO, MEXICO

A DISSERTATION

SUBMITTED TO THE GRADUATE FACULTY

in partial fulfillment of the requirements for the

degree of

DOCTOR OF PHILOSOPHY

BY

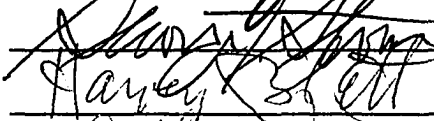
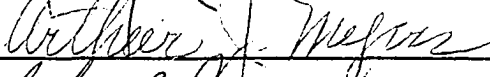
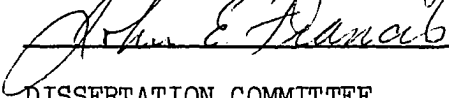
CLAYTON RALPH NICHOLS

Norman, Oklahoma

1970

THE GEOLOGY AND GEOCHEMISTRY OF THE PATHÉ GEOTHERMAL  
ZONE, HIDALGO, MEXICO

APPROVED BY

  
\_\_\_\_\_  
  
\_\_\_\_\_  
  
\_\_\_\_\_  
  
\_\_\_\_\_

DISSERTATION COMMITTEE

## ABSTRACT

### THE GEOLOGY AND GEOCHEMISTRY OF THE PATHÉ GEOTHERMAL

#### ZONE, HIDALGO, MEXICO

The Mexican government's Comisión Federal de Electricidad has operated a 3500 kw turbo generator plant at the Pathé geothermal field in northwest Hidalgo, Mexico since 1958. The present investigation examines the variables which control the alteration product mineralogy developed in an active hydrothermal area. Exploratory drilling has reached a depth of 1286 m without drilling through the Tertiary volcanic sequence of interbedded rhyolite pumice tuffs and flow breccia, andesite and olivine basalt. The vertical chemical variation as determined by quantitative chemical analyses by x-ray fluorescence does not indicate an obvious overall differentiation trend. Five K/Ar age determinations of Pathé samples by R. E. Denison, Mobil Field Research Laboratory, indicate Pliocene emplacement dates (4.2 to 6.7 m. y.) for the volcanic sequence.

Low pressure steam at temperatures of 100° to 150° C is produced from a 1200 m long portion of a north-south trending high-angle fault. A second set of east-west trending normal faults has produced a series of grabens and horsts parallel to an area of subsidence through the Pathé field. Steam is present at shallow depth and constitutes a hazard in the clay mines which are present along the thermally active portion of the fissure. The mines work a one-meter wide vertical seam of hydrothermal montmorillonite, zeolite and quartz, thus allowing a first-hand inspection of the "plumbing" of a geothermal system. Chalcedonic and euhedral quartz, dioctahedral montmorillonite, and stilbite are the commonly associated near-surface vein minerals. The low iron, high magnesium montmorillonite is stable at the highest temperatures observed in the Pathé field (approximately 150° C), and yields exceptionally strong (00) diffraction intensities. Altered wallrock within a basaltic tuff section exposed in a mine shaft perpendicular to the main fault indicates a zone of weathering, then progressive chloritization and silicification as the fissure is approached.

Mineralogical variations with depth include an increase in the amount of vein calcite accompanied by a decrease in quartz. The zeolites mordenite, laumontite, heulandite and analcite are locally present. Kaolinite, illite and calcite cuttings from depths greater than 700 m (T = 150° C) indicate that a zone of acid leaching and "K-fixation" may be present at depth. The mineralogical distribution is assumed to reflect the alkaline, magnesium-rich, potassium-deficient nature of the Pathé steam. Montmorillonite is stable at relatively high temperatures (100° to 150° C) within the fissures as a result of the high ratio of sodium to potassium in the thermal system. Caution must be exercised in the utilization of the montmorillonite-illite transformation without considering the chemical environment.

## ACKNOWLEDGMENTS

The writer expresses his sincere appreciation to Dr. Charles J. Mankin for his guidance and seemingly endless patience throughout this study. The author also expresses his gratitude to Dr. Harvey Blatt, Dr. John E. Francis, Dr. Arthur J. Myers, and Dr. George T. Stone who read the manuscript and offered many helpful suggestions: to Dr. Hal Noltimier, Mr. William H. Bellis and fellow graduate students for their helpful discussions of the study; to Dr. R. E. Denison and the Mobil Research and Development Corporation for their generous contribution of radiometric dates; to Mrs. Linda Hare for technical assistance in the laboratory investigation, to Mrs. Marian Clark and John Langford for assistance in drafting.

Special thanks are extended to Ing. Guillermo P. Salas, Director, Consejo de Recursos Naturales No Renovables, Dr. Liberto de Pablo and Dr. William A. Salas for their assistance in organizing the field investigation and preliminary laboratory study in Mexico, and to numerous employees of the Comision Federal de Electricidad, including Ing. Frederico Mooser, Mr. Bernard Pomade, Mr. Peter Powers, Havier Montes de Oca and others for their cooperation and assistance with the field geologic investigation. The financial assistance of the Geology and Geophysics Foundation, The University of Oklahoma and the Instituto de Geologia, Universidad Nacional Autonoma de Mexico is gratefully acknowledged.

## TABLE OF CONTENTS

|  | Page |
|--|------|
| ABSTRACT .....   | iii  |
| ACKNOWLEDGMENTS .....                                      | iv   |
| LIST OF TABLES .....                                       | vii  |
| LIST OF ILLUSTRATIONS .....                                | viii |
| INTRODUCTION .....   | 1    |
| General Statement .....                                    | 1    |
| Purpose of the Investigation .....                         | 1    |
| Location and Accessibility .....                           | 3    |
| Previous Investigations .....                              | 5    |
| History of the Development of the Pathe Geothermal Zone .. | 6    |
| Scope of the Present Investigation .....                   | 11   |
| STRATIGRAPHY .....   | 15   |
| Basement Rocks of Pre-Tertiary Age .....                   | 15   |
| Jurassic System or Older .....                             | 17   |
| Metasedimentary Rocks .....                                | 17   |
| Las Trancas Formation .....                                | 17   |
| Cretaceous System .....                                    | 17   |
| El Doctor Limestone .....                                  | 17   |
| Soyatal and Mexcala Formations .....                       | 18   |
| Extrusive Volcanic Rocks of Tertiary Age .....             | 18   |
| Oligocene-Miocene (?) Volcanic Rocks (Undivided) .....     | 18   |
| Extrusive Volcanic Rocks of Pliocene Age .....             | 19   |
| Interstratified Volcanic Unit .....                        | 19   |
| Rhyolite Unit .....  | 22   |
| Basalt Unit .....  | 24   |
| Pumice Tuff Unit .....                                     | 36   |
| Don Guinyo Tuff .....                                      | 37   |
| Intrusive Volcanic Rocks of Pliocene Age .....             | 38   |
| Rhyolite Porphyry Unit .....                               | 38   |
| Rhyolite Felsite Dikes .....                               | 39   |
| Recent Fluvial Deposits .....                              | 40   |
| Origin of the Pathe Volcanic Sequence .....                | 41   |

|  | Page |
|--|------|
| STRUCTURE .....  | 43   |
| Regional Structural Setting .....                            | 43   |
| Structure of the Pathé Geothermal Field .....                | 45   |
| Structural Control of the Steam Distribution .....           | 49   |
| MINERALOGY AND DISTRIBUTION OF THE ALTERATION PRODUCTS ..... | 52   |
| Sampling Procedures .....                                    | 52   |
| Analytical Techniques .....                                  | 53   |
| Deuteric Alteration and Chemical Weathering .....            | 55   |
| Wallrock Alteration .....                                    | 63   |
| El Carmen Mine .....   | 63   |
| El Carmen #2 Mine .....                                      | 67   |
| Tizpathe Mine .....  | 71   |
| Santa Rosa Mine .....  | 78   |
| El Coh Mine .....  | 79   |
| Alteration of the Pathé Cores .....                          | 82   |
| Wells 8, 9 and 11 .....                                      | 82   |
| Wells 4 and 5 .....  | 88   |
| Well 7 .....   | 92   |
| GEOCHEMICAL CONTROL OF THE ALTERATION .....                  | 93   |
| Geochemical Environment of the Pathé Geothermal Zone .....   | 93   |
| Temperature .....  | 93   |
| Solution Chemistry .....                                     | 96   |
| SiO <sub>2</sub> .....                                       | 100  |
| CaCO <sub>3</sub> .....                                      | 102  |
| Ca, Na and K .....   | 102  |
| Mg .....   | 103  |
| Mineral Stabilities .....                                    | 104  |
| Montmorillonite-Illite .....                                 | 104  |
| Kaolinite .....  | 105  |
| Silica Minerals .....  | 107  |
| Calcite .....  | 107  |
| Zeolites .....   | 108  |
| Chlorite-Montmorillonite .....                               | 108  |
| Pyrite .....   | 108  |
| CONCLUSIONS .....  | 110  |
| SELECTED REFERENCES .....                                    | 113  |
| APPENDICES .....   | 117  |

LIST OF TABLES

| Table  | Page |
|--|------|
| 1. Stratigraphic Columns in Parts of Queretaro, Hidalgo and N. E. Mexico, Mexico ..... | 16   |
| 2. Chemical Analyses by X-ray Fluorescence .....                                       | 21   |
| 3. Chemical Analyses by X-ray Fluorescence of Alteration Products .....                | 65   |
| 4. Lattice Spacing Data for Trioctahedral Chlorite-Smectite Minerals .....             | 70   |
| 5. Chemical Calculations: Pathé Montmorillonite .....                                  | 77   |
| 6. Analcite-Wairakite Powder Data .....  | 91   |
| 7. Chemical Analyses of Geothermal Solutions and Condensate .....                      | 98   |

## LIST OF ILLUSTRATIONS

| Figure   | Page |
|--|------|
| 1. Location Map .....  | 4    |
| 2. Mine, Well and Sample Location Map of Pathé Geothermal<br>Zone .....  | 9    |
| 3. Pathé Cliff Measured Section .....  | 32   |
| 4. Mineralogical Variation: El Carmen Mine .....   | 64   |
| 5. X-ray Diffraction and DTA Data: Saponite-Chlorite .....   | 68   |
| 6. X-ray Diffraction and DTA Data: Pathé Montmorillonite .....   | 74   |
| 7. X-ray Diffraction Data: El Coh Mine .....   | 80   |
| 8. X-ray Diffraction Data: Zeolites .....  | 84   |
| 9. X-ray Diffraction Data: Illite-Montmorillonite .....  | 87   |
| 10. Calculated Boiling Curve and Temperature Log, Well 8 .....   | 95   |
| 11. Solubilities of Amorphous Silica and Quartz as a<br>Function of Temperature .....  | 99   |
| 12. Calculated Geothermal Temperature Based on SiO <sub>2</sub> .....  | 101  |
| 13. Stability Relations in the System Na <sub>2</sub> O-Al <sub>2</sub> O <sub>3</sub> -SiO <sub>2</sub> -H <sub>2</sub> O<br>at Elevated Temperatures ..... | 106  |
| 14. Zeolites as a Function of H <sub>2</sub> O, Al/S: and the Energy<br>Index .....  | 109  |

| Plate  | Page |
|--|------|
| I. Reconnaissance Geologic Map of the Tecozautla-Cadereyta Area, Hidalgo and Queretaro, Mexico ..... in Pocket |      |
| II. Geologic Map: Pathé Geothermal Zone, Hidalgo and Queretaro, Mexico ..... in Pocket                         |      |
| III. Textures of Igneous Rocks ..... 25  | 25   |
| IV. Photomicrographs of Volcanic Rocks ..... 27  | 27   |
| V. Photomicrographs of Volcanic and Epiclastic Rocks ..... 29  | 29   |
| VI. Pathé Cliff Section ..... 31   | 31   |
| VII. Views of the Pathé area ..... 33  | 33   |
| VIII. View of the Main Fissure, Pathe' Fault ..... 47  | 47   |
| IX. El Coh Mine ..... 54   | 54   |
| X. Photomicrographs of Alteration Products ..... 58  | 58   |
| XI. Scanning Electron Micrographs of Alteration Products ..... 60  | 60   |
| XII. Scanning Electron Micrographs of Clay ..... 62  | 62   |
| XIII. Scanning Electron Micrographs of Zeolite ..... 89  | 89   |
| XIV. Lithology, Temperature and Alteration Product Mineralogy: Pathé Cores ..... in Pocket                     |      |

THE GEOLOGY AND GEOCHEMISTRY OF THE PATHÉ GEOTHERMAL ZONE,  
HIDALGO, MEXICO

INTRODUCTION

General Statement

The major geothermal systems of the world have been extensively investigated during the past twenty years in conjunction with their exploitation as sources of steam for the generation of "geothermal power." The general geologic similarities of these occurrences, particularly their relation to tectonism and volcanism, have been well established. In contrast with these general similarities involving their geologic setting, a marked diversity is seen when the mineralogy of their associated alteration products is considered. This diversity is not surprising considering the interplay of source rock, temperature, and solution chemistry which occurs in the geothermal environment.

Purpose of the Investigation

The purpose of this investigation is to examine the geology and mineral chemistry of the Pathé geothermal zone, Hidalgo, Mexico. An important objective was a determination of the variables which control the alteration product mineralogy in the Pathé geothermal zone and a comparison of the chemical environment there with that of other geothermal systems. Investigators of geothermal systems have long recognized the important

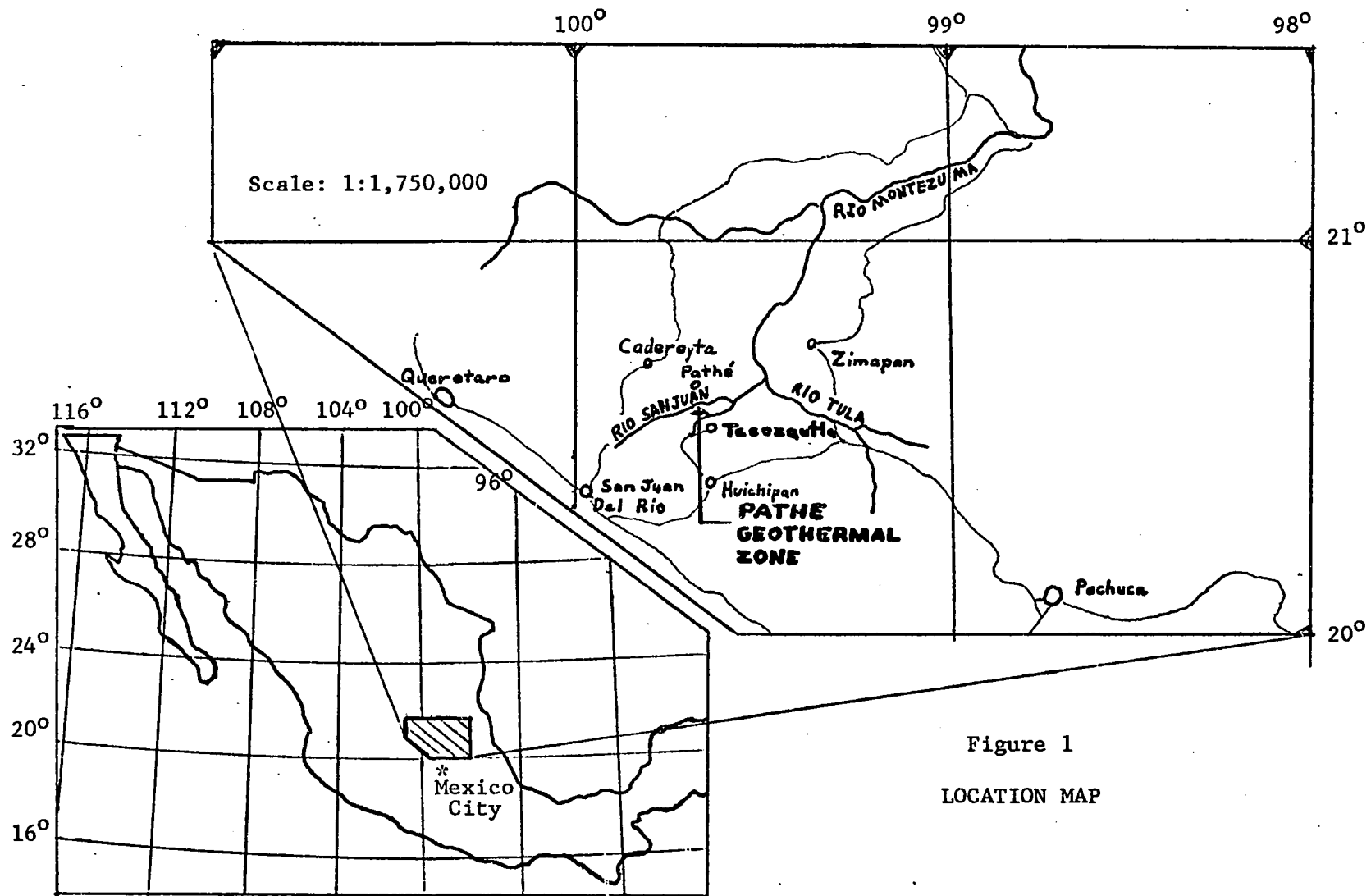
role of temperature in the control of alteration product zonation (Fenner, 1936; Steiner, 1967). Montmorillonite, a highly-hydrated, relatively low temperature clay mineral is transformed into the micaceous clay mineral illite with increasing temperature. Recently Burst (1969) has demonstrated the control of temperature rather than pressure or "geologic age" in the transformation of montmorillonite to illite which occurs during the diagenesis of marine sediments.

Exploration of the Pathe zone has provided an opportunity to examine the stability fields of a low temperature mineral assemblage (montmorillonite + zeolite + calcite + quartz) under more closely determined conditions than are ordinarily possible. The Comisión Federal de Electricidad has made available for mineralogical and petrographic study 1588 m of cores obtained from five exploration wells drilled within the Pathé Geothermal Zone. Extensive clay mining within the thermal area to depths limited by the escape of steam into the mine shafts allows a direct observation of the wallrock alteration in progress, and a firsthand observation of the fault control of both the steam distribution and alteration. The true three-dimensional nature of the alteration may be examined by considering both the near-surface, laterally variable wallrock alteration, and the vertical variation produced by increasing temperature with depth as observed in deep cores and drill cuttings. A preliminary investigation indicated that montmorillonite was the primary phyllosilicate vein mineral within the steam-bearing fissures. The presence of this low temperature mineral as a vein deposit suggested that factors in addition to temperature exerted an important control on the alteration product mineralogy at Pathé.

### Location and Accessibility

The Pathe geothermal zone is situated 135 km north-northwest of Mexico City and 70 km east of Queretaro at lat 20°35' N., long 99°42' W. (Fig. 1 and Plate 1). The field office of the Comisión Federal de Electricidad, a 3,500 kw generator plant, and the steam-producing wells are on the east bank of the Rio San Juan in the State of Hidalgo. The river is the boundary between Hidalgo to the southeast and Queretaro to the northwest. Steam production is localized within a 1,200 m long by 600 m wide zone but warm spring activity is present along an east-west trending fault through the area for a distance of at least seven kilometers. An area of 25 km<sup>2</sup> surrounding the Pathé camp was mapped at a scale of 1:5,000 in conjunction with the study (Plate 2 in pocket).

Access to the Pathé area is provided by a hard surface highway which connects Huichapan and Tecozautla, 9.5 km to the southeast. Six kilometers of dirt road that extends north from the highway at a point five kilometers west of Tecozautla serves the Pathé camp and the clay mines of the area. A rough truck road connects the camp with the village of Pathé, three kilometers to the north in the state of Queretaro, and eventually with Cadereyta, 17 km further to the northwest. The Rio San Juan is known as the Rio Montezuma downstream from its junction with the Rio Tula 22 km east of Pathe. At that point the river's course turns sharply to the north. The deep gorges of the Rio San Juan, the Rio Montezuma, various tributary streams of the Rio Montezuma to the north of Pathé, and the mountainous nature of the terrain serve to isolate the region immediately east and northeast of Pathé. Access to this area is only by means of trails or helicopter. The low-water crossing at Pathé



is the last vehicular crossing of the river for a distance of 100 km to the east and northeast.

In sharp contrast with the relatively uninhabited, inaccessible land to the northeast, the area immediately south of the Pathé zone is a 3 km wide floodplain of a tributary stream, the Rio San Francisco. The plateau south of the valley of the Rio San Francisco, and southeast of Tecozautla is capped by extensive deposits of tuff and basalt. Huichapan, the major center of commerce in the area, serves as a railhead and is on a highway connecting Mexican Highways 57 and 85.

#### Previous Investigations

Mooser (1967) has mapped the volcanic and major tectonic features of the Trans-Mexico Volcanic Belt (neovolcanic zone) from aerial photos at a scale of 1:50,000. His mapping reveals the probable trend of this zone of Late Tertiary to Recent volcanic activity along a 1000 km arc extending from Baha California to the Gulf of Mexico. The relationship of this zone to the other major tectonic features of Mexico is shown on a 1:500,000 scale map by de Cserna (1961).

Prior to 1952, detailed geologic investigations along the northern margin of the Trans-Mexico Volcanic Belt were restricted primarily to the mining areas such as the Pachuca-Del Monte and Zimpan districts (Plate 1). In 1952, Segerstrom began mapping the Bernal-Jalpan area (25 km northwest of Pathé at its nearest point) in cooperation with the Instituto Nacional Para la Investigacion de Recursos Minerales and the United States Geological Survey (Segerstrom, 1961). In a companion study of the Geology of south-central Hidalgo and northeastern Mexico, Segerstrom (1962) mapped

an area to the east which extends to within 16 km of the Pathé area, and includes both the Zimpan and Pachuca-Del Monte mining districts.

Detailed investigations of the Zimpan and Pachuca districts are pertinent to the present study because they reveal aspects of the regional setting not apparent in the Pathé area. Simons and Mapes (1956) studied the geology of the Zimpan mining district 23 km northeast of Pathé, and described in detail the petrology of a well-exposed section of Tertiary igneous rocks. The study of the Pachuca-Del Monte district (Geyne, et al., 1963) summarizes the wealth of geologic knowledge gained over 400 years of mining experience in one of the world's most important silver-producing areas. Its detailed petrographic descriptions, chemical analyses and age correlations provide a starting point for volcanic-rock correlations within the northern portion of the Trans-Mexico Volcanic Belt.

#### History of the Development of the Pathé Geothermal Zone

Published accounts of the early development of the Pathé geothermal field include a paper by de Anda, Isita, and Elisondo (1961) and a thesis by H. Alonso Espinosa (1961). Both of these studies review geothermal exploration in Mexico by the Comisión Federal de Electricidad with emphasis on the Pathé zone. Information contained in these two reports (particularly sample logs of wells not cored, temperature measurements, and chemical analysis of condensates produced by the wells) was utilized extensively in the present study.

Geological considerations which led to the choice of Pathé as Mexico's first geothermal power project were summarized by de Anda, et al. (1961, p. 153):

. . . Pathé was originally chosen because it presented evidence of attractive geothermal activity--that is, thermal springs and fumaroles at boiling point, a great amount of geyseric rock, mineralized rocks with sulfides, alteration of primary rocks giving place to important deposits of caolinite, veins of gypsum and profound erosion in preferential directions with fractures. Some chemical analyses were made of the water of various springs, and it appeared opportune to start an exploratory perforation. . . .

Another consideration which favored the choice of the Pathé area was its relative accessibility. Nine mining claims for "caolin" were being produced from the geothermal zone (Esquivel and Zamora, 1958) and the area was served by a truck road.

The initial well sites were chosen primarily on the basis of a photogeologic study of the area. The wells were drilled at the intersection of north-south and east-west trending fractures. Figure 2 shows the well locations and their relation to the important structural fractures. Well 1 was begun in August, 1955, utilizing percussion drilling equipment. A dominantly basalt and basaltic-tuff section was penetrated to a depth of 236 m, and in January, 1956, the well exploded shortly after samples indicated the penetration of a rhyolitic breccia capped by pumice. The maximum temperature measured in the hole prior to the blowout was 150° C.

Producing wells were then drilled 210 m northeast (well 2A) and 206 m southeast (well 3) of well 1. In 1959, a generator plant with a maximum-rated capacity of 3500 kw was put into production utilizing the dry steam produced by well number 2A. Subsequent attempts at locating usable steam met with mixed results. Diamond cored exploration wells drilled to the southwest and east (wells 4 and 5) indicated relatively low temperatures along the fracture zones away from the central, highly-altered valley. Wells 6 and 7 were drilled on the main north-south

Figure 2

MINE, WELL AND SAMPLE LOCATION MAP,  
PATHE GEOTHERMAL ZONE

Mine Locations

The clay vein along the Pathe fault has been mined continuously from the El Carmen to the Santa Rosa mines. Symbols reflect the location of the more recently active entrance shafts. Three types of mine samples were collected; underground samples from measured traverses perpendicular to the vein, spot samples collected underground, and samples collected from the mine dumps.

Well Locations

Samples of the cores from wells 4, 5, 8, 9 and 11 are described in Appendix B. The lithology, mineralogy of the alteration products, and recorded temperatures of these wells are shown in Plate XIV. Well locations are also indicated on Plate II.

Surface Sample Locations

Spot samples and samples from measured traverses were collected to represent both the fresh rock and surficial alteration. Not shown are surface sample locations 21 through 25 from the north flank of Cerro Peligroso, 200 m southwest of El Carmen.

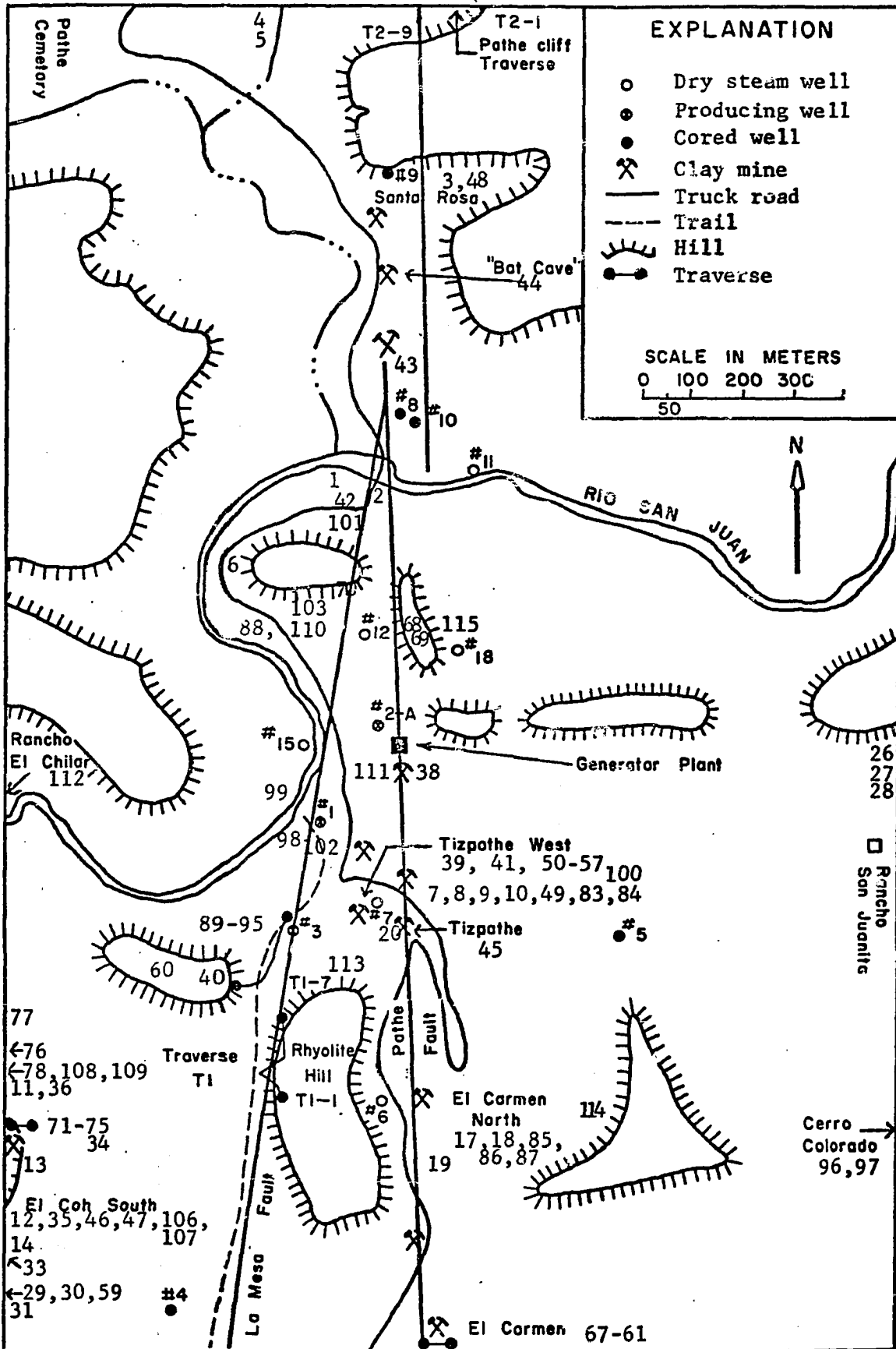


Figure 2

trending fracture south of well 2A and encountered elevated temperatures but no producible quantities of steam. Four wells were then drilled north of the Rio San Juan along the trace of the main north-south fault. Elevated temperatures were encountered just north of the river (150° C in well 8), but no steam production was obtained. Three of these wells were diamond-cored (wells 8, 9, and 11). Exploration was then concentrated within the main valley and production was obtained from wells 13A and 17, both of which were drilled on the trace of the north-south fault. Well 15 was drilled on the west bank of the river with the hope of intersecting the fault zone at greater depth, but this well was dry as were several additional wells drilled on the east side of the main fault.

During 1967 and 1968, C. J. Banwell directed an intensive geophysical and geochemical exploration of Mexico's geothermal resources. The program concentrated on the application of techniques such as isotope and resistivity surveys to the more promising thermal fields. In 1969, a preliminary low-frequency, ground-noise survey of the Pathé zone was conducted by Mr. G. T. Clacey, consulting geophysicist with the Field Geology Division of the Federal Comisión de Electricidad. His survey indicated a ground-noise anomaly in the geothermal zone which increased in magnitude to the northwest towards Cadereyta. Benard Pomade, cartographer with the Field Geology Division, then undertook the reconnaissance mapping of the area indicated in Plate I under the supervision of F. Mooser, and with the cooperation of the present author (Nichols and Pomade, 1970). Mapping was done from aerial photographs on a 1:100,000 scale Mexico Army topographic map and field checking was accomplished mainly by helicopter reconnaissance. Mapping by Segerstrom (1961, 1962) was

also utilized in the preparation of Plate I, which includes an extrapolation across the Pathé volcanic field of structures from adjacent areas mapped by Segerstrom.

Present activity at the Pathé camp is mainly concerned with maintaining the steam production. With time, the wells have tended towards higher water production, lowered temperatures and eventually a cessation of natural production as a result of ground water encroachment, mineral deposition within production tubing or a combination of these factors. The maximum temperature recorded during the drilling of the 18 exploration and production wells at Pathé was 160° C. The estimated maximum temperature for the thermal system as calculated from the SiO<sub>2</sub> content of the steam is approximately 150° to 160° C. The condensate from the Pathé wells has a higher Mg content and Na/K ratio than "average" steam-producing wells. Its total solids content of 1200 ppm reflects the relatively low temperature of the Pathé system. The maximum steam production achieved has been 14 tons per hour with a pressure of 2.8 Kg/cm<sup>2</sup>.

#### Scope of the Present Investigation

The primary objective of the present investigation was to document the zeolite and phyllosilicate alteration assemblages present in the mines and cores from the Pathé zone. A detailed knowledge of the volcanic section and structural geology was an important prerequisite to the alteration study. However, the extensive alteration, closely-spaced faulting, relative monotony of the volcanic section, and surficial cover by recent fluvial and pyroclastic deposits had prevented a detailed determination of the local volcanic section. It was anticipated that the present study,

by incorporating petrographic examinations, mineralogical determinations by x-ray diffraction, chemical analyses of the individual rock units and detailed surface mapping at a scale of 1:2000 would be able to contribute to the understanding of the geology of the zone. This portion of the project would provide a starting point for the study of the alteration produce mineralogy and geochemistry.

Dr. Liberto de Pablo, Dr. C. J. Mankin, and the author visited the Pathé zone during an initial sample collecting trip in August, 1967. Vertical aerial photographs with a scale of 1:24,000 were provided by the Consejo de Recursos Naturales No Renovables and a preliminary laboratory investigation of the samples was begun in the x-ray laboratory, School of Geology and Geophysics, University of Oklahoma. Field work was accomplished during the period January 1 through March 1, 1968, and the author also had the opportunity to observe the electron-optical research being conducted by de Pablo on the structure of the Pathé montmorillonite.

Much time in the field was consumed by surface sampling and checking the numerous fractures visible on aerial photographs. Most of the relatively small area mapped at a scale of 1:2000 (25 km<sup>2</sup>) is accessible only by foot trails. The cores of five wells were described and sampled (Plate XIII). A final aspect of the field investigation was sampling alteration products associated with the thermal activity in the clay mines. One open pit mine (Fig. 2) is located one kilometer southwest of the main valley; the rest of the mines are narrow, vertical cuts which follow the main fault planes. Access to the lower reaches of the mines is provided by notched poles which are wedged into crevasses. The

"ladders" are removed from mines not being actively worked so access is usually restricted to the particular area being mined. Access is further limited by heat, water levels, and local concentrations of bats. During summer months, mining is restricted to the hours of darkness because daytime temperatures within the mines during hot days are unbearable. During the winter, mining is usually discontinued at noon in the "hot" sections of the mines. Several inclined tunnels intersect the main clay vein and these provided an opportunity to examine lateral variations in the wall-rock alteration.

A total of 210 samples collected from outcrops, mines and cores were examined utilizing equipment of the X-ray Laboratory, School of Geology and Geophysics, University of Oklahoma. Sample locations and descriptions are included as Appendix B. Petrographic examinations and chemical analyses by x-ray fluorescence of relatively unaltered samples of various lithologies in the area provided reference data for the alteration studies. X-ray diffraction data were utilized as a supplement to standard petrographic techniques in the characterization of olivine, pyroxene and feldspar, and as a primary means of identifying zeolites and phyllosilicate phases. The x-ray diffraction techniques employed for clay mineral identification included obtaining diffractometer patterns of randomly oriented powder samples, (001) oriented slides prepared by sedimentation, oriented slides "solvated" by ethylene glycol, and slides subjected to heat treatments. The above techniques are described by Brown (1961). Mineral separations for detailed analyses was accomplished by means of "hand-picking" and by size distribution separations based on

differential settling velocities in distilled water as described in Appendix A.

Quantitative x-ray fluorescence analyses were obtained using a Siemens-Halske sequential x-ray fluorescence spectrometer, model SRS-1 and sample preparation techniques described in Appendix A. High-temperature stability studies were accomplished by means of a Robert L. Stone x-ray diffractometer furnace and recording assembly installed on a Corelco x-ray diffractometer. Differential thermal analyses obtained with a Robert L. Stone model DTA-13M furnace and recording assembly were utilized primarily to characterize the dehydration behavior of the clay minerals.

Dr. R. E. Denison, Senior Research Scientist of the Rock Dating Section, Mobil Field Research Laboratories, Dallas, Texas, generously provided K/Ar dates for five samples from the cores and outcrops of the Pathé area. These were selected to determine the time span represented by the Pathé volcanic sequence. This aspect of the study is being expanded through the cooperation of the C.F.E. to include additional dates from other sites along the northern margin of the "Neo Volcanic Zone."

## STRATIGRAPHY

### Basement Rocks of Pre-Tertiary Age

Rocks of pre-Tertiary age do not crop out within the Pathé geothermal zone, and have not been identified in cores or cuttings from the wells, which have reached a maximum depth of 1286 m (well 7). Limited exposures of Upper Cretaceous clastic rocks and limestones are present 10 km southeast of Tecozautla along the axis of the San Lorenzo Syncline (Plate I) and are assumed to be present at depth at Pathé. Extensive uninterrupted outcrops of Jurassic and Cretaceous sedimentary rocks form the mountainous areas to the northwest, north, and northeast of Pathé. A consideration of these formations is relevant to the present study as they may constitute the "plumbing" of the Pathé geothermal system and thus exert an influence on the chemistry of the circulating thermal fluids. The following brief review is extracted from studies by Segerstrom (1961, 1962). The Pathé stratigraphic column, dated in part by radiometric dating, is compared with columns reported from other areas within the Tertiary volcanic belt in Table 1. Radiometric dating of the Tertiary volcanic sequence indicated a generally younger age than had been previously assumed on the basis of stratigraphic relations and geomorphology.

16  
TABLE 1

STRATIGRAPHIC COLUMNS IN PARTS OF QUERETARO, HIDALGO, AND N.E. MEXICO

| Sys-tem     | Series  | Bernal-Jalpan<br>Segerstrom-1961 | Pathe-Huichipan-<br>Tecoautla   | S. Central Hidalgo and<br>N.E. Mexico, Segerstrom<br>(1961)               |   |
|-------------|---|----------------------------------|---|---|---|
| QUATERNARY  | Pleistocene and Recent  | Clastic deposits, caliche        | Fluvial deposits Rio San Francisco and Rio San Juan<br>Basalt (Huichipan) | Clastic deposits Caliche, basalt  |   |
|             |   | Basalt                           | Don Guinyo Tuff<br>4.2 ± 0.3 m.y.<br>4.3 ± 0.3 m.y.                       | Tarango and Atotonilco El Grande formations (clastic deposits)            |   |
|             | Pumice Tuffs  |                                  | San Juan group (includes San Cristobal "basalt")                          |   |   |
|             | Basalt Unit<br>6.3 ± 0.2 m.y.<br>6.3 ± 0.2 m.y.<br>6.4 ± 0.2 m.y.<br>6.5 ± 0.2 m.y. |                                  |   | Jalpan andesite   |   |
|             | Andesite  |                                  |   | Rhyolite Unit   | Don Guinyo Tuffs zumate (andesitic to dacitic flows) and Tezuantia (rhyolitic to rhyodacite) formations |
|             |   |                                  | Rhyolite Porphyry<br>6.6 ± 0.1 m.y.<br>6.7 ± 0.1 m.y.                     |   |   |
|             |   | Basalt-Andesite Unit             |   |   |   |
|             | TERTIARY  | Pliocene                         | Basalt  | Oligocene-Miocene (?)<br>Undifferentiated (chiefly rhyolite and andesite) | Pachuca Group (rhyolite, andesite and dacite flows)   |
|             |   |                                  | Rhyolite  |   |   |
|             |   | Miocene                          | El Morro fanglomerate   | El Morro fanglomerate   |   |
|             |   |                                  |   |   | Oligocene   |
|             | Eocene  |                                  |   |   |   |
| Paleocene   |   |                                  |   |   |   |
|             | CRETACEOUS  | Upper                            | Mexcala fm.   | Mexcala fm.   | Mexcala Mendez fm.  |
| Soyatal fm. |   |                                  | Cuantla fm.   | Soyatal and Cuantla fm.   |   |
| Lower       |   | El Doctor ls.                    | El Doctor ls.   | El Doctor Limestone   |   |
|             |   |                                  |   | Santurio fm. (ls.)  |   |
| JURASSIC    | Upper   | Las Trancas formation            | ???   | Las Trancas formation   |   |
|             | Lower   |                                  |   |   |   |
| PALEOZOIC?  |   | Schist, quartzite                |   |   |   |

### Jurassic System or Older

Metasedimentary rocks. Metamorphic rocks including mica schists and quartzites crop out along the crest of the El Chilar anticline 38 km northwest of Pathé. These are the oldest rocks recognized near the area of this study (Middle Jurassic or older), and are overlain unconformably by the Las Trancas Formation of Middle or Upper Jurassic age.

Las Trancas Formation. Segerstrom (1961, p. 30) characterized the Las Trancas Formation as ". . . black, thinly fissile phyllitic shale containing sandstone and claystone concretions, detrital mica and interbeds of coarse graywacke, the graywacke in places contains pebble conglomerate." The present thickness of the formation ranges from a maximum of 500 to 1000 m to 0 where it has been completely removed by erosion along the crest of the El Chilar anticline.

### Cretaceous System

El Doctor Limestone. The Las Trancas Formation is overlain by the El Doctor Limestone of Middle Albian to Early Cenomanian age. At the type locality, near the village of El Doctor, Queretaro, the formation consists of four facies: shallow water biostrome, conglomerate, thick limestone beds with chert nodules, and thin-bedded limestone with abundant chert lenses (Wilson, et al., 1955). The El Doctor Formation is resistant to erosion and produces a topography characterized by rugged mountains and steep-walled canyons. Near the type locality the maximum measured thickness of the El Doctor Limestone is 1500 m. Isolated exposures of the limestone are present throughout the Tertiary volcanic belt east and south of Pathé; the nearest is 10 km southeast of Tecozautla.

Soyatal and Mexcala formations. North of Pathé in the Bernal-Jalpan area mapped by Segerstrom (1961), the El Doctor Limestone is overlain by thin-bedded, fine-grained, dark-gray limestone with interbedded shale, mudstone and siltstone of the Soyatal Formation. Higher in the section a gradational boundary is observed with the upper, predominantly clastic portion of the unit designated the Mexcala Formation.

#### Extrusive Volcanic Rocks of Tertiary Age

The pre-Tertiary basement rocks of the Pathé field are overlain by a volcanic section of undetermined total thickness. Drilling reached a depth of 1286 m (well 7) without drilling through the Tertiary volcanic section. The composition of these lavas and clastic volcanic rocks varies from rhyolite to olivine basalt. A review of the investigations of nearby volcanic areas by Geyne, et al. (1963), Segerstrom (1961, 1962), and Simons and Mapes (1956) reveals a similar lithologic variability. These rocks have been dated on the basis of paleontological evidence in interbedded sedimentary rocks as Oligocene to Miocene in age. The Pathé stratigraphic column and stratigraphic columns extracted from the aforementioned references are included as Figure 4.

#### Oligocene-Miocene (?) Volcanic Rocks (Undivided)

The oldest rocks of probable Tertiary age encountered at Pathé comprise a thick sequence of interbedded rhyolitic flows, tuff and flow breccia. The unit has been recognized only in cuttings from well 7 at depths below 650 m. Severe circulation losses in the well between depths of 600 and 800 m resulted in poor sample returns and prevented the determination of the exact top of the lower rhyolite unit. Cuttings from a

depth of 750 m to the termination of drilling at a depth of 1265 m indicate a predominantly rhyolitic lithology.

The Oligocene-Miocene (?) volcanic rocks consist of compact non-porphyrific rhyolite and tuff. The partially devitrified brown groundmass of the rhyolite contains abundant microcrystalline quartz "blebs" which are preferentially oriented to give a strongly banded appearance to much of the rock. Spherulitic intergrowths of quartz and feldspar are present locally within the groundmass. Several fragments of rhyolite contain relic glass shards indicating the presence of pyroclastic units. Chips of an andesite (?) lava are locally common indicating the presence of andesite within the predominantly rhyolite sequence. The andesite consists of plagioclase microlites set in a dark, magnetite-rich, glassy groundmass. Secondary quartz and calcite are common, and the rock is highly altered.

The known thickness of the Oligocene-Miocene (?) volcanic rocks in well 7 is approximately 600 m. Rhyolite of Oligocene to Miocene age is the dominant lithology in the Bernal and Queretaro volcanic fields west of the Pathé zone. The oldest known Tertiary formation in the Pachuca district to the east is the Santiago Formation (Fries, et al., 1963, p. 32). It consists of interbedded andesite to rhyolite lava flows, flow breccias, and tuffs of Oligocene age. The maximum exposed thickness of the Santiago Formation is 480 m, but its base has not been penetrated.

#### Extrusive Volcanic Rocks of Pliocene Age

Interstratified Volcanic Unit. Overlying the Oligocene-Miocene (?) volcanic rocks is a sequence of nonporphyritic, fine-grained andesite and

basalt lavas and rhyolite tuffs. Near the top of the unit the basic flows become increasingly interbedded with rhyolitic lavas and tuffs similar to the overlying rhyolite unit. The top of the interstratified volcanic unit is here defined as the base of the massive flow-breccia of the overlying continuous silicic sequence of the rhyolite unit.

The andesite flow rocks are red-brown to light purple and are finely vesicular. They contain sparse microphenocrysts of normally zoned plagioclase (An<sub>50</sub>) and augite set in a pilotaxitic groundmass of slender plagioclase microlites. Brown glass, magnetite, and pyroxene are present in the groundmass.

One flow from the upper portion of the unit was identified by chemical analysis (Table 2, Col. 1) as basalt (Nockolds, 1954); it contains abundant magnetite grains and acicular crystallites. It has an intergranular texture similar to that of the olivine basalt sequence which overlies the upper rhyolite unit.

The rhyolite tuffs interbedded with the basic lavas display a distinctive lenticular texture suggestive of the partial collapse and welding of pumice tuff. Flattened dark-green pumice fragments one to two cm in diameter are set in a more compact light-green groundmass (Plates III & V). In thin section, the flattened pumice fragments and glass shards are seen to wrap around quartz phenocrysts suggesting the partial collapse and welding of the tuff. Subhedral to euhedral quartz phenocrysts from 0.5 to 2.0 mm in diameter are common. Chlorite and a micaeous clay identified by x-ray diffraction as mixed-layer illite-montmorillonite are common alteration products of the pumice. A chemical analysis of the pumice tuff is included in Table 2 (Col. 9) and denotes a rhyolite composition.

TABLE 2

## CHEMICAL ANALYSES BY X-RAY FLUORESCENCE

|                                 | 1<br>5-392 | 2<br>5-246 | 3<br>M-112 | 4<br>M-97 | 5<br>T2-1 | 6<br>M-118 | 7<br>11-134 | 8<br>5-415 | 9<br>5-302 | 10<br>5-461 | 11<br>T1-1 | 12<br>M-25 | 13<br>11-140 | 14<br>M-67 |
|---------------------------------|------------|------------|------------|-----------|-----------|------------|-------------|------------|------------|-------------|------------|------------|--------------|------------|
| SiO <sub>2</sub>                | 48.9       | 49.6       | 49.6       | 51.1      | 51.7      | 65.8       | 73.0        | 75.2       | 75.4       | 77.1        | 78.2       | 78.4       | 80.00        | 83.6       |
| Al <sub>2</sub> O <sub>3</sub>  | 15.0       | 15.8       | 16.4       | 15.3      | 16.7      | 14.2       | 12.0        | 13.7       | 10.6       | 12.1        | 8.7        | 12.2       | 8.8          | 5.9        |
| Fe <sub>2</sub> O <sub>3</sub>  | 9.6        | 8.32       | 10.55      | 8.32      | 8.67      | 6.40       | 2.33        | 2.67       | 2.27       | 4.22        | 3.33       | 0.95       | 3.35         | 2.95       |
| M <sub>g</sub> O                | 10.25      | 9.19       | 4.62       | 6.05      | 5.32      | 0.42       | 1.91        | 1.12       | 0.22       | ND          | ND         | 0.09       | .2           | 1.62       |
| CaO                             | 9.26       | 9.95       | 9.35       | 9.82      | 9.09      | 1.89       | 0.46        | 0.08       | 1.14       | 0.68        | .05        | 0.10       | .03          | 0.16       |
| Na <sub>2</sub> O               | 3.27       | 2.85       | 3.47       | 2.60      | 3.55      | 4.62       | 1.30        | 1.72       | 2.65       | 0.66        | .50        | 2.75       | 1.73         | 0.07       |
| K <sub>2</sub> O                | 0.42       | 0.73       | 0.46       | 0.65      | 1.02      | 3.14       | 4.57        | 3.82       | 3.20       | 2.03        | 6.09       | 4.06       | 3.82         | 1.02       |
| TiO <sub>2</sub>                | 1.48       | 1.11       | 2.48       | 1.37      | 1.03      | 0.50       | 0.27        | 0.20       | 0.13       | 0.29        | 0.41       | 0.08       | 0.21         | 0.36       |
| MnO                             | .12        | 0.14       | 0.18       | 0.13      | 0.14      | 0.09       | 0.02        | 0.03       | 0.03       | 0.03        | Tr         | Tr         | .01          | Tr         |
| P <sub>2</sub> O <sub>5</sub>   | .31        | 0.34       | 0.45       | 0.32      | 0.33      | 0.15       | .07         | 0.07       | 0.06       | 0.08        | 0.09       | .04        | .08          | 0.06       |
| S                               | .10        | 0.06       | 0.06       | 0.25      | 0.10      | -          | 1.09        | 0.29       | 0.22       | -           | 0.14       | -          | 1.24         | 0.29       |
| H <sub>2</sub> O <sup>f</sup> * | 1.00       | 0.36       | 0.54       | 1.75      | 0.80      | 1.20       | 0.41        | 2.71       | 3.38       | 2.00        | 0.86       | 0.50       | .16          | 2.71       |
| H <sub>2</sub> O <sup>-</sup>   | 1.20       | 1.00       | 1.50       | 1.40      | 0.80      | .20        | 2.50        | 0.10       | 0.10       | 1.60        | 2.2        | 1.30       | .50          | 1.00       |
| Totals                          | 100.91     | 99.45      | 99.66      | 99.06     | 99.25     | 98.61      | 99.93       | 101.01     | 99.40      | 100.69      | 100.54     | 100.47     | 100.13       | 99.74      |

\*H<sub>2</sub>O<sup>f</sup> determined by adjusting ignition loss at 1000° C for S content.

The most complete cored section of the interstratified volcanic unit is from well 5, where 160 m of the unit were penetrated before drilling was terminated within the sequence at a depth of 544 m. The maximum probable thickness of the interstratified volcanic unit in well 5 is 250 m. The unit is not exposed in the Pathé zone. A lithologically similar unit, the Corteza Formation (Geyne, et al., 1963, p. 34) is present overlying the Santiago Formation in the Pachuca district.

Rhyolite Unit. Overlying the interstratified volcanic unit is the most distinctive unit in the Pathé zone, a thick rhyolite flow rock and tuff sequence here designated the rhyolite unit. The unit is readily recognized in both cuttings and cores by its green color, abundant quartz phenocrysts, and abundant pyrite.

The basal beds of the rhyolite unit commonly are coarse, compact flow-breccias which contain angular, cobble-size fragments of brown to green rhyolite. These angular fragments are set in a compact, flow-banded aphanitic groundmass of almost pure, microcrystalline quartz. No mafic minerals were observed.

Overlying the basal rhyolite flow breccia is a thick rhyolite tuff section. This unit is characterized by abundant embayed, subhedral to euhedral quartz phenocrysts with the bipyramidal habit characteristic of volcanic quartz. The quartz phenocrysts, which average one to three mm in diameter, constitute 10 to 15 percent of the tuff. Also present are euhedral to subhedral sanidine phenocrysts averaging two mm in diameter. The matrix consists of fine quartz and pyrite grains set in a light-green to brown groundmass of devitrified glass shards. Montmorillonite and clinoptilolite are the dominant alteration products of the glass.

The uppermost member of the upper rhyolite unit is a compact, pink to cream lithic rhyolite tuff (Plate III), which is partially welded and more resistant to erosion than the underlying, extensively altered rhyolite tuff. It may represent the inner welded portion of an originally much thicker tuff section. The upper unwelded portion of the tuff sequence may have been removed by erosion, a common feature of ashflow tuffs (Ross and Smith, 1961). The texture of this upper compact zone is generally similar to that of the immediately underlying tuffaceous zone, the main difference is the more vitric nature of the upper zone. The upper zone contains more pyrite and no montmorillonite or zeolite. Chemical analyses indicate a rhyolite composition with unusually high sulphur content as a result of the pyrite (Table 2, Columns 7 and 13).

Every well drilled at Pathé, with the exception of well 3, encountered the rhyolite unit. Well 3 was drilled in a graben and apparently was terminated at a depth just above the top of the unit. Wells 4, 5, 7 and 10 penetrated a total thickness of 100 to 200 m of the unit. Two-hundred meters of the unit is underlain by basalt in well 10, but the original thickness is assumed to have been greater prior to the erosion of the unwelded upper portion. Whole rock K/Ar dates of  $5.4 \pm 0.2$  million years (m. y.) and  $5.1 \pm 0.1$  m. y. were obtained from a vitric sample of the unit (#11-140). This date appears slightly young in view of two older dates ( $6.4 \pm 0.2$  m. y. and  $6.5 \pm 0.2$  m. y.) obtained from an overlying basalt unit. The whole-rock basalt determinations are assumed to be more accurate, but the Pliocene date obtained from the rhyolite is in general agreement with the other dates.

Basalt Unit. The upper rhyolite unit is overlain by a basalt unit which crops out in most of the Pathé zone. This unit is defined as the sequence of olivine basalt and interbedded basic tuffs, bentonite and scoria which overlie the upper rhyolite unit. The basalts possess a variety of textures varying from intergranular to hyaloophitic (Plate IV). They generally are divisible into two distinct groups: a very fine-grained, olive-gray, pyroxene-rich basalt with intergranular texture, and a glassy basalt with coarse feldspar laths. Whole rock K/Ar determinations of two samples of fine-grained, non-vesicular intergranular basalt yielded dates of  $6.4 \pm 0.2$  m. y. and  $6.5 \pm 0.2$  m. y. (T2-1), and  $6.3 \pm 0.2$  m. y. and  $6.3 \pm 0.2$  m. y. (#5-246). Sample T2-1 was collected from the uppermost flow at the "Pathé Cliff" section, and is typical of the extensive basal flow which caps the fault blocks north of the Rio San Juan. Sample #5-246 (well 5; depth 246 m) is representative of the 250-m-thick basalt unit cored in well 5.

The intergranular basalt is uniformly gray to olive-gray and is commonly streaked with red-brown hematite stains. Olivine phenocrysts altered to red-brown "iddingsite" give the hand specimen a porphyritic appearance. Basalt from the lower portion of the member contains abundant grains of pigeonite(?) and grains and rods of wilmenite. Upward in the section, the proportion of groundmass magnetite decreases, whereas the proportion of plagioclase ( $An_{54-56}$ ) increases. Sparse, partially resorbed plagioclase phenocrysts two to three mm in length with reversed zoning occur in much of the intergranular basalt.

Magnesium-rich olivine ( $2V = 90^\circ$ ,  $For_{85}$ ) occurs as phenocrysts which constitute 5 to 7 percent of the rock. The outer rim of the

## Plate III

## TEXTURES OF IGNEOUS ROCKS

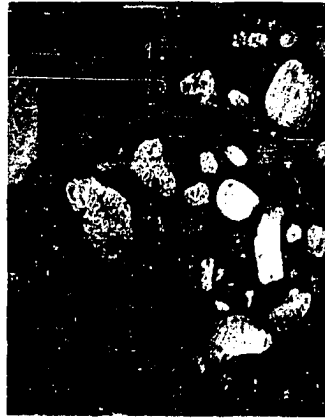
All samples were photographed in reflected light and with the exception of B are oriented with tops up. All magnifications are x 1.

- A. Sample 9-47: Vesicular hyaloophitic basalt. Fibrous mordenite within vesicles.
- B. Sample T1-4: Silicified lapilli tuff from the hill southeast of well 3. Top of the sample is to the left.
- C. Sample 11-134: Rhyolitic tuff. Partially welded zone which overlies the rhyolite unit.
- D. Sample 5-294: Zeolitized rhyolitic tuff.
- E. Sample 5-495: Partially welded pumice tuff. Darker areas are collapsed pumice fragments.
- F. Sample 4-18: Lithic tuff. Block-sized fragments of basalt locally present.
- G. Sample T1-1: Rhyolite felsite. Flowbanded dike rock.
- H. Sample 5-415: Welded tuff. Collapsed pumice in a vitric groundmass.

PLATE III



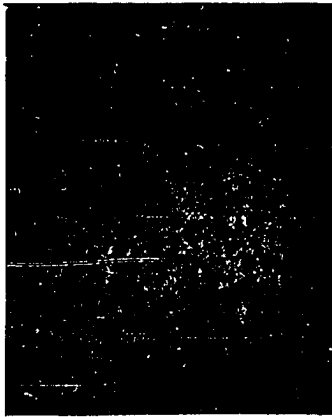
A



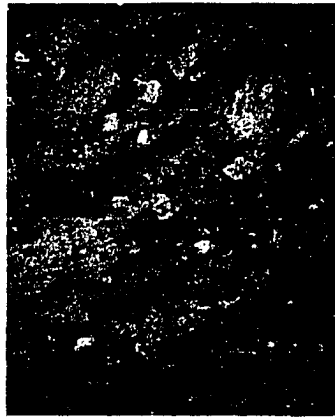
B



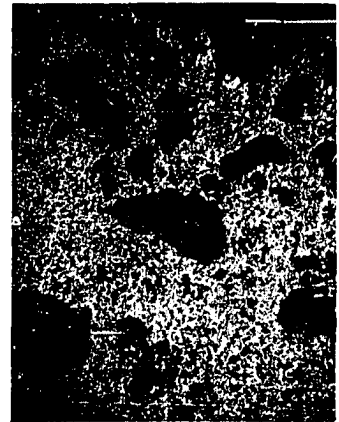
C



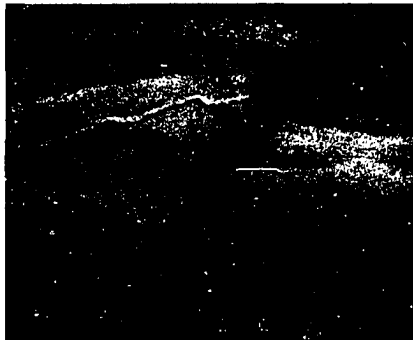
D



E



F



G



H

## Plate IV

## PHOTOMICROGRAPHS OF VOLCANIC ROCKS

- A. Sample M-21: Olivine basalt. Euhedral olivine crystals displaying rim alteration to "iddingsite". Crossed polars.  
X25
- B. Sample T2-1: Basalt. Intergranular texture with crowded plagioclase laths. Crossed polars.  
X2.5
- C. Sample M-38: Amygdular basalt. Amygdular calcite and stilbite. Plagioclase laths in tachylyte groundmass. Crossed polars.  
X2.5
- D. Sample M-1: Basalt. Aggregates of coarse plagioclase laths in tachylyte. Crossed polars.  
X2.5
- E. Sample 5-246: Basalt. Illmenite rods in a clinopyroxene-rich groundmass. Plain.  
X25
- F. Sample 4-383: Basaltic andesite. Pilotaxitic texture. Note orientation of plagioclase microlites. Plain light.  
X10

PLATE IV



A



B



C



D



E



F

## Plate V

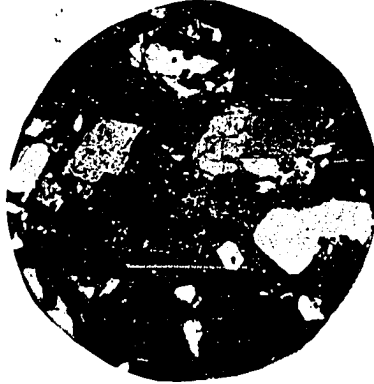
PHOTOMICROGRAPHS OF VOLCANIC AND  
EPICLASTIC ROCKS

- A. Sample 11-198: Rhyolite tuff. Bipyramidal, resorbed quartz phenocryst in a fine ash matrix. Crossed polars.  
X15
- B. Sample 11-138: Rhyolite tuff. Fractured sanidine and quartz phenocrysts in a fine ash matrix. Crossed polars.  
X60
- C. Sample T2-3: Volcanic ash. Horizontal, hematite-rimmed glass shards and fine, angular, basaltic clasts. Sample from Pathé cliff measured section. Plain light.  
X15
- D. Sample 5-144: Lithic tuff. Clasts include pumice, basalt and quartz crystals. Plain light.  
X15
- E. Sample 5-302: Lapilli tuff. Quartz and sanidine phenocrysts. Collapsed pumice lapilli. Disseminated fibrous zeolite (mesolite?). Plain light.  
X15
- F. Sample 4-125: Lithic tuff. Angular basalt clasts in calcite and zeolite matrix. Sample characteristic of basaltic tuff in upper basalt unit. Plain light.  
X15
- G. Sample 5-415: Welded tuff. Collapsed pumice in a vitric groundmass. Plain light.  
X15
- H. Sample 110: Volcanic sandstone. Lithic and crystal fragments in opaline cement. Associated with abundant silicified wood on east bank of Rio San Juan at Campo de Pathé. Plain light.  
X15
- I. Sample M-118: Don Guinyo welded tuff. Zoned, resorbed plagioclase phenocrysts in brown glass. Sparse quartz crystals. Crossed polars.  
X15

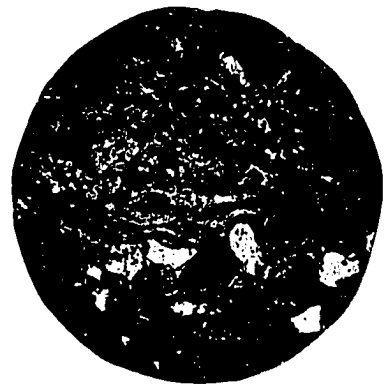
PLATE V



A



B



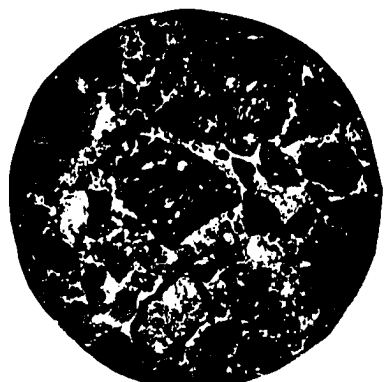
C



D



E



F



G



H



I

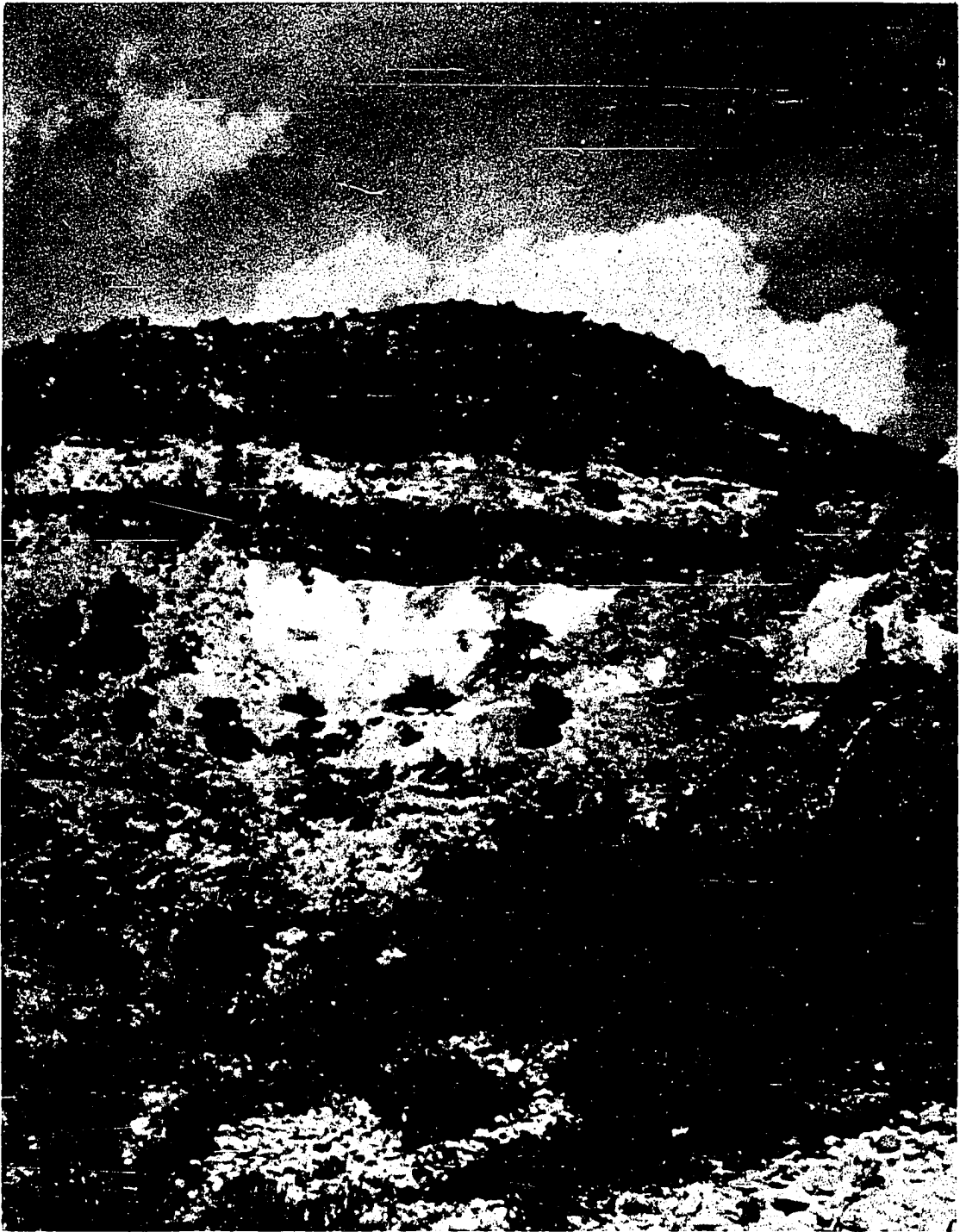


PLATE VI

PATHE' CLIFF SECTION

Photo by C. J. Mankin

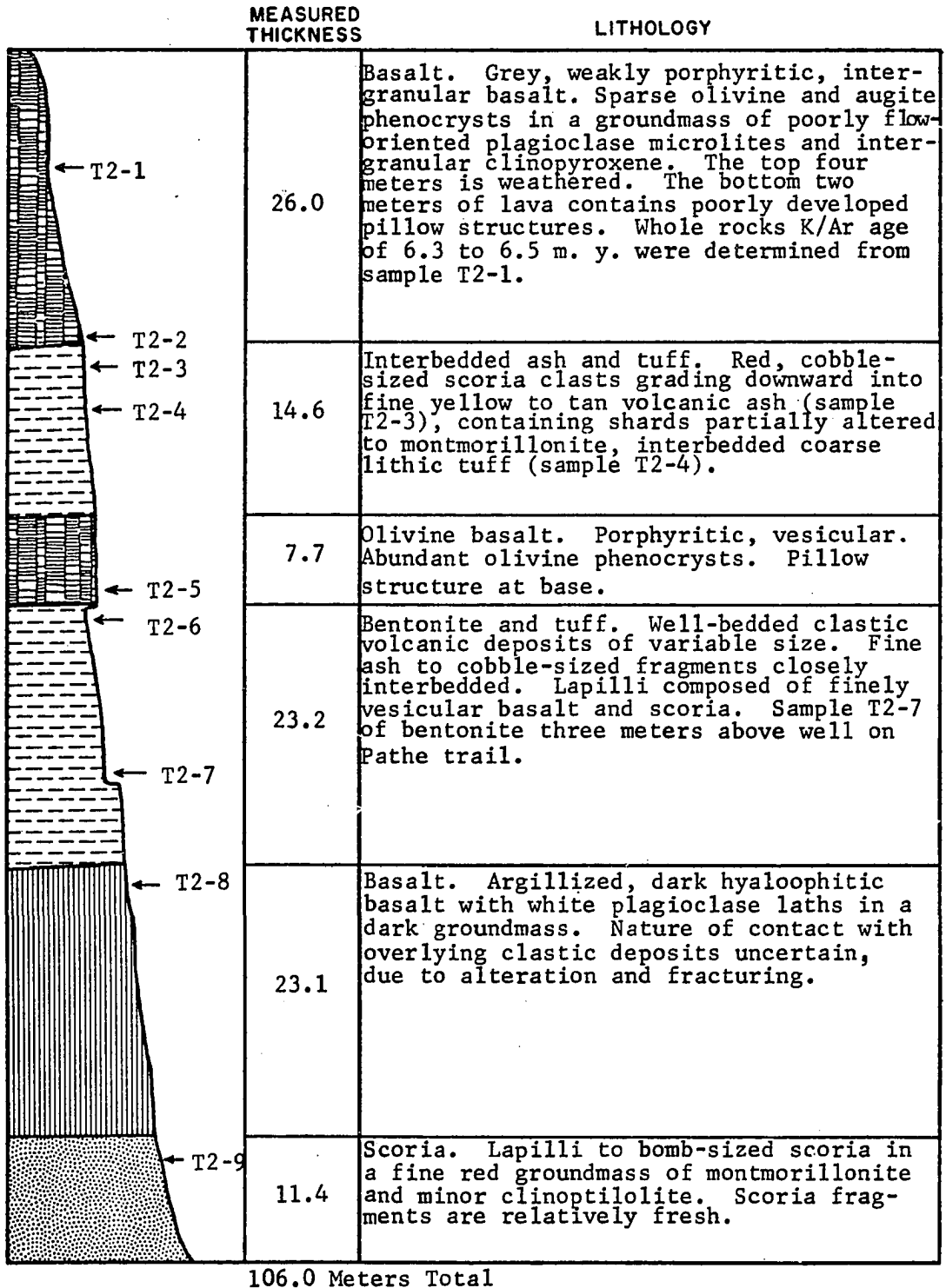


Figure 3

PATHE CLIFF MEASURED SECTION



A



B

PLATE VII  
VIEWS OF THE PATHÉ AREA

- A. Bedded pumice tuff of Pliocene age. This erosional remnant one kilometer west of the El Coh mine is preserved within a depression in the underlying basalt unit.
- B. Cerro Colorado scoria cones of probable Pliocene age. The two kilometer in diameter cluster of cones is situated four kilometers east of the Campo de Pathé.

olivine phenocrysts are commonly altered to brownish-red "iddingsite" which appears to consist of intimately mixed mica and hematite or goethite. A chemical analysis of the basalt flow which caps the fault blocks north of the Rio San Juan is included in Table 2 (Column 5).

An unusual textural feature is locally present in the lower portion of this basalt member. Extremely fine individual grains of pyroxene averaging 0.03 mm locally dominate the rock. They are crudely lath-shaped and are present in aggregates which possess optical continuity. Plagioclase microlites are present but constitute less than 50 percent of the rock and magnetite rods are common. An analysis of this basalt is included in Table 2 (Column 2).

The second major basalt type is commonly light gray with visible plagioclase laths in the glassy groundmass. Much of this basalt is coarsely vesicular or amygdular (Plate III). The spherical to distinctly elongate vesicles range from 0.5 to 2 cm in diameter. Common amygdular fillings include calcite, microcrystalline quartz, zeolites and montmorillonite. Stubby plagioclase laths averaging 2 by 0.5 mm and having a composition range of An<sub>60</sub> to An<sub>68</sub> are set in a partially devitrified tachylyte groundmass. Pyroxene and olivine phenocrysts are present but not as common as in the denser basalt member.

These glassy basalts are relatively susceptible to alteration and chlorite, calcite, clinoptilolite, nontronite, saponite, montmorillonite, sericite and biotite are present as alteration products. The cores of plagioclase laths are commonly replaced by calcite and montmorillonite in the more highly altered rocks near the fault zones.

Scoriaceous agglomerates, basaltic tuff, and volcanic ash are interstratified with the basalt flows. The scoriaceous agglomerates commonly contain cobble-size scoria fragments in a finer scoriaceous matrix. In thin section the matrix material is seen to consist of plagioclase microlites in a red-glass groundmass which is altered to clinoptilolite and montmorillonite. Dips of the agglomerate are highly variable and indicate subaerial deposition on rough erosional surfaces.

All gradations from coarse agglomerates, finer tuff-breccia, and lapilli tuff to fine volcanic ash are present. A widespread, distinctive lapilli-tuff bed consists of subrounded to angular, basaltic felsite and scoria fragments 0.25 to 1 cm in diameter closely packed in a groundmass of calcite. Individual 3 to 15 cm-thick beds of the tuff display graded bedding. Beds of bentonitic ash with a thickness of 1 to 2 m underlie the basalt lavas which cap the higher hills in the Pathé zone. They weather to a yellow color and are readily distinguishable from the reddish-brown, scoriaceous beds which commonly form vertical cliffs in the deeper canyons.

A large, dissected, scoriaceous cinder cone of Pliocene (?) age is situated on the south bank of the Rio San Juan immediately north of Tecozautla. In the area south of this cone, known locally as Cerro Colorado, there are crudely linear trends of scoria present within the valley of the Rio San Francisco. The east-west trending scoria appears to coincide with regional fractures present beneath the Recent fluvial cover. The slopes of Cerro Colorado as well as the scoria fields in the river valley contain red to purple scoriaceous bombs in a highly-altered, reddish-brown, glassy groundmass which is finely vesicular. Clinoptilolite,

montmorillonite, and calcite are present both as amygdular fillings and alteration products of the glassy groundmass. The composition of the plagioclase microlites in the groundmass was not determined, but the rock has an average basaltic composition (Table 2, Column 4). The cone appears to be younger than the basaltic cap rock of the surrounding hills but its highly dissected state indicates an age not younger than Pliocene. Similar scoria interbedded with the upper flows of the olivine-basalt unit indicates a close temporal relationship with the basalt unit.

The sequence of basalt and interbedded pyroclastic rocks has a total measured thickness of 400 m within the central-graben zone. The unit thins to 200 m over the uplifted fault blocks just north of the Rio San Juan (wells 8, 10 and 11). A measured section of the upper, predominantly pyroclastic portion of the unit is described in Figure 5 and shown in Plate VI. A probable source of the basaltic flows which cap the tilted fault blocks north of the Rio San Juan is a 200 m high basaltic hill four kilometers north of the village of Pathé.

Pumice Tuff Unit. A sequence of coarse pumice tuffs interbedded with siltstones and mudstones overlies the lavas and tuffs of the olivine basalt unit in the valley of the Rio San Francisco. A well-indurated upper portion of the unit forms the rimrock south and southwest of Tecozautla and west and northwest of Huichipan. North of the Rio San Francisco, the pumice tuff is locally preserved within depressions on the surface of the underlying basalt. According to Mooser (personal communication, 1970) the source of the pumice tuff is the Cerro Nado Caldera 20 km southwest of San Juan del Rio.

The pumice tuff is readily distinguishable from the underlying basaltic tuffs by its coarse (1 to 5 m diameter) cellular pumice fragments, generally unaltered, uncemented condition, and higher silt content. The pumice tuff unit was not dated radiometrically, but a Pliocene age is required because it overlies the basalts and underlies the Don Guinyo tuff, both of Pliocene age.

Don Guinyo Tuff. An extensive welded tuff unit extends from the vicinity of Ixmiquilpan, Hidalgo, to within 7 km southeast of Tecozautla and 2 km east of Huichapan, where it overlies the pumice tuff unit. The stratigraphic position and age of the Don Guinyo tuff is relevant to the present study as it provides a link between the Pathé volcanic sequence and the extensively studied but radiometrically undated Pachuca volcanic series (Segerstrom, 1962). The type locality and lithology of this unit are described by Segerstrom as follows: (Seegerstrom, 1962, pp. 113-114)

Well-indurated andesite or dacite tuff and breccia with horizontal lenses of black glass (welded tuff or ignimbrite) cover extensive areas along the highway between Ixmiquilpan and Huichapan north of Golondrinas and in the vicinity of Tula. The name Don Guinyo is here proposed for this tuff which appears to have been deposited on an irregular erosion surface. The type locality is near a high bridge that crosses Arroyo de Don Guinyo between Ixmiquilpan and Huichapan; it furnishes good hand specimens of welded tuff. Under the microscope the tuff shows excellent collapsed pumice texture, plagioclase of about  $Ab_{30}$  is abundant and orthopyroxene is also fairly abundant. This rock is probably low-silica dacite and is close to andesite. . . . Several welded tuff layers, each a few meters thick, are interbedded with other pyroclastic beds to a total thickness of about 170 m at the base of Cerro Xicuco and along Arroyo de Don Guinyo.

A chemical analysis of a sample collected from the type locality at the west side of the road at the northwest end of the bridge reveals a dacite composition (Table 2, Column 6). Plagioclase K/Ar determinations

of this same sample yielded the youngest dates obtained in the present investigation ( $4.2 \pm 0.3$  m. y. and  $4.3 \pm 0.3$  m. y.).

#### Intrusive Volcanic Rocks of Pliocene Age

Rhyolite Porphyry Unit. Two parallel hills one kilometer south of the main geothermal zone constitute the exposures of the rhyolite porphyry unit. Sanidine separated from a sample from the northern hill yielded K/Ar dates of  $6.6 \pm 0.1$  m. y. and  $6.7 \pm 0.1$  m. y. (M-25), the oldest dates obtained from the Pathé samples.

The hills appear to be the northern and southern flanks of a downfaulted rhyolite dome. The rhyolite exposed on the more gentle northern slope of the northernmost hill (Cerro Peligroso) is extensively argillized but is overlain by relatively fresh basaltic tuff. A regolith developed on the flanks of the dome has been preserved beneath the basalt unit.

In hand specimen the rhyolite porphyry is light pink to white; weathered specimens are chalky. Quartz phenocrysts from one to four mm in diameter distinguish the porphyritic rhyolite from any other rock unit which crops out in the Pathé area.

In thin section, the unit is seen to consist of euhedral to subhedral, bipyramidal quartz and sanidine phenocrysts in a partially devitrified groundmass, which varies from slightly to strongly spherulitic (Plate V). Scattered microlites of sanidine are present in the glassy matrix. The chemical analysis of the unit reveals an exceptionally high  $\text{SiO}_2$  content, 78 percent (Table 2, Column 12).

A similar texture was observed in thin sections of extensive kaolinitized rhyolite encountered at a depth of 15 m in the El Coh mine.

At this location the nature of the rhyolite porphyry cannot be determined due to the extensive argillation and cover by overlying tuff beds.

Rhyolite Felsite Dikes. A one-meter-wide, near-vertical dike of felsite trending north 20° east is exposed in the saddle at the north end of the central graben zone. Similar felsite caps the southern slope of the hill immediately south of the central drilling zone. The felsite locally displays purple, yellow, and brown banding of the "wonderstone" type (Plate III). Much of the rock is dark reddish-brown. In thin section the rock appears to be cryptocrystalline; scattered quartz grains are the only recognizable mineral constituents. The fresh felsite is generally more vitric, whereas the altered rock assumes a light pink color and a tripolitic texture.

Outcrops of felsite are limited to the dike and flow rocks on the surface of the southwestern dipping fault block which forms the southern wall of the main geothermal area. Felsite is absent from the highest point of the hill (the northwest corner) but thickens to the southwest along the trend of the dike. The unit has a maximum exposed thickness of three meters at the southern limit of its exposure at the point where the "La Mesa" trail crosses the Rio San Francisco.

The basaltic tuff section underlying the rhyolite has been silicified to the extent that the two are readily differentiated only by the occasional presence of relic clastic texture in the altered tuff. A chemical analysis of the felsite (Table 2, Column 11) indicates a rhyolite composition with an  $\text{SiO}_2$  content of 78.2 percent and 6.09 percent  $\text{K}_2\text{O}$ . An analysis of the silicified tuff from the fault zone (Table 2,

Column 14) reveals an even higher  $\text{SiO}_2$  content (83.6 percent) but a low  $\text{K}_2\text{O}$  content (1.02 percent) indicating the addition of  $\text{SiO}_2$  and the leaching of  $\text{K}_2\text{O}$ .

#### Recent Fluvial Deposits

Fluvial deposits of an unusual character are present along both the Rio San Juan and the Rio San Francisco within the geothermal zone. The present channels of both rivers contain cobble-size volcanic rock fragments cemented by siliceous sinter at a point where the main fault zone crosses the river channel. A one-meter-high waterfall immediately downstream from the crossing of the Rio San Juan marks the downstream edge of the fault zone and the silicification. The same type of siliceous sinter "pavement" caps an older terrace level 50 m downstream from the present river crossing and 5 m above the present river channel.

Siliceous sinter covers the fan-shaped area extending from the sites of former thermal springs and fumaroles (de Anda, et al., 1961), near the center of the graben area to the east bank of the Rio San Juan. The sinter beds along the Rio San Juan contain abundant silicified wood and cactus. Associated with the silicified wood is a volcanic lithiarenite which contains well-sorted angular fragments of the dominant volcanic rock types of the area (basalts, andesites and rhyolites) in a siliceous groundmass (Plate V). Similar silica-cemented arenites are present along the trend of the fault zone responsible for the erosional cut through "La Mesa." Their silicification indicates that the past geyser activity included this now-cooled portion of the fault system.

### Origin of the Pathé Volcanic Sequence

The rocks of the Pathé geothermal field display a lithologic variability which is characteristic of the basalt-andesite-rhyolite volcanic association of orogenic regions (Turner and Verhoogan, 1960, p. 272). Other investigations within the states of Queretaro and Hidalgo have revealed a similar association which is generally characteristic of the entire Tertiary volcanic belt of the Mexican central highlands. The San Juan volcanic field of Colorado and New Mexico represents the northernmost extension of the belt. The volcanic rocks of the San Juan area have been erupted throughout a radiometrically dated period of at least 23.5 m. y. (Lipman, 1969). This also appears to have been the approximate time span of the Tertiary volcanic belt of Mexico. The oldest flows of the Pachuca group in the Pachuca-Monte de Real district are of probable Eocene or Early Oligocene age (Geyne, et al., 1963).

Previous investigators of Mexican Tertiary and Quaternary volcanism (de Cserna, 1961; Geyne, et al., 1963) have noted that rhyolitic to andesitic compositions are characteristic of the Tertiary volcanic belt. Olivine basalts are considered more typical of the generally east-west trending Neo-volcanic belt. The present investigation and those of adjoining areas (Seegerstrom, 1961 and 1962) have revealed that the above generalization must be applied with caution, as lithologies as diverse as olivine basalt and rhyolitic tuff are often interstratified.

Wise (1969) concluded from a study of the Mt. Hood area in the Cascade Range that there has been repeated generation of olivine basalt and subsequent differentiation to andesites throughout much of Cenozoic

time. Some differentiation on this scale (basalt → basaltic andesites) may have occurred at Pathé, but the vast bulk of rhyolitic material seems to necessitate two separate sources of magma generation, one in the upper mantle, the other in the crust. Tectonic events which accompanied the generation of magma with rhyolitic to intermediate composition in Oligocene and Miocene time were also accompanied by basalt-producing processes in Pliocene time.

## STRUCTURE

### Regional Structural Setting

The Pathé geothermal field is situated on the northern margin of a volcanic belt of probable Pliocene to Recent age which traverses Mexico from northwest to southeast (Trans-Mexico Volcanic Belt). Pathé also lies within the Tertiary volcanic belt near its junction with the Sierra Madre Oriental (Plate I). During the Laramide Orogeny (Late Cretaceous to Late Eocene time) the Mesozoic sedimentary rocks of the region were folded and locally overthrust to the northeast. The intense folding involves principally the Las Trancas and El Doctor formations exposed in the mountainous regions to the north and east of Pathé and possibly underlying the Pathé zone. The major folds of the region such as the San Lorenzo syncline and El Chilar anticline characteristically are complex with numerous smaller folds superimposed on the major structure (Segerstrom, 1961). The Las Trancas formation of Jurassic age is characteristic of the outcrops of major anticlinal trends and the Mexcala formation of Upper Cretaceous age is indicative of a synclinal trough. This series of southeast trending anticlines and synclines probably continues into the Pathé geothermal area under the Cenozoic cover (Plate I). One of the structures, the San Lorenzo syncline, can be traced for a distance of 105 km to the southwest

(Segerstrom, 1961, p. 61-62). This syncline is expressed topographically as a low which passes 14 km east of Pathé. The axis of a small anticline seven kilometers to the west of this syncline is shown on a map of the region of south-central Hidalgo and northeastern Mexico (Segerstrom, 1962) trending toward the town of Tecozautla. If this trend continues beneath the Cenozoic cover, the anticlinal axis passes approximately six or seven kilometers east of the Pathé zone.

Faulting associated with early Tertiary folding of the Cretaceous and Triassic sedimentary rocks is dominantly normal and the strikes of the faults parallel the axial trends of the folds. Tectonic activity immediately preceding or accompanying the Tertiary volcanism in central Mexico and the southwestern United States is characteristically of the "Basin and Range" type. Normal faulting with attendant graben and horst development has been reported in the San Juan field (Wise, 1969) and the Pachuca district (Geyne *et al.*, 1963).

An east-west trending fault zone of regional extent bounded by Pathé on the north and Tecozautla on the south passes through the Pathé zone. According to Mooser (1968, personal communication) this zone is part of a fracture zone which parallels the axis of the Trans-Mexico Volcanic Belt. Mooser (1967) mapped the Quaternary cones and faults associated with this belt at a scale of 1:50,000. He describes the Trans-Mexico Volcanic Belt as (p. 102):

. . . an intermittent zone of crustal fracturing, varying in width and extending from the southern Gulf of California straight through the continent to southeastern Mexico, at which point, however, it does not link up with the Guatemalan Volcanic Belt. East and west of the Tuxtla volcanoes the belt is interrupted, probably due to the presence of great thicknesses of

marine sediments, which owing to their plasticity and weight prevent dikes from rising to the surface. The new map also proves that Colima, Tancitaro and Popocatepetl volcanoes do not belong to a continental prolongation of the marine Clarion Fracture Zone, as previously supposed, but that these structures grew on separate side branches of the main belt.

Mooser, Nairn and Noltimier (1970) have recently theorized that the Trans-Mexico Volcanic Belt represents the sub-continental path of a branch of the East Pacific Rise. Additional geologic investigations of the volcanic belt including age determinations by radiometric and paleomagnetic dating, gravity surveys, and chemical and petrographic analyses of the volcanic sequence, have been initiated by these authors.

H. Espinosa et al. (1964) compiled a list of approximately 100 thermal springs in Mexico; most of these lie within or adjacent to the volcanic belt as mapped by Mooser thereby implying a genetic relationship between the volcanic belt and the geothermal springs.

#### Structure of the Pathe' Geothermal Field

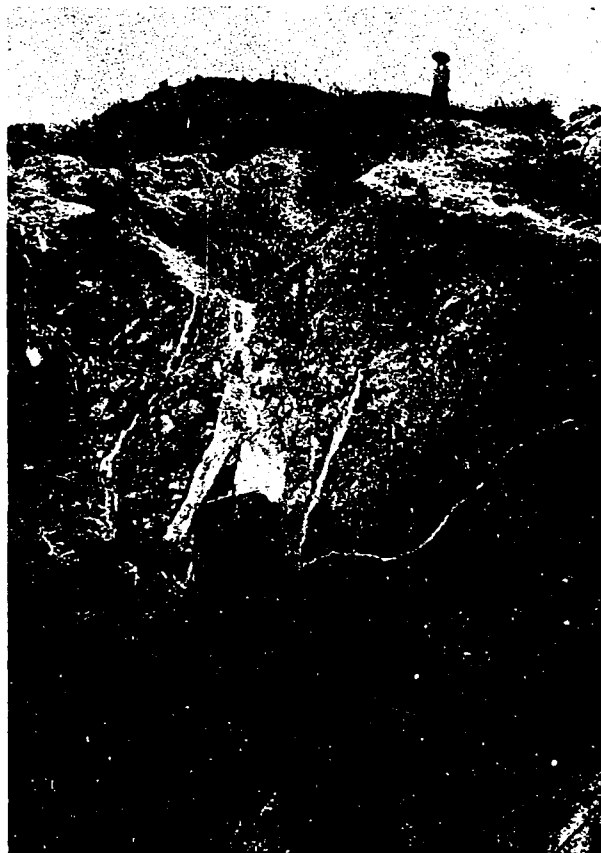
The Pathe' volcanic sequence is a generally east-west trending volcanic "embayment" extending into the Sierra Madre Oriental to the east at a point where the structural trend of the folds changes from northwest-southeast to north-south (Plate I). The northern margin of this volcanic extension is along an east-west line passing through Bernal, Zimapan, and continuing on 35 km to the east.

The volcanic rocks capping the region along the Rio San Francisco and the Rio San Juan have been block faulted by two sets of normal faults at approximately right angles (Plate II). One set of faults trends north-south, and the individual faults are more or less regularly spaced at intervals of 1.5 km. The individual blocks north of

the Rio San Juan are tilted to the southeast. The north-south faults are high-angle faults with dips at the surface of  $85^{\circ}$  to  $90^{\circ}$ . At one fault intersection one and one-half kilometers east of the main Pathé fault, a left-lateral, strikeslip component of movement of three or four meters is indicated by horizontal slickensides and the slight displacement of the older east-west trending fractures. Vertical displacement appears to be only 10-20 m at the surface but increases with depth to a maximum of 180 m as indicated by the displacement in the cores of the rhyolite unit. The faults may be traced for a distance of eight to ten kilometers north of the Rio San Juan. Near the point of their disappearance the drainage patterns assume a northwest-southeast orientation paralleling the shallow Cretaceous structures.

The principal north-south fault through the Pathé field is herein referred to as the Pathé fault (Plate VIII). Within the steam-producing zone there are two additional north-south trending, closely-spaced faults. The westernmost (referred to herein as the La Mesa fault) may be traced through the pumice tuff deposits and across La Mesa, three kilometers to the south. Fault movement continuing at least through Pliocene time is thus inferred.

The east-west striking set of normal faults has produced a series of grabens and horsts as illustrated in Plate II. The low-water ford of the Rio San Juan is situated on the major horst of the series, which separates the main graben of the steam-producing zone to the south from a smaller graben to the north. The top of the upper rhyolite unit is displaced 20 m downward in the northern graben and 180 m in the steam-producing area to the south. The wedge-shaped area of maximum



A



B

PLATE VIII  
VIEWS OF THE MAIN FISSURE, PATHÉ FAULT

- A. Collapsed mine entrance above present Tizpathe mine. The montmorillonite-zeolite-quartz vein widens at depth. Wallrock is silicified basaltic tuff.
- B. View north along Pathé fault. Entrance to Tizpathe mine is near middle of picture. Generator plant directly overlies the fault which may be traced 12 km north past mountain on horizon.

subsidence is bounded by the Pathé fault on the east and the La Mesa fault to the west. The southern margin of the down-dropped block is an east-west trending fault which parallels the southern flank of Cerro Grande.

An additional east-west trending graben is present south of the geothermal zone in the valley of the Rio San Francisco. The structure is indicated by the downfaulting of the central portion of a rhyolite dome producing two subparallel hills from the northern and southern flanks of the dome. Pliocene tuffs and alluvium are present at the surface of the graben, which has not been explored for possible steam production by drilling.

The entire Pathé zone may also lie on the eastern margin of a larger north-south trending graben. The principal north-south trending faults such as the Pathé fault are downthrown to the west. At distances greater than six kilometers west of the Pathé fault, the north-south faults are downthrown to the east (Plate I).

All of the fault blocks and superimposed clastic volcanic deposits of Pliocene age south of the Rio San Juan dip  $5^{\circ}$  to  $15^{\circ}$  to the south. These dips are constant over the individual fault blocks and are readily distinguishable from the highly variable dips displayed by volcanic units with primary dips. Primary dip angles of up to  $40^{\circ}$  were measured on beds of a scoriaceous flow-breccia underlying the olivine basalt. Dip angles of  $10^{\circ}$  to  $30^{\circ}$  were measured on the highly fractured basalt and scoriaceous agglomerate flows of the northwest slope of Cerro Grande, which appears to be a small eruption center (Plate VII).

Closely spaced jointing is well developed within the fracture zones. Numerous small, east-west trending normal faults with vertical displacements of less than five meters are present throughout the Pathé zone. Their strikes may be traced across the surfaces of the basalt blocks by the closely spaced jointing and fracturing which produced "flagstone" shaped individual fragments.

#### Structural Control of the Steam Distribution

Faults serve a dual function in the operation of major conventional geothermal systems. They provide a path for the lateral and downward circulation of relatively cool, dense, surface water to the contact zone with heated rocks. Faults also provide the channels for the upward migration of the heated, lighter fluids through otherwise impermeable strata. This structural control of steam distribution has been well established by the drilling and clay mining in the Pathé geothermal area.

At Pathé, steam is present within a relatively limited portion of the main Pathé fault and two of its branches. The presence or absence of steam within a particular segment of the fault zone may be determined by a direct examination of the fissure. This unusual opportunity to observe the internal plumbing of a geothermal system is permitted by the continuous clay mines which follow the fault zones (Plate VIII). Clay mines within the central steam producing zone are all "hot" mines. Because of the heat escaping from the clay-bearing fissures the mines can be worked only at night and in the early morning hours. At the time of this investigation (January, 1968) steam was escaping into one mine (the Tizpathe) at a depth of approximately 30 m below the valley floor.

Mines directly north of the Rio San Juan (the Santa Rosa) and south of the Cerro Grande fault (El Carmen) are warm but not unbearably hot. These warm, inactive mines are presently occupied during daylight hours by thousands of bats. The Pathé cemetery to the north and the Rio San Francisco to the south mark the limits of hydrothermal alteration along the main Pathé fault zone. A second smaller, less obvious, steam-bearing fault lies 30 m west of and parallel to the main fault. Its surface expression is now obscured, but its trace is obvious in aerial photographs which predate the drilling activity.

Observations within the mines explain some of the difficulties encountered during attempts to produce steam from the main fault. The steam-bearing fissures are remarkably narrow (ordinarily one meter wide or less) and tend to be self sealing. At the relatively shallow depths penetrated by mining (less than 100 m) the fissures are clogged by secondary minerals and only narrow "chimneys" are presently steam-bearing at shallow depths.

East-west cross-faulting has served to localize the steam at other areas of less intense past or present geothermal activity to the east and west of the Pathé fault. One and one-half kilometers west of the Pathé field a large open pit kaolin mine known as "El Coh" is situated within a fault-bounded block at the intersection of major east-west and north-south faults (Plate I). East of the Pathé fault, the intersections of north-south faults with the Cerro Grande fault are marked by warm springs such as those at the Banos de Tashido. The Cerro Grande fault may be the deep "feeder fault" for the thermal system. The near-surface movement of steam and heated water is

localized at the intersections of east-west faults and north-south faults which have been more recently active.

## MINERALOGY AND DISTRIBUTION OF THE ALTERATION PRODUCTS

### Sampling Procedures

Samples of both fresh and altered rocks were collected for an evaluation of the mineralogical and chemical changes which accompany the hydrothermal alteration in the Pathe' thermal area. Sixteen samples were collected from two traverses in the vicinity of well 3 for a comparison of the lithology and alteration product mineralogy on the east and west sides of La Mesa fault (Fig. 2). Well 3 is in the bottom of an arroyo with steep slopes rising to the southeast and southwest. The lower portions of the slopes are covered by slumping bentonite but undisturbed samples of basaltic tuff were obtained by digging to a depth of approximately one-half meter. One of the traverses extends from a cement claim marker in the rhyolite cap rock of the hill on the east 55 m to the bottom of the arroyo. The second traverse extends southwest 150 m from well 3 to the volcanic conglomerate caprock of the hill to the southwest.

Wall rock samples were also collected from the two kilometer-long argillized portion of the Pathe' fault as permitted by accessible portions of the El Carmen, El Carmen #2, Santa Rosa and Tizpathe mines. Six samples were collected for an examination of possible zoning of the wall rock alteration from a 38 m long traverse perpendicular to the Pathe' fault at the El Carmen mine (Fig. 2). A total of 120 surface and

clay-mine samples were collected including three "hot samples" which were collected from active steam-producing vents.

Sampling at the El Coh mine consisted of samples one to three kilograms in weight selected to represent obvious variations in the degree of alteration or lithology. Vertical sampling of the east walls of the open pit was designed to determine vertical mineralogical and chemical variations with respect to the present soil zone (Plate IX).

Ninety core samples were collected from the 1600 m of excellent two and one-half inch diameter cores obtained during the exploration program (1956-1960). The locations of the wells cored (wells 4, 5, 8, 9, and 11) are shown in Figure 2. These cores were generously made available for study at the Pathé drilling camp by the Comisión Federal de Electricidad and were examined and described by the author at the Pathé camp. Ninety samples of the cores were selected as representative of the lithology and alteration; these were then transported to the laboratory of the Consejo de Recursos Naturales No Renovables, Mexico City, for preliminary x-ray diffraction analysis and preparation of thinsections. At the completion of the field phase of the investigation, the samples were shipped to the X-ray Laboratory, School of Geology and Geophysics, University of Oklahoma, for additional laboratory analysis.

#### Analytical Techniques

The samples were first hand ground in an agate mortar to pass a 200 mesh screen. Splits of the samples were then utilized to obtain bulk powder x-ray diffractograms and diffractograms of oriented



A



B

PLATE IX  
EL COH MINE

- A. Small, east-west trending apparent reverse fault, east wall of El Coh mine. Bedded clastic volcanic deposits of variable composition and size altered to kaolinite which grades downward into montmorillonite.
- B. South wall of El Coh mine. Workings on this face have been abandoned due to slides. Note the north-south trending normal fault.

sedimented slides if phyllosilicate minerals were believed present. The oriented slides were routinely subjected to solvation with ethylene glycol as a measure of the expandability of 14 A clay minerals. Selected samples were heat treated to 600° C for one-half hour as a test for the presence of chlorite. Quantitative chemical analyses by x-ray fluorescence were performed on splits of thirty samples utilizing a Siemens-Halske Sequential X-ray Fluorescence Spectrometer. Scanning electron microscopy was utilized as a supplement to thinsection petrography in examining mineralogical and textural relationships at magnifications greater than 150 x. The accompanying electron micrographs were obtained with a JOELCO Model JSM2 scanning electron microscope housed in the X-ray and Electron Microscopy laboratory of the School of Geology and Geophysics, University of Oklahoma and operated by Mrs. Linda Hare. Detailed sample preparation techniques and the analytical procedures utilized for the x-ray diffraction analysis, differential thermal analysis, scanning electron microscopy, and quantitative x-ray fluorescence analysis are contained in Appendix A. Sample descriptions are given in Appendix B.

#### Deuteric Alteration and Chemical Weathering

Samples of basaltic lavas collected at distances greater than 20 to 50 m from major fractures are relatively "fresh". The only alteration commonly observed is the conversion of the outer rim of euhedral olivine phenocrysts to "iddingsite" (Plate IV). "Iddingsite" consists of goethite-or hematite-stained montmorillonite and is generally of deuteric origin (Deer, Howie and Zussman, 1962, Vol. 1). There is evidence

at Pathé, however, that the same process may be accomplished during an early stage of hydrothermal alteration of the olivine basalts (Plate X).

Samples of scoria collected from Cerro Colorado, the "badlands" at Rancho San Juanita, Cerro Grande, and an unnamed hill one-half kilometer south of Rancho El Chilar (Fig. 2) all indicate the ubiquitous formation of clinoptilolite and montmorillonite. They are present both as alteration products of the hematite-stained glassy groundmass and as amygdular fillings. The basic ash and tuff beds likewise contain montmorillonite and clinoptilolite or calcite as devitrification products regardless of their proximity to fault zones. Discrete clay particles were not recognized in a scanning electron microscope study of a weathered basic ash (Plate XIA) although the presence of montmorillonite was indicated by x-ray diffraction. By way of contrast, the hydrothermal montmorillonite associated with the steam-bearing fissures has a larger particle size and is easily recognized at relatively low magnifications (Plate XII).

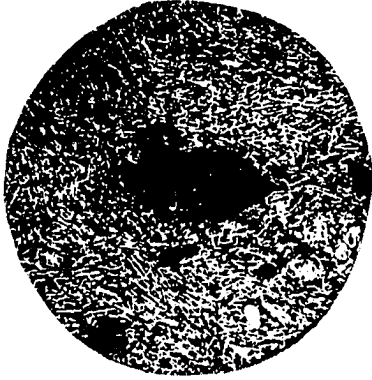
The weathering of rhyolite porphyry to montmorillonite was observed on the north slope of Cerro Peligroso. Relatively fresh quartz and sanidine phenocrysts are in a vitric groundmass which has been partially altered to montmorillonite. Weathering is assumed to be the altering process, as the argillation is a surface feature of the unfaulted portion of the rhyolite dome. The presence of a regolith is supported by the unaltered state of the overlying basaltic tuffs which are in direct contact with the altered rhyolite. The rhyolite at the west end of Cerro Peligroso locally displays silicification

## Plate X

## PHOTOMICROGRAPHS OF ALTERATION PRODUCTS

- A. M-19: Basalt. "Iddingsite" alteration of olivine phenocryst. Note flow-oriented plagioclase microlites. Plain light. Sample collected 11 m east of Pathé fault at Cerro Grande.  
X15
- B. M-19A: Argillized basalt. Extensive montmorillonite development as fracture filling and replacement of basalt. Sample collected 10 m east of Pathé fault at Cerro Grande. Plain light.  
X15
- C. M-69: Amygdular basalt. Note internal alteration of plagioclase laths to montmorillonite and calcite. Tachylyte matrix. Crossed polars.  
X15
- D. 8-69: Argillized basalt. Mordenite (fibers), montmorillonite and clinoptilolite. Crossed polars.  
X15
- E. M-7: Vein deposit, Tizpathe mine. Boxwork of earlier-formed chalcedony and euhedral quartz. Minor montmorillonite and stilbite. Crossed polars.  
X15
- F. M-13: Kaolinized rhyolite tuff, El Coh mine. Fractured sanidine and quartz phenocrysts in a kaolinite matrix. Crossed polars.  
X15

PLATE X



A



B



C



D



E



F

## Plate XI

## SCANNING ELECTRON MICROGRAPHS OF ALTERATION PRODUCTS

- A. T2-3: Volcanic ash. Montmorillonite and clinoptilolite are indicated by x-ray diffraction but discrete clay particles were not recognized in electron micrographs. Elongate structures are individual glass shards.  
X800
- B. M-38: Amygdular basalt. Arcuate montmorillonite flakes are enclosed by stilbite in the interior of an amygdule.  
X1600
- C. 5-498: Zeolitized scoria. Laumontite (upper right) developed as an alteration product of scoria.  
X500
- D. M-13: Kaolinized rhyolite tuff. Kaolinite developed by near-surface acid leaching of rhyolite tuff. The rounding of the kaolinite flakes and the association of minor montmorillonite indicate that the kaolinite may not be stable under present chemical conditions.  
X3000

PLATE XI



A



B



C



D

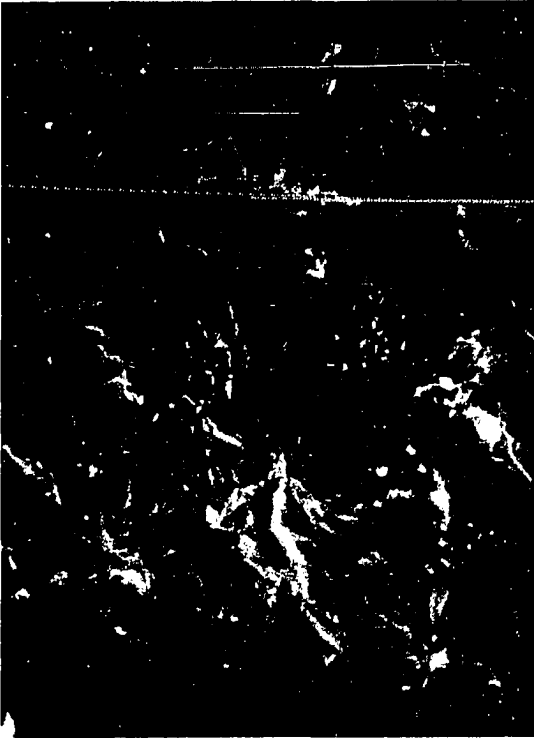
## Plate XII

## SCANNING ELECTRON MICROGRAPHS OF CLAY

The accompanying electron micrographs were obtained from samples of the Pathé montmorillonite collected at the Tizpathe mine.

- A. M-8: Montmorillonite spherulites. Curling of clay flakes is produced by dehydration during sample coating in a vacuum.  
X1000
- B. M-8: Montmorillonite and stilbite. Note porous nature of sample and preferred orientation of clay flakes.  
X2700
- C. M-7: Stilbite. Fibers are intimately associated with montmorillonite. Production of fibers by the fraying of coarser laths was observed.  
X3000
- D. M-8: Montmorillonite. Individual flakes are curled yielding a "flame" texture. Note the thin flake which has partially broken loose from the substratum and formed a scroll.  
X16,500

PLATE XII



A



B



C



D

superimposed on the weathering. Hand specimens of rhyolite collected there contain an argillized, chalky interior and a thin surficial veneer of silica apparently produced by thermal solutions.

### Wallrock Alteration

#### El Carmen Mine

An inclined access tunnel at the El Carmen mine provides an excellent opportunity to observe lateral variations in the chemistry and mineralogy perpendicular to the Pathé fault within a basaltic tuff sequence. The 38 m long, east-west trending tunnel is cut entirely within basaltic tuff, which crops out south of the Sierra Grande fault and east of the Pathé fault. On the west side of the Pathé fault at the El Carmen mine, silicified tuff one to three meters in thickness covers the basaltic tuff. The relatively unaltered tuff at the entrance to the shaft (east end) is weathered, but coarse, dark basalt fragments are clearly visible in a lighter matrix. As the north-south trending main fracture is approached, the tuff changes to light green and minor disseminated pyrite appears. At a horizontal distance of 10 m from the fracture, the rock is compact in contrast with the friable nature of the unaltered tuff, and the clastic texture is no longer visible. The altered wallrock within five meters of the vein is a silicified, dark-green, pyrite-rich clay.

Mineralogical variation within the sequence as revealed by x-ray diffraction analysis is shown in Figure 4 and the chemical analyses are included in Table 3 (Cols. 8, 9, 10, and 11). Weathering of the basaltic tuff has produced dioctahedral montmorillonite and calcite

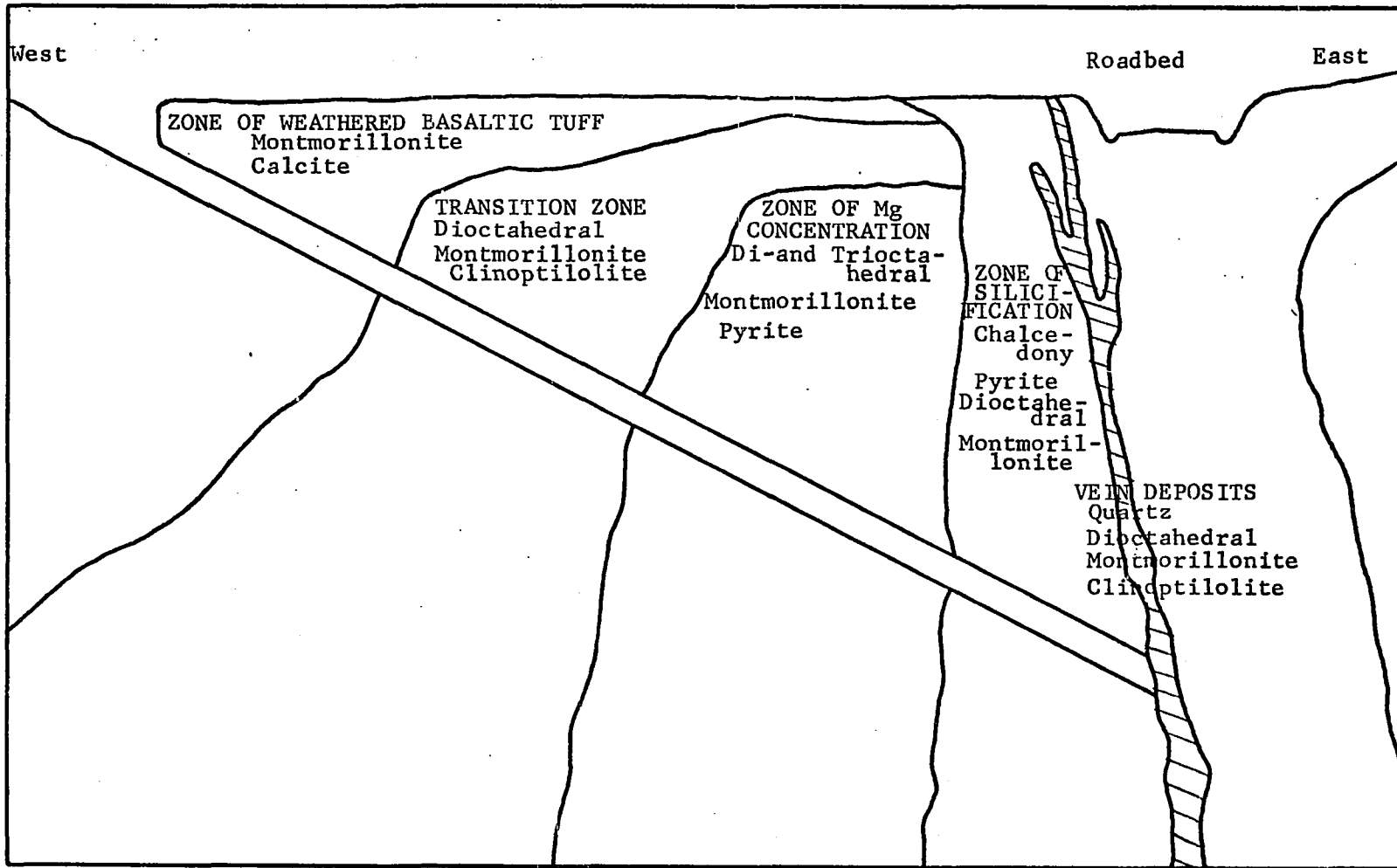


Figure 4

MINERALOGICAL VARIATION: EL CARMEN MINE

TABLE 3

CHEMICAL ANALYSES BY X-RAY FLUORESCENCE OF ALTERAT

|                                | 1 †<br>24 | 2<br>M-8 | 3<br>M-54<br>Bulk | 4<br>M-54<br><14 | 5<br>M-48 | 6<br>M-108 | 7<br>M-109 | 8<br>M-61 | 9<br>M-62 | 10<br>M-63 | 11<br>M-65 | 12<br>M-85 | M  |
|--------------------------------|-----------|----------|-------------------|------------------|-----------|------------|------------|-----------|-----------|------------|------------|------------|----|
| SiO <sub>2</sub>               | 51.5      | 54.5     | 48.9              | 50.6             | 52.7      | 47.7       | 59.7       | 41.2      | 45.7      | 46.6       | 61.6       | 50.2       | 4  |
| Al <sub>2</sub> O <sub>3</sub> | 19.44     | 20.7     | 21.3              | 21.9             | 16.4      | 19.4       | 26.2       | 9.9       | 10.6      | 12.2       | 14.2       | 8.8        | 36 |
| Fe <sub>2</sub> O <sub>3</sub> | .10       | ND       | ND                | ND               | 0.53      | 5.41       | 2.04       | 7.59      | 7.37      | 5.76       | ND         | 6.56       | 2  |
| MgO                            | 5.07      | 5.45     | 6.50              | 6.82             | 8.45      | 3.74       | 0.11       | 12.9      | 11.05     | 15.0       | 8.13       | 22.0       | 0  |
| CaO                            | .48       | 2.53     | 1.08              | 1.15             | 2.65      | 1.08       | ND         | 5.21      | 0.90      | 1.62       | 0.63       | 0.20       | 0  |
| Na <sub>2</sub> O              | .20       | 0.43     | 0.09              | 0.23             | 0.06      | 0.16       | 0.36       | 0.21      | 0.13      | ND         | 0.11       | 0.07       | 0  |
| K <sub>2</sub> O               | -         | 0.07     | 0.05              | 0.05             | 0.10      | 0.07       | 0.02       | 1.18      | 1.00      | 0.78       | 0.11       | 0.90       | 0  |
| TiO <sub>2</sub>               | -         | 0.02     | ND                | ND               | 0.03      | 2.03       | 0.33       | 0.78      | 0.87      | 0.92       | ND         | 0.72       | 3  |
| MnO                            | -         | 0.02     | 0.01              | 0.01             | Tr        | 0.03       | Tr         | 0.08      | 0.03      | 0.12       | 0.01       | 0.16       |    |
| P <sub>2</sub> O <sub>5</sub>  | -         | 0.08     | 0.07              | 0.06             | 0.07      | 0.21       | 0.04       | 0.18      | 0.12      | 0.14       | 0.05       | 0.10       | 0  |
| S                              | -         | 0.09     | ND                | ND               | ND        | 1.49       | 0.95       | 0.07      | 0.16      | 2.24       | 0.13       | 1.37       | 0  |
| H <sub>2</sub> O <sup>†*</sup> | 8.04      | 4.91     | 7.80              | 8.20             | 5.40      | 7.01       | 9.95       | 11.23     | 8.54      | 6.76       | 8.07       | 5.83       | 12 |
| H <sub>2</sub> O <sup>-</sup>  | 14.50     | 11.20    | 14.20             | 11.00            | 13.60     | 11.60      | 0.30       | 9.40      | 13.50     | 7.80       | 6.90       | 3.60       | 1  |
| Totals**                       | 99.33     | 100.01   | 100.00            | 100.02           | 99.99     | 99.93      | 100.00     | 99.93     | 99.97     | 99.94      | 99.94      | 100.51     | 99 |

\*H<sub>2</sub>O<sup>†</sup> is ignition loss at 1000° C adjusted for S content.

\*\*Analyses for "light elements" were performed under vacuum conditions which result proportional to the state of hydration. Weight percentages obtained under these conditions are 100% less total H<sub>2</sub>O.

† Analysis reported by Ross and Hendricks (1945) for montmorillonite from Mexico

TABLE 3

## X-RAY FLUORESCENCE OF ALTERATION PRODUCTS

| 8     | 9     | 10    | 11    | 12     | 13    | 14    | 15     | 16    | 17    | 18    | 19    | 20     |
|-------|-------|-------|-------|--------|-------|-------|--------|-------|-------|-------|-------|--------|
| M-61  | M-62  | M-63  | M-65  | M-85   | M-71  | M-72  | M-73   | M-74  | M-19A | M-19B | 4-140 | 9-47   |
| 41.2  | 45.7  | 46.6  | 61.6  | 50.2   | 43.2  | 37.8  | 39.3   | 46.1  | 47.5  | 47.6  | 41.4  | 53.5   |
| 9.9   | 10.6  | 12.2  | 14.2  | 8.8    | 36.2  | 24.8  | 19.8   | 16.4  | 14.5  | 14.8  | 11.8  | 16.3   |
| 7.59  | 7.37  | 5.76  | ND    | 6.56   | 2.94  | 21.1  | 23.6   | 10.6  | 4.13  | 8.20  | 6.93  | 7.02   |
| 12.9  | 11.05 | 15.0  | 8.13  | 22.0   | 0.02  | 0.03  | 0.64   | 4.72  | 6.86  | 11.69 | 11.77 | 1.87   |
| 5.21  | 0.90  | 1.62  | 0.63  | 0.20   | 0.79  | 0.16  | 0.65   | 1.78  | 1.89  | 9.20  | 7.76  | 5.66   |
| 0.21  | 0.13  | ND    | 0.11  | 0.07   | 0.07  | 0.23  | 0.23   | 0.28  | 0.35  | 2.71  | 0.22  | 3.00   |
| 1.18  | 1.00  | 0.78  | 0.11  | 0.90   | 0.02  | ND    | 0.03   | 0.04  | 0.80  | 0.61  | 0.30  | 1.58   |
| 0.78  | 0.87  | 0.92  | ND    | 0.72   | 3.13  | 2.03  | 1.76   | 1.62  | 1.34  | 0.87  | 1.07  | 2.82   |
| 0.08  | 0.03  | 0.12  | 0.01  | 0.16   | Tr    | 0.14  | 0.05   | 0.11  | 0.11  | 0.11  | 0.14  | 0.13   |
| 0.18  | 0.12  | 0.14  | 0.05  | 0.10   | 0.36  | 0.13  | 0.20   | 0.10  | 0.10  | 0.29  | 0.20  | 0.39   |
| 0.07  | 0.16  | 2.24  | 0.13  | 1.37   | 0.07  | ND    | 0.32   | 0.05  | 0.13  | ND    | ND    | 5.16   |
| 11.23 | 8.54  | 6.76  | 8.07  | 5.83   | 12.13 | 13.6  | 7.98   | 5.75  | 10.97 | 1.40  | 9.6   | 0.74   |
| 9.40  | 13.50 | 7.80  | 6.90  | 3.60   | 1.00  | 1.00  | 5.50   | 12.40 | 11.2  | 2.50  | 8.8   | 0.28   |
| 99.93 | 99.97 | 99.94 | 99.94 | 100.51 | 99.93 | 99.92 | 100.06 | 99.95 | 99.88 | 99.98 | 99.99 | 100.97 |

S content.

under vacuum conditions which result in dehydration and a weight total overage  
percentages obtained under these "dry" conditions were recalculated to total

5) for montmorillonite from Mexico.

which grades laterally into dioctahedral montmorillonite and clinoptilolite, which is associated with minor introduced quartz.

The chemical analyses indicate an increase in  $\text{SiO}_2$  (41.2% to 61.6%) a decrease in  $\text{Fe}_2\text{O}_3$  (7.59% to not detected), and a decrease in  $\text{CaO}$ ,  $\text{Na}_2\text{O}$  and  $\text{K}_2\text{O}$  as the vein is approached. An unexpected result was the revelation of a zone of MgO concentration (15% MgO) near the vein. X-ray diffraction data indicates the presence of both di- and trioctahedral montmorillonite within this zone, five to ten meters east of the vein.

The vein-filling material at the intersection of the access tunnel and the near vertical fissure has been removed by mining, but remnants preserved in pockets suggest that the quartz-dioctahedral montmorillonite-clinoptilolite assemblage present in the El Carmen mine is similar to that presently being mined in the Tizpathe mine 700 m to the north.

Removal of the clay-bearing vein in the El Carmen mine provides an unusual opportunity to observe the geometry of the fault surface and shape of the vein. Over much of its length the montmorillonite-bearing seam is a void filling rather than a replacement feature. The displacement of the "zig-zag" surfaces of the hanging and foot walls of the fault leaves a near-vertical, open fissure which alternately swells to a maximum horizontal width of several meters then narrows to thicknesses of less than a meter.

Outcrops of basaltic ash and lithic tuff which parallel the west side of the main Pathé steam-bearing zone indicate that the width of the altered area, as marked by the beginning of silicification and

the addition of pyrite to the rock, averages 10 to 20 m on each side of the fault zone. Saponitic montmorillonite is present as an alteration product of both tuff and as an amygdular filling in basalt along the trend of the fissure.

#### El Carmen #2 Mine

This MgO concentration parallel to the vein is most pronounced in the El Carmen #2 mine, which is situated on the same vein 100 m north of the El Carmen. Here a dense clay zone 10 m east of the fissure contains a relatively pure, mixed layer, chlorite-saponite clay mineral with a MgO content of 22.0% (Table 3, Col. 12). X-ray diffraction data for the montmorillonite-chlorite is shown in Figure 5 and compared in Table 4 with other reported trioctahedral chlorite-montmorillonites. The diffraction data are characteristic of those minerals in which 14 Å chlorite layers and 15 Å montmorillonite layers alternate regularly yielding a basal spacing of about 29 Å and a regular series of orders is produced. Ethylene glycol expansion affects the montmorillonite but not the chlorite layer yielding a composite 31.5 Å spacing. Heat treatments to 600° C collapses the montmorillonite layer to approximately 10 Å which, combined with the 14 Å spacing of chlorite, yields a 24 Å periodicity. The chemical data for the clay is shown in Table 4. The trioctahedral (060) nature of the clay is confirmed by its high-magnesium versus aluminum content. A differential thermal analysis pattern of the material shown in Figure 5 indicates the mixed montmorillonite-chlorite nature of the material. A low temperature endothermic reaction typical of montmorillonite is combined with the high temperature

Figure 5

## X-RAY DIFFRACTION AND DTA DATA: SAPONITE-CHLORITE

Differential Thermal Analysis Instrument Data: Sample M-85

Robert L. Stone Model DTA-13M  
Inconel sample holder  
Nitrogen purging gas  
Heating rate: 10° C per minute  
Microvolt setting: 225

## A. DTA Pattern

X-ray Diffraction Instrument Data: Sample M-85

Siemens x-ray generator with horizontal goniometer  
Operated at 35 kilovolts and 18 milliamps  
Nickel-filtered Cu K-alpha radiation  
Scanning rate: 1° 2 per minute  
Scintillation counter  
Oriented sample on glass slides (C and D) and ceramic slide (B)

B. Sample heated to 600° C and cooled

C. Sample solvated for 8 hours with ethylene glycol

D. Sample sedimented and humidified

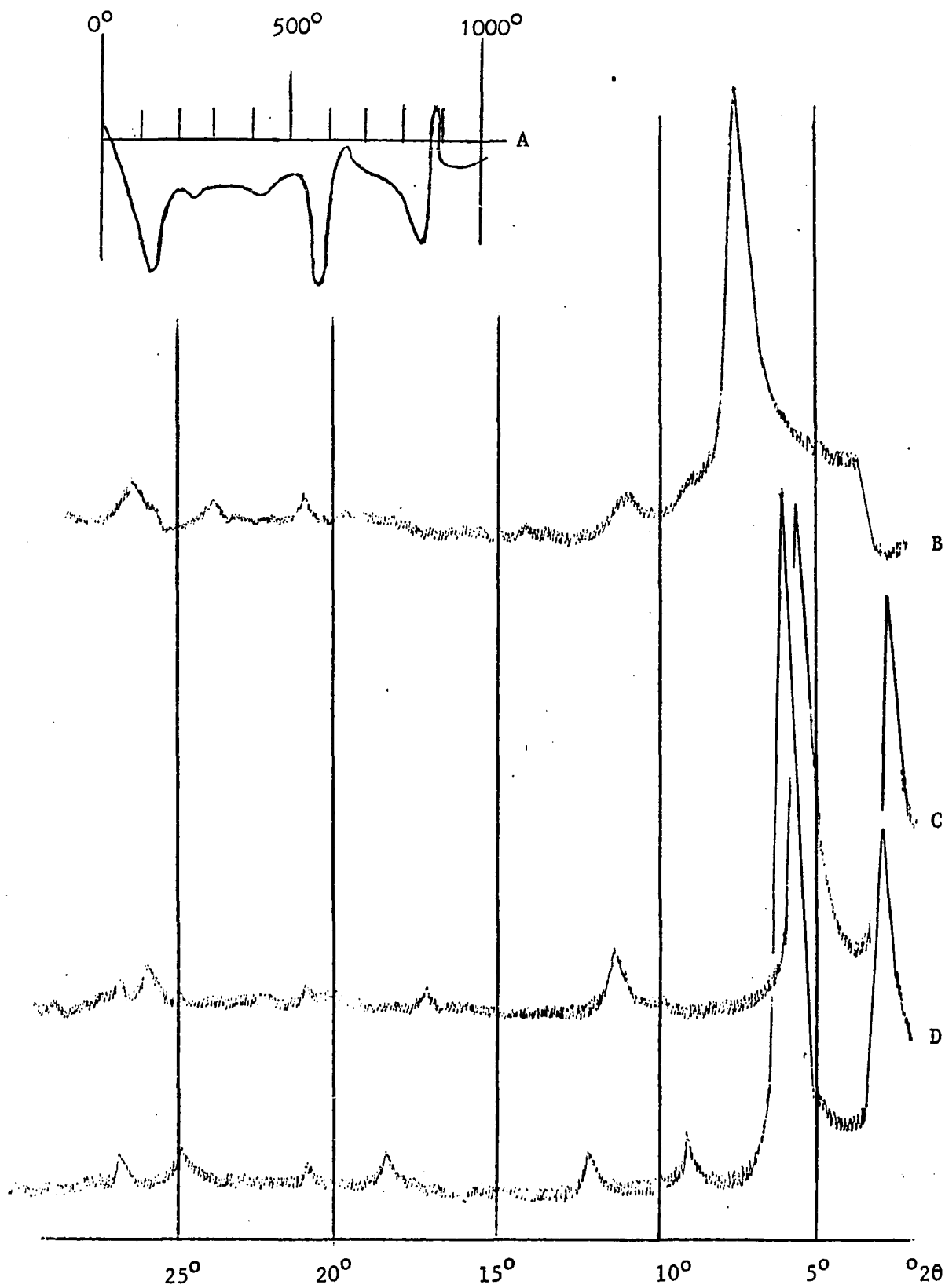


Figure 5

TABLE 4

LATTICE SPACING DATA FOR TRIOCTAHEDRAL CHLORITE-  
SMECTITE MINERALS

| Name                         | Reference<br>Reported in<br>Brown (1961) | d(00 $\ell$ ) Å |                                      |                          | d(060)<br>Å |
|------------------------------|--|-----------------|--------------------------------------|--------------------------|-------------|
|                              |  | Untreated       | Ethylene<br>Glycol(1)<br>Glycerol(2) | After<br>500°-<br>600° C |             |
| Saponite-Chlorite            | This Study                               | 29.0            | 31.1 (1)                             | 24.0                     | 1.538       |
| Montmorillonite-<br>Chlorite | Earley, Brindley<br><u>et al.</u> (1956) | 29.1            | 32.0 (2)                             | 23.8                     | 1.542       |
| Chlorite-Vermi-<br>culite    | Bradley, Weaver<br>(1956)                | 29.2            | 31.0 (1)                             | 24.0                     | 1.54        |
| Chlorite-Vermi-<br>culite    | Gallitelli<br>(1956)                     | 28.8            | 31.8 (2)                             | 23.2                     | 1.536       |

endothermic reaction more characteristic of chlorite decomposition. The low amount of aluminum in the analysis, combined with the slight 200° C endothermic reaction indicates that the montmorillonite component may be transitional to vermiculite (Brown, 1961).

#### Tizpathe

Production of steam and associated water in the zone has resulted in a lowering of the water table to a depth of 100 m, and, as a result, deeper mining has been made possible. The Tizpathe, the main mine presently being worked in the Pathé zone, is located on the Pathé fault east of well 7 (Fig. 2). The main vein is reached by numerous vertical shafts both north and south of the Pathé camp entrance road and by a spiraling inclined tunnel which approaches from the west. The area presently being mined lies at a depth of approximately 30 m below the valley floor and is reached by descending notched poles wedged into the one-meter-wide, near-vertical fissure.

The wallrock on the west side of the main vein at Tizpathe is olivine basalt. Thin-section examination of the basalt collected approximately six meters west of the vein indicates an extensive argillation of the groundmass plagioclase feldspar and all mafic constituents with only a relic intergranular or intersertal (?) texture remaining. Samples of vein material collected from a steam-bearing fissure at a depth of approximately 30 m in the Tizpathe mine reveal that the mineralogy of the veins in the Tizpathe is similar to that observed in the El Carmen mine. Dominant vein minerals in the order of abundance are chalcedonic to euhedral quartz, dioctahedral montmorillonite,

and stilbite with local minor occurrences of pyrite and free sulphur. Massive blocks of chalcedonic quartz and zeolite constitute the vein material in much of the fissure and clay occurrences are localized. Individual blocks of quartz two meters long and one meter thick mark the surface trace of the fissure in the vicinity of the mine.

The smaller fissure 30 m west of the main fissure at the Tizpathe also contains montmorillonite, stilbite and chalcedony as the dominant vein minerals. Fluorite and gypsum, not recognized in the main fissure, are present in samples from the surface exposure of the vein and in a "hot" sample collected from a depth of 15 m (Fig. 2). The order of mineral formations, as indicated by zonation of void-filling veins, was chalcedony and montmorillonite, stilbite, fluorite and euhedral quartz and lastly gypsum.

In hand specimen much of the vein quartz seems to be rather porous; this observation is confirmed by thin-section studies. The porous quartz is composed of microcrystalline aggregates of chalcedony which form the linear walls of triangular areas into which euhedral quartz crystals have grown (Plate X). The crystals are oriented with their c-axes perpendicular to the chalcedony walls. Stilbite crystals with a sheath-like habit have grown within the voids not occupied by euhedral quartz. Montmorillonite is present both as a void filling and as a replacement product of earlier formed stilbite. Vein montmorillonite typically is non-pleochroic to slightly pleochroic in brown and occurs as fine-grained aggregates which display a common optical orientation. Spherulites and a few vermicular aggregates composed of extremely thin, parallel platelets are present.

The pure montmorillonite rarely occurs in larger than "fist-size" aggregates. Scanning electron microscopy and x-ray diffraction investigations of these "pure" clay samples indicate that stilbite and to a lesser extent quartz are usually present associated with the clay. Shown in Plate XI are some of the textures observed at magnifications of 1000 x to 16,500 x. The splitting of stilbite laths to produce finer hair-like fibers was observed; these fibers are most abundant in open spaces within the clay-chalcedony vein material (Plate XI, C).

The delicate scroll structure shown in Plate XI (D) illustrates the sensitivity of the montmorillonite to the vacuum required during sample coating for scanning electron microscopy. The scroll appears to be a single clay flake which curled as a result of stresses caused by the dehydration. It is apparent from the delicate nature of the flakes that a reduction of particle size might result from the normal dispersion of the clay for x-ray diffraction or transmission electron microscopy. The scroll is approximately 6  $\mu$  long.

Montmorillonites are normally so poorly crystalline that single-crystal x-ray data are unobtainable. Montmorillonite from the Pathé fault zone possesses a normal particle size (less than one or two microns in diameter as determined by Stokes law settling velocity determinations) but yields extraordinarily intense (00) diffraction intensities (Fig. 6). Dr. de Pablo, who suggested the present investigation of the Pathé zone's geology and geochemistry, is investigating the detailed structure of the "Pathé montmorillonite" by means of selected area electron diffraction in the laboratories of the Instituto de Geologia, Universidad de Mexico.

Figure 6

## X-RAY DIFFRACTION AND DTA DATA: PATHÉ MONTMORILLONITE

Differential Thermal Analysis Instrument Data: Sample M-8

Robert L. Stone Model DTA-13M  
Inconel sample holder  
Helium purging gas  
Heating rate: 10° C per minute  
Microvolt setting: 360

A. DTA Pattern

X-ray Diffraction Instrument Data: Sample M-8

Norelco x-ray generator with vertical goniometer  
Operated at 40 kilovolts and 20 milliamps  
Nickel-filtered Cu K-alpha radiation  
Scanning rate: 1° 2 $\theta$  per minute  
Scintillation counter  
Oriented sample on glass slides except F

B. Sample at 200° C

C. Sample solvated for 8 hours with ethylene glycol. Scale factor 1x16x1

D. Sample solvated for 8 hours with ethylene glycol. Scale factor 1x256x0.6

E. Sample sedimented and humidified

F. Sample on vaseline-coated glass slide

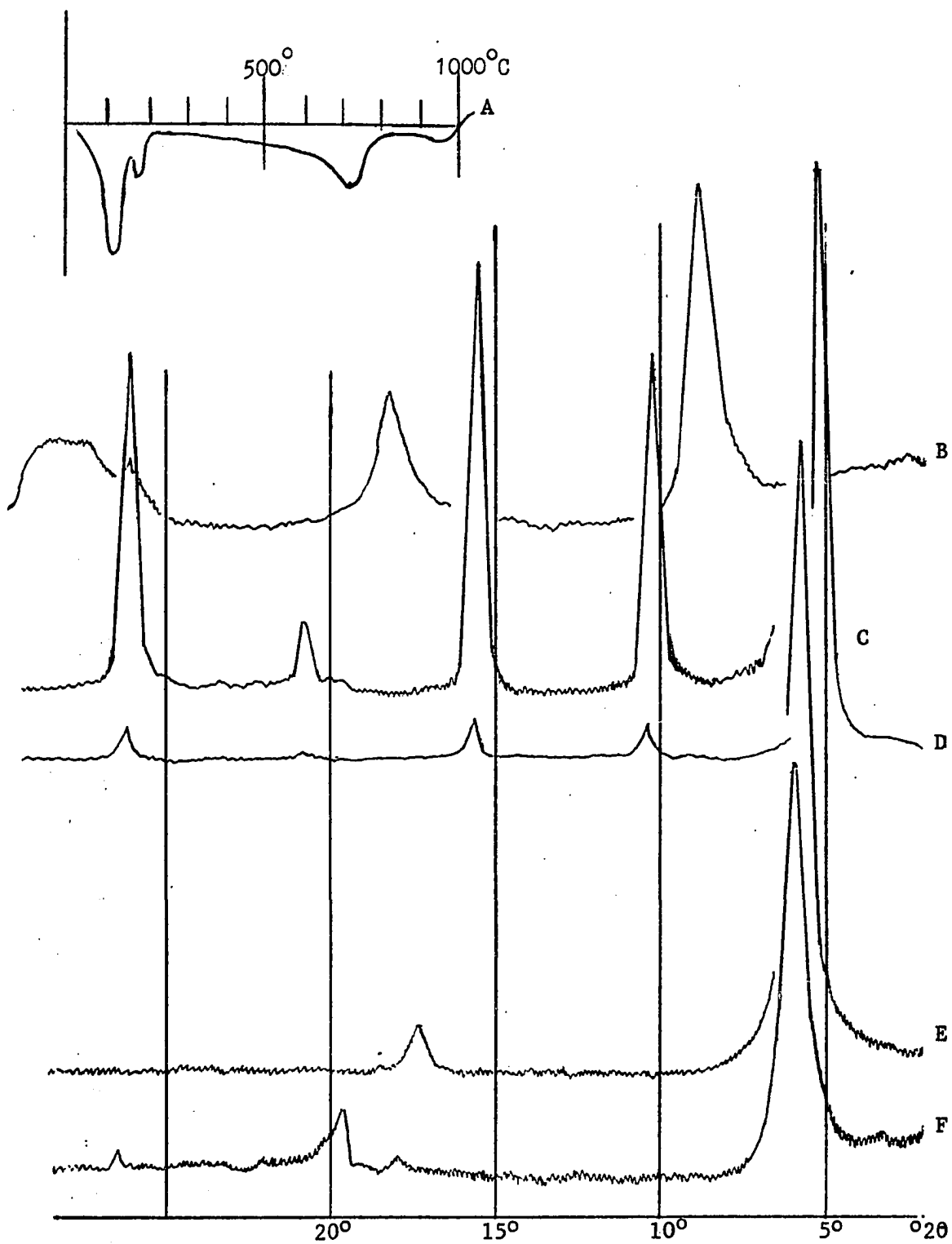


Figure 6

Chemical and x-ray data for the clay are presented in Figure 6 and Table 3 (Cols. 2, 3 and 4). Also shown for comparison (Table 3, Col. 1) is an analysis listed by Ross and Hendricks (1945, analysis number 24) which is described as being from an unknown Mexican locality. According to de Pablo (personal communication, 1968) this montmorillonite is from the Pathé mine. Ross and Hendricks noted that the clay contained the lowest iron content of montmorillonite analyses reported in their investigation (0.10 percent  $\text{Fe}_2\text{O}_3$ ). The equivalency of the two clays is indicated by the low iron analysis recorded in the present study. A theoretical structure calculated by Ross and Hendricks (1945) reveals that the clay is a high-magnesium dioctahedral montmorillonite with a formula  $(\text{Si}_{3.85} \text{Al}_{0.15}) (\text{Al}_{1.56} \text{Mg}_{0.57}) (\text{Ca}, \text{Na})_{0.11}$ . Other formulas calculated by the method of Ross and Hendricks and chemical data from the present investigation are included in Table 5.

Seven basal orders are readily obtained from (00 $\ell$ )-oriented samples prepared by the sedimentation and evaporation of montmorillonite-containing fluids on glass plates. Analysis of the clay by differential thermal analysis, diffractometer heating furnace and measurement of weight loss reveal no additional or unusual features (Fig. 6). The heating behavior is similar to that reported for normal montmorillonite by Rowland *et al.*, (1956). Low temperature dehydration and collapse of the structure to 9.8 Å is complete at 200° C. A slow dehydration which begins at approximately 300° C is terminated by the destruction of the structure and a strong endothermic reaction at approximately 700° C. Preliminary examination of the data indicates that the unusual diffraction properties of the clay may result from its unusual chemical purity

TABLE 5

## CHEMICAL CALCULATIONS: PATHE MONTMORILLONITE

| Sample  | Formulae*   |
|---|---|
| Theoretical<br>Structure<br>Ross and Hendricks<br>(1945, p. 48) | $(Al_{1.67} Mg_{.33}) (Si_4 O_{10}) (OH)_2 Na_{.33}$                        |
| #24<br>Ross and Hendricks<br>(1945)                             | $(Al_{1.56} Mg_{.57}) (Si_{3.84} Al_{.15} O_{10}) (OH)_2 (Ca, Na)_{.11}$    |
| M-8<br>Bulk Sample  | $(Al_{1.64} Mg_{.58}) (Si_{3.90} Al_{.10} O_{10}) (OH)_2 (Ca, Na, K)_{.45}$ |
| M-54<br>1 u   | $(Al_{1.60} Mg_{.74}) (Si_{3.71} Al_{.29} O_{10}) (OH)_2 Ca_{.22}$          |

\*Formulae calculated according to the method of Ross and Hendricks (1945) assuming 22 negative charges per unit and exchangeable bases totaling 0.33<sup>+</sup>.

and ordering (regular superposition of layers) rather than from any major structural modification.

#### Santa Rosa Mine

The clay-bearing fissure of the main fault has been mined north of the Rio San Juan for a distance of one kilometer. The main vein is closely paralleled by the Pathe' road as it follows the east side of the north-south arroyo. The altered wallrock in this portion of the fracture is basalt containing laboradorite laths ( $An_{60-68}$ ) in a black glass groundmass. The course of the fissure north of the river is marked by a white silicified ridge 10 m high, containing large blocks of chalcedonic quartz similar to those near the Tizpathe mine. These mines are also "hot" mines, and the alteration observed in the wallrock at the Santa Rosa mine is generally similar to that of the Tizpathe. The alteration zone is five to ten meters wider at the Santa Rosa mine, which is indicative of the greater reactivity of the glass-rich groundmass of the basalt in this area.

Lateral redistribution of iron and development of a gossan-like iron boxwork laterally away from the fissure is a feature unique to the Santa Rosa mine. Associated with hematite and goethite is a blue-green waxy "turquoise-like" clay. X-ray diffraction and chemical data (Table 3, Col. 5) indicate that the clay is dioctahedral montmorillonite with a high magnesium content and higher iron content than that observed at the main fissure. Samples of Santa Rosa as well of those of Tizpathe and El Carmen indicate that low-iron, dioctahedral montmorillonite, chalcedony, and crystalline euhedral quartz, and stilbite or clinoptilolite constitute the primary vein filling.

## El Coh

Open pit mining one and one-half kilometers southwest of Pathé has revealed a sequence of basalt and basaltic tuff overlying a down-faulted block of intermediate to rhyolitic tuff (Fig. 2). Supergene alteration in the down-faulted area has produced a complex deposit containing both kaolin and montmorillonite in close association. The east face of the pit clearly shows the bedded nature of the clastic rocks and their textural variability (Plate IX). The top, light colored, one-half meter of material contains kaolinite which grades downward through a mixed kaolinite-montmorillonite zone into beds containing a high iron oxide concentration and montmorillonite. Beneath the foot wall of the small, reverse fault is a white to pink clay identified by x-ray diffraction (Fig. 7) as montmorillonite with minor kaolinite. The gradational sequence to the left of the fault consists of altered andesite, whereas the montmorillonitic material beneath the fault zone has developed from a dacitic to rhyolitic clastic pumice tuff. Chemical data for the section is presented in Table 3 (Cols. 13 through 16).

A relatively sharp kaolinite-montmorillonite contact is present in a fault zone which forms the north margin of the pit. North of the fault mining has exposed green, dioctahedral iron-rich montmorillonite associated with abundant pyrite. South of the fault at a distance of one and one-half meters montmorillonite grades into white kaolinite containing cubic pyrite crystals which range in diameter from one-half to one and one-half centimeters. Chemical analyses of the kaolinite and montmorillonite (Table 3, Cols. 6 and 7) indicate retention of the relatively unoxidized pyrite within the kaolinite. The close association

Figure 7

## X-RAY DIFFRACTION DATA: EL COH MINE

X-ray Diffraction Instrument Data

Norelco x-ray generator with vertical goniometer  
Operated at 40 kilovolts and 20 milliamps  
Nickel-filtered Cu K-alpha radiation  
Scanning rate: 1° 2θ per minute  
Scintillation counter  
Bulk samples on vaseline slides

- A. Sample M-75: Montmorillonite and kaolinite
- B. Sample M-74: Montmorillonite
- C. Sample M-73: Montmorillonite and kaolinite
- D. Sample M-71: Kaolinite

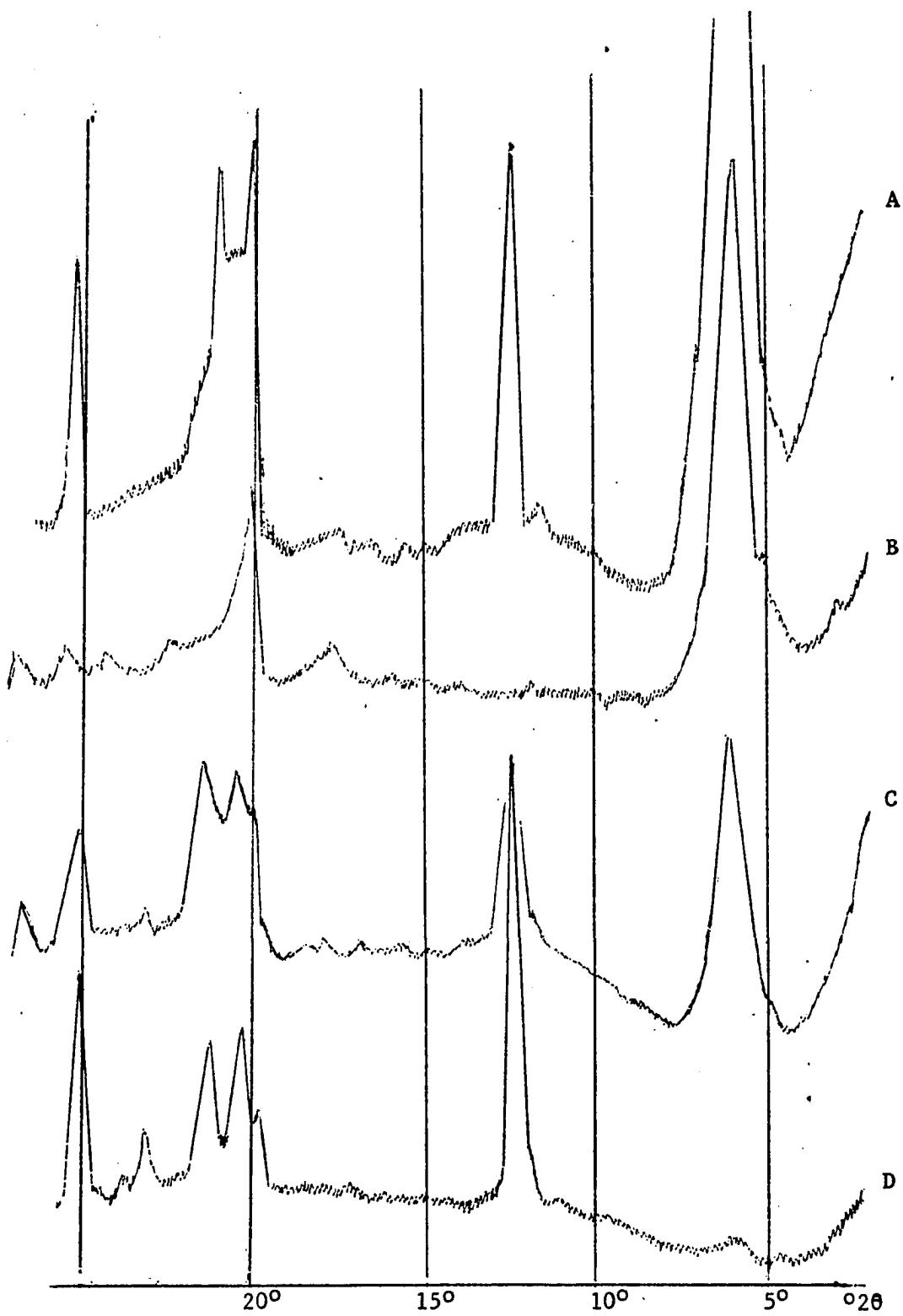


Figure 7

of kaolin and montmorillonite is also present in a small pit one kilometer west of the main El Coh mine where coarse clastic volcanic fragments of intermediate composition have altered to a kaolin and montmorillonite assemblage. A geochemical feature of El Coh similar to that of the Santa Rosa mine is the lateral and vertical migration of iron from the area of maximum hydrothermal activity (Plate IX). This mobilization and removal of Fe and its concentration around the margin of the deposit is similar to Fe mobilization described by Keller and Hanson (1968 and 1969) at other Mexican hydrothermal kaolin deposits.

#### Alteration of the Pathé Cores

The possible vertical variation in alteration-product mineralogy as a function of temperature can be considered by comparing relatively high and low temperature cores from the Pathé field. Lithologies, alteration-product mineralogy and temperatures measured during the drilling of wells 4, 5, 8, 9 and 11 are shown in Plate XIV (in pocket). X-ray diffractograms of representative zeolite-bearing samples are shown in Figure 8.

#### Wells 8, 9 and 11

Wells 8, 9, and 11 were drilled near the Pathé fault north of the Rio San Juan (Fig. 2). Both wells 9 and 11 encountered maximum temperatures of less than 100° C. Well 8 was drilled directly down the fracture zone and encountered highly-altered rock and vein filling at shallow depth. The altered wallrock in the upper portion of the cores is similar to that observed in the Santa Rosa mine. The basic, glass-rich basalt is highly altered in the core from well 8 and relatively

Figure 8

## X-RAY DIFFRACTION DATA: ZEOLITES

X-ray Diffraction Instrument Data

Siemens x-ray generator with horizontal goniometer  
Operated at 35 kilovolts and 18 milliamps  
Nickel-filtered Cu K-alpha radiation  
Scanning rate:  $1^{\circ} 2\theta$  per minute  
Scintillation counter  
Bulk samples on vaseline-coated glass slides

- A. Clinoptilolite: Sample 5-144. Lithic tuff
- B. Stilbite: Sample M-49. Vein deposit
- C. Laumontite: Sample 5-498. Andesite
- D. Mordenite: Sample 8-69. Fracture filling in basalt

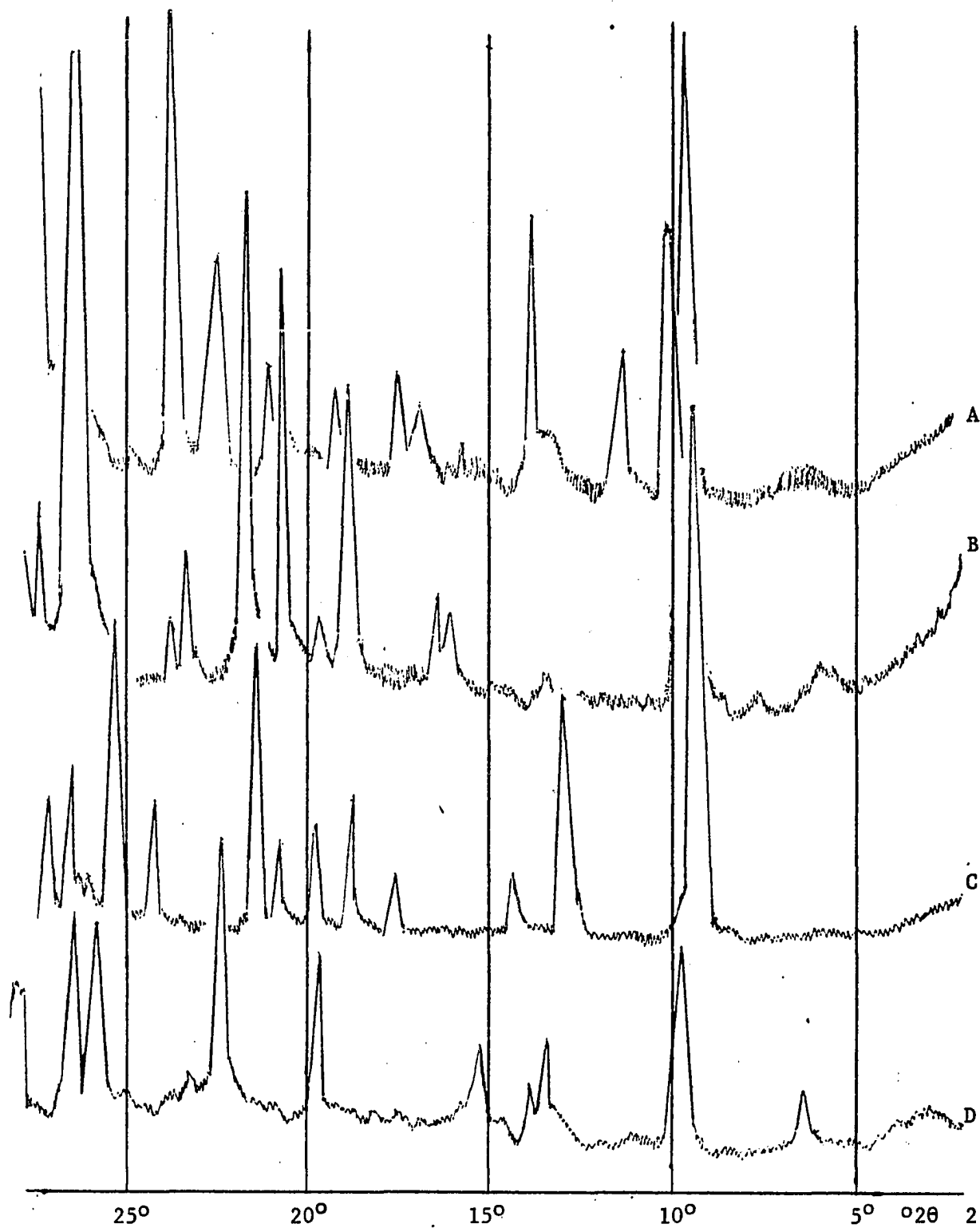


Figure 8

fresh in well 9. In well 8 alteration of the stubby plagioclase laths ( $An_{60-68}$ ) is pervasive. In wells 9 and 11, the alteration of basalt is restricted to the immediate vicinity of smaller fractures and veins. The vein filling in well 8 contains a higher percentage of calcite relative to clinoptilolite as compared to wells 9 and 11. Montmorillonite was the dominant alteration product within the veins in the upper basalt section of all three wells.

In wells 9 and 11, the temperature was below  $100^{\circ}$  C and the pumice and glass groundmass of the rhyolite units are not argillized. In well 8, however, the dominant alteration products in the corresponding rhyolite unit are mixed-layer illite-montmorillonite clay, quartz, and montmorillonite. The corresponding section in the wells 9 and 11 contains montmorillonite and clinoptilolite as a sparse alteration product of pumice in the green rhyolitic tuff section. In all three cores the upper partially welded portion of the rhyolite unit has remained relatively unaltered.

Well 8 intersected the foot wall of the fault and passed into cooler basalt at a depth of 175 m. The clay contained within the fissure zone at a temperature of  $150^{\circ}$  C was montmorillonite, whereas the clay away from the fissure in the less-altered rhyolite pumice zone was mixed-layer illite-montmorillonite (Fig. 9). The vein-filling minerals in the larger fractures encountered in drilling all three wells were chalcedony and montmorillonite with minor clinoptilolite. The fractured basalt in well 11 at a depth of 65 m contains laumontite and calcite as the alteration products. Well 9 contains saponite as an amygdular

Figure 9

## X-RAY DIFFRACTION DATA: ILLITE-MONTMORILLONITE

X-ray Diffraction Instrument Data

Siemens x-ray generator with horizontal goniometer  
Operated at 35 kilovolts and 18 milliamps  
Nickel-filtered Cu K-alpha radiation  
Scanning rate:  $1^{\circ} 2\theta$  per minute  
Scintillation counter  
Samples sedimented on glass slides

- A. Illite: Sample 5-415. Welded tuff
- B. Illite-Montmorillonite: Sample 8-141. Solvated with ethylene glycol. Rhyolite tuff
- C. Illite-Montmorillonite: Sample 8-141. Rhyolite tuff
- D. Montmorillonite: Sample 8-120. Vein deposit

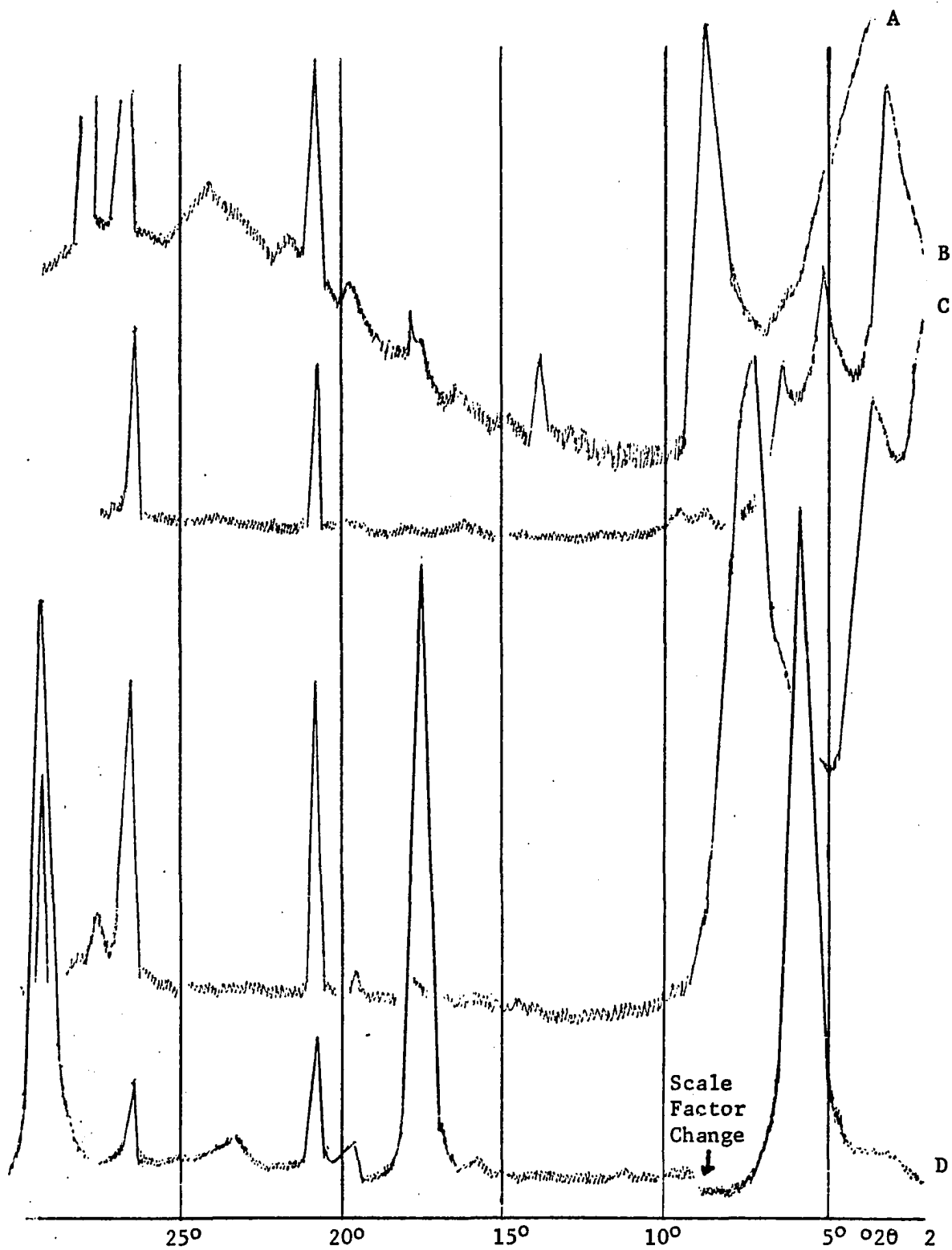


Figure 9

filling at a depth of 78 m and a temperature of 80° C. Pyrite is a common vein material at all depths drilled.

#### Wells 4 and 5

In the deep, comparatively cool wells 4 and 5 basalt is relatively unaltered. Alteration is confined primarily to the immediate vicinity of fractures, and to the beds of scoriaceous agglomerate, basic lithic tuffs, and bentonitic ash associated with the upper basalt sequence. In both cores, dioctahedral montmorillonite and clinoptilolite dominate the basic clastic volcanic sequence. Saponite is present in well 4 as an amygdular filling and laumontite is locally present in well 5 as an alteration product of scoria (Plate XI).

Differences in the alteration products of the rhyolite unit are observed in comparing the two wells. Well 4 contains the montmorillonite-clinoptilolite assemblage common throughout the green tuff section in wells 8, 9 and 11, whereas well 5 contains zeolites of the analcrite-wairakite group as the dominant alteration products of the rhyolite pumaceous tuff. Scanning electron micrographs of sample #5-350 reveal the presence of euhedral to subhedral zeolite crystals within the tuff (Plate XIII). The crystals commonly display extensive replacement by a "cotton-like" alteration product containing clay and quartz. Most of the crystal forms observed appeared cubic (or pseudocubic) and several distinctly elongated crystals were observed.

Wairakite and analcrite x-ray diffraction data reported by Kiss and Page (1969) and Coombs (1955) are compared in Table 6 with data for the Pathé material. The Na zeolite, analcrite, indexes as a cubic

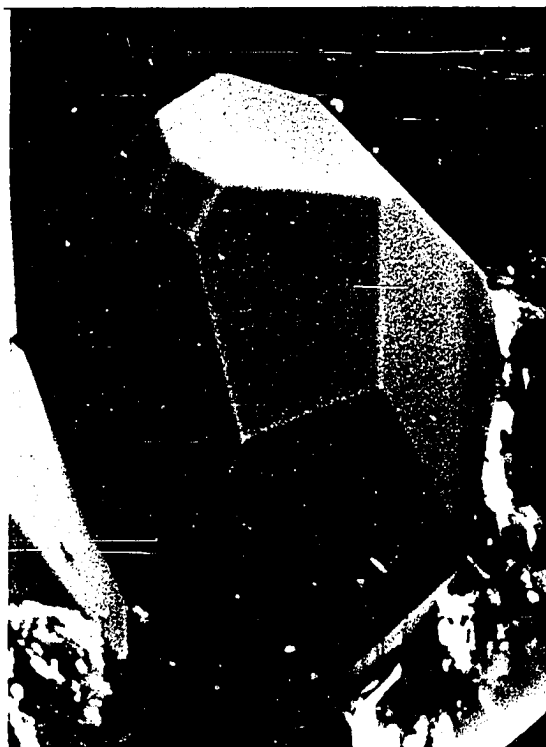
## Plate XIII

## SCANNING ELECTRON MICROGRAPHS OF ZEOLITES

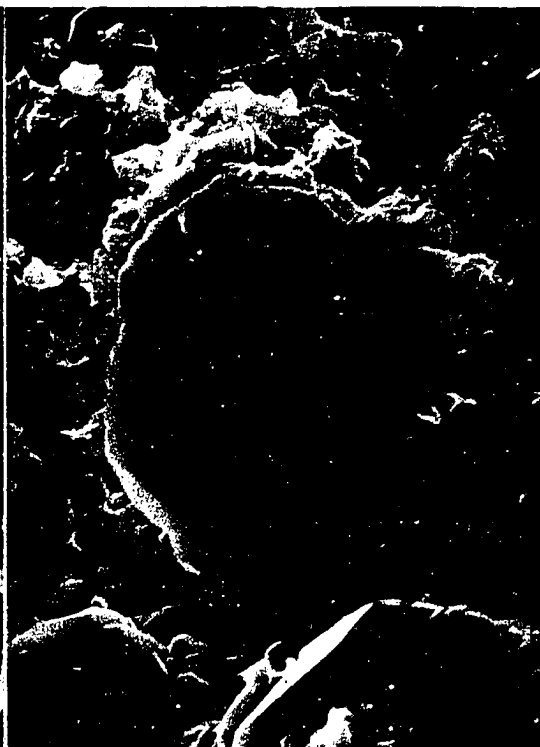
The accompanying electron micrographs were obtained from sample 5-350, an analcrite-rich lapilli tuff.

- A. Analcite. Unaltered euhedral crystal identified by x-ray diffraction as Ca-rich analcrite.  
X375
- B. Partially argillized analcrite. Upper surface of the crystal is unaltered. The lower portion has been replaced by a clay identified by x-ray diffraction as illite-montmorillonite.  
X1000
- C. Partially argillized analcrite. Left side of the crystal has been extensively replaced by a cotton-like aggregate of clay (?) and euhedral quartz crystallites.  
X500
- D. Elongate analcrite crystal. Analcrite enclosed in a matrix of doubly terminated quartz crystallites and clay.  
X2000

PLATE XIII



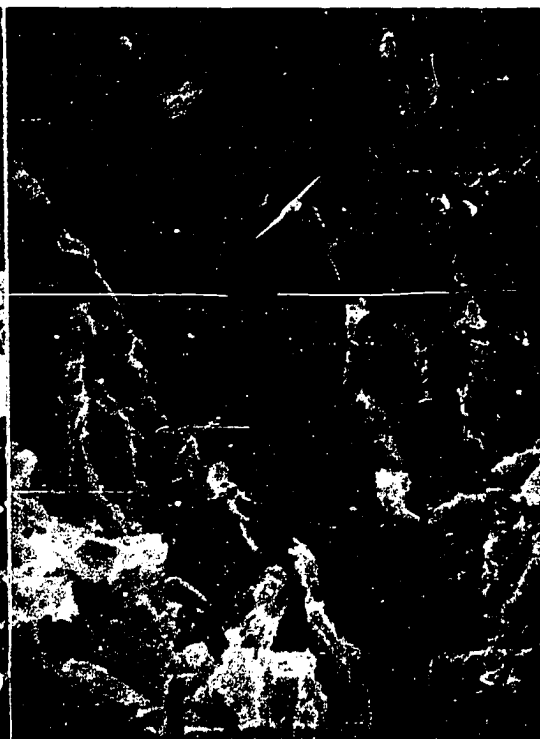
A



B



C



D

TABLE 6

## ANALCITE-WAIRAKITE POWDER DATA

| hkl | Analcite <sup>1</sup> |    | Wairakite <sup>1</sup> |         | Wairakite <sup>2</sup> |    | Analcite(?)#5-350 |    |
|-----|-----------------------|----|------------------------|---------|------------------------|----|-------------------|----|
|     | d(Å)                  | I  | d(Å)                   | I       | d(Å)                   | I  | d(Å)              | I  |
| 200 | 6.87                  | 1  | 6.85                   | 4       | -                      | -  | -                 | -  |
| 211 | 5.61                  | 8  | 5.57                   | 8       | 5.56                   | 9  | 5.57              | 8  |
| 220 | 4.86                  | 4  | 4.84                   | 4       | -                      | -  | -                 | -  |
| 321 | 3.67                  | 2  | 3.64                   | 3       | -                      | -  | -                 | -  |
| 400 | 3.43                  | 10 | 3.42<br>3.39           | 6<br>10 | 3.41                   | 10 | 3.42              | 10 |
| 332 | 2.925                 | 8  | 2.909<br>2.897         | 5<br>3  | 2.91                   | 9  | 2.914             | 4  |
| 422 | 2.801                 | 2  | 2.783<br>2.770         | 1<br>1  | -                      | -  | -                 | -  |
| 431 | 2.693                 | 5  | 2.680<br>2.67          | 4<br>1  | -                      | -  | 2.683             | 2  |
| 521 | 2.505                 | 5  | 2.50<br>2.489          | 1<br>4  | -                      | -  | -                 | -  |

<sup>1</sup>Coombs (1955)<sup>2</sup>Kiss and Page (1969)

structure but the indexing of wairakite, its Ca analogue has proven more difficult. Both cubic and pseudocubic tetragonal structures have been postulated. X-ray data for the Pathe zeolite is closer to that reported for analcite, but deviation from the analcite data is sufficient to infer limited Ca substitution. The dense, welded rhyolitic rock interbedded with the interstratified volcanic unit of well 5 contains a small amount of 10 Å mica (illite) as an alteration product.

#### Well 7

Cuttings of rhyolite from depths between 700 and 1286 m in well 7 contain illite, kaolinite and calcite as the dominant alteration products. The kaolinite here is the only known occurrence of the mineral outside of the surficial deposits in the El Coh mine area. The measured temperature below a depth of 400 m in well 7 was 150° C.

## GEOCHEMICAL CONTROL OF THE ALTERATION

### Geochemical Environment of the Pathé Geothermal System

An important objective of this investigation was a determination of the variables which control the alteration-product mineralogy in the Pathé geothermal zone and a comparison of the chemical environment there with that of other geothermal systems. In terms of the classic, somewhat arbitrary, schemes of classifying processes of rock alteration, the environment of Pathé is best described as hydrothermal. Much of the alteration has been and continues to be produced by the mineralogical and chemical interaction of rocks and hot water.

The temperature and chemistry of the thermal solutions together with a weaker influence exerted by the chemistry and mineralogy of the wallrocks have controlled the mineral assemblages produced at Pathé. Total pressure may safely be ignored as a variable influencing alteration product stabilities within the shallow depths considered here. Steiner (1969), Muffler and White (1969) and Burst (1969) have shown total pressure to have no effect at depths greater than those reached at Pathé.

#### Temperature

The maximum temperatures present within the Pathé geothermal system (150°-160° C) are transitional between the upper limits of

diagenesis and the lower temperature limits of the zeolite facies of metamorphism (Fyfe, et al., 1958). The temperature-depth curves for the Pathé wells have previously been reported by de Anda et al. (1964). Temperature data from five logs abstracted from this source, with the logs of lithology and alteration product mineralogy are shown in Plate XIV.

The maximum temperature recorded during the drilling exploration of the Pathé geothermal system was 160.5° C. This temperature was recorded by means of a thermistor (semi-conductor resistance thermometer) during the drilling of well 3. Well 5, drilled 100 m east of the Pathé fault encountered the lowest geothermal gradient measured within the Pathé area (140° C per km). Maximum temperatures were encountered by the steam-producing wells drilled down the main Pathé fissure. Their temperature graphs closely approximate a theoretical boiling point curve calculated as described by White (1968). The temperature gradients of these wells reach a maximum of approximately 150° C and continue relatively unchanged with deeper drilling (Fig. 10). Deep drilling in most of the world's known geothermal systems has shown this achievement of a "base temperature" to be present. This achievement of a base temperature is interpreted by White (1968) as representing the equilibrium temperature reached by the deeply circulating water in the lower portion of the thermal system which is receiving heat by conduction from rocks.

A relatively narrow temperature span exists between the lower limits of steam at the boiling point under surface pressure conditions (94° C) and the maximum measured temperature (160° C) of the Pathé system.

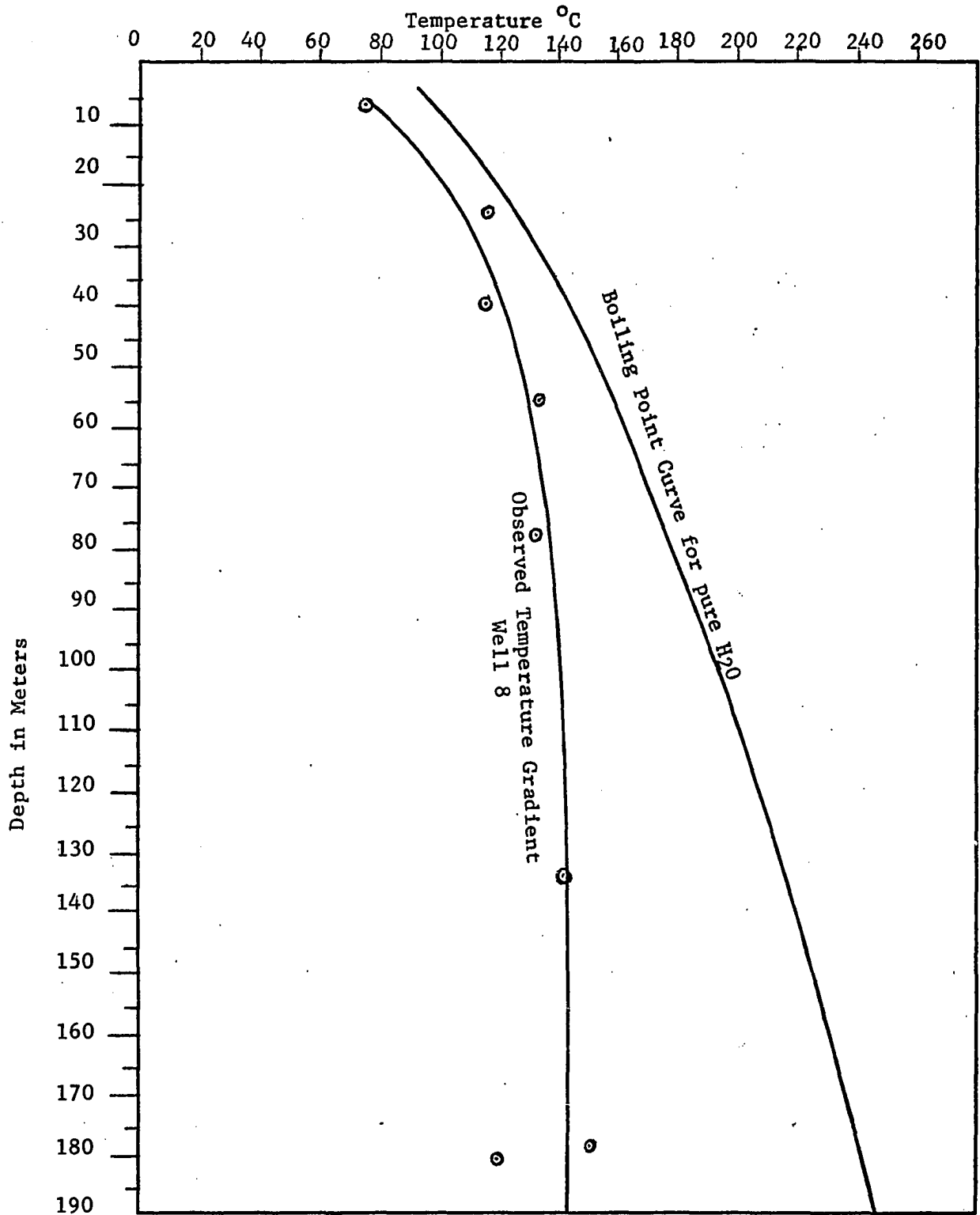


Figure 10

CALCULATED BOILING CURVE AND TEMPERATURE LOG, WELL 8  
 Theoretical Boiling Point Curve Calculated as Described by White (1968)  
 Assuming Water Table @ 5 m and Elevation of 1700 m

Within this narrow temperature range only minor temperature-controlled variations exist in the mineralogy of the vein deposits. The influence of temperature is more indirect; it is exerted through solubility changes in the rapidly ascending thermal solution. A major variation in the "degree of alteration" is present between the 160° C maximum and 20° to 25° C minimum rock temperature which exist in close proximity.

#### Solution Chemistry

Major geothermal systems are envisioned as large-scale convective cells in which cool meteoric water circulates to depths greater than two or three kilometer depths and is there heated by contact with rock heated by conduction from cooling magma. The heated water rises to the surface driven by a pressure differential stemming from its lower density as compared to that of the cooler, more dense water around the peripheral area (White, 1968, pp. 8-12). Emanations from the magma may mingle with the upward migrating meteoric water, but isotopic ratios of geothermal fluids and surface waters from the same areas are interpreted as indicating a very minor magmatic contribution. Plots of the  $O_{18}/O_{16}$  ratio versus the deuterium/hydrogen (D/H) ratio for surface water-geothermal water pairs reveal a variation in the  $O_{18}/O_{16}$  ratio, and the D/H ratios for any area are constant. The  $O_{18}$  is enriched in the thermal water as a result of its reaction with silicate and/or carbonate rocks. The D/H ratio is constant for both the surface and thermal water in each of the areas thus investigated. Craig (1956) estimated the possible maximum magmatic contribution to the steam to be less than five percent. Thus the solution chemistry of a geothermal system is largely a function

of the base temperature of the deeply circulating water and the nature of the strata encountered by the circulating water. Allen and Day (1935) described the concept of obtaining large concentrations of elements such as chlorine, fluorine, sulphur and arsenic from rock at depth in a large spring system simply by leaching as "unthinkable". Recent laboratory investigations by Ellis and Mahon (1964) have shown the concentrations of all elements in normal geothermal brines to be well within the range of values which could be extracted in a large circulating system by heated water.

A chemical analysis of steam from well 1 was made in the laboratories of the Comisión Federal de Electricidad in 1956. This analysis is shown in Table 7, together with an analysis of Wairakie steam reported by Ellis and Wilson (1960). The composition of the steam indicates that it is nearest to the "Type A" chloride thermal waters described by Ellis and Mahon (1964). The water is alkaline (pH 9.3) with a predominance of Na, Cl,  $\text{SO}_4$ ,  $\text{CO}_3$  and  $\text{SiO}_2$ . The water differs from normal "Type A" water in that it has a relatively low Cl/ $\text{SO}_4$  and a high Na/K ratio. It is best described as an intermediate type. Other unusual aspects of the Pathé steam are its high Mg and relatively low  $\text{SiO}_2$  content compared to that of other geothermal systems.

The solubilities of amorphous silica and quartz are shown as a function of temperature in Figure 11. The steam produced by well 1 at a temperature of  $94^\circ\text{C}$  is supersaturated with respect to quartz (solubility of 50 to 55 parts per million) but undersaturated with respect to amorphous silica (solubility of approximately 380 parts per million).

TABLE 7

## CHEMICAL ANALYSES OF GEOTHERMAL SOLUTIONS AND CONDENSATE

| Analyses<br>in ppm | Hole #44<br>Wairakei <sup>1</sup> | Hole #219<br>Rotorua <sup>1</sup> | Well #1<br>Pathe | Hole #38,<br>Wairakei <sup>2</sup> |
|--------------------|-----------------------------------|-----------------------------------|------------------|------------------------------------|
| Ca                 | 17                                | 1                                 | 36               | 29.6                               |
| Mg                 | 0.03                              | 0.06                              | 48               | 2.2                                |
| Na                 | 1320                              | 375                               | 590              | 1320                               |
| K                  | 225                               | 35                                | ND               | 175                                |
| HBO <sub>2</sub>   | 117                               | 25.4                              | 28               | -                                  |
| CO <sub>2</sub>    | 19                                | 206                               | 235              | -                                  |
| SO <sub>4</sub>    | 36                                | 12                                | 169              | -                                  |
| Cl                 | 2260                              | 355                               | 144              | -                                  |
| H <sub>2</sub> S   | -                                 | 36                                | 15               | -                                  |
| SiO <sub>2</sub>   | 640                               | 405                               | 143              | -                                  |
| pH                 | 8.6                               | 9.4                               | 9.3              | -                                  |

<sup>1</sup>Ellis and Mahon (1964)

<sup>2</sup>Ellis and Wilson (1960)

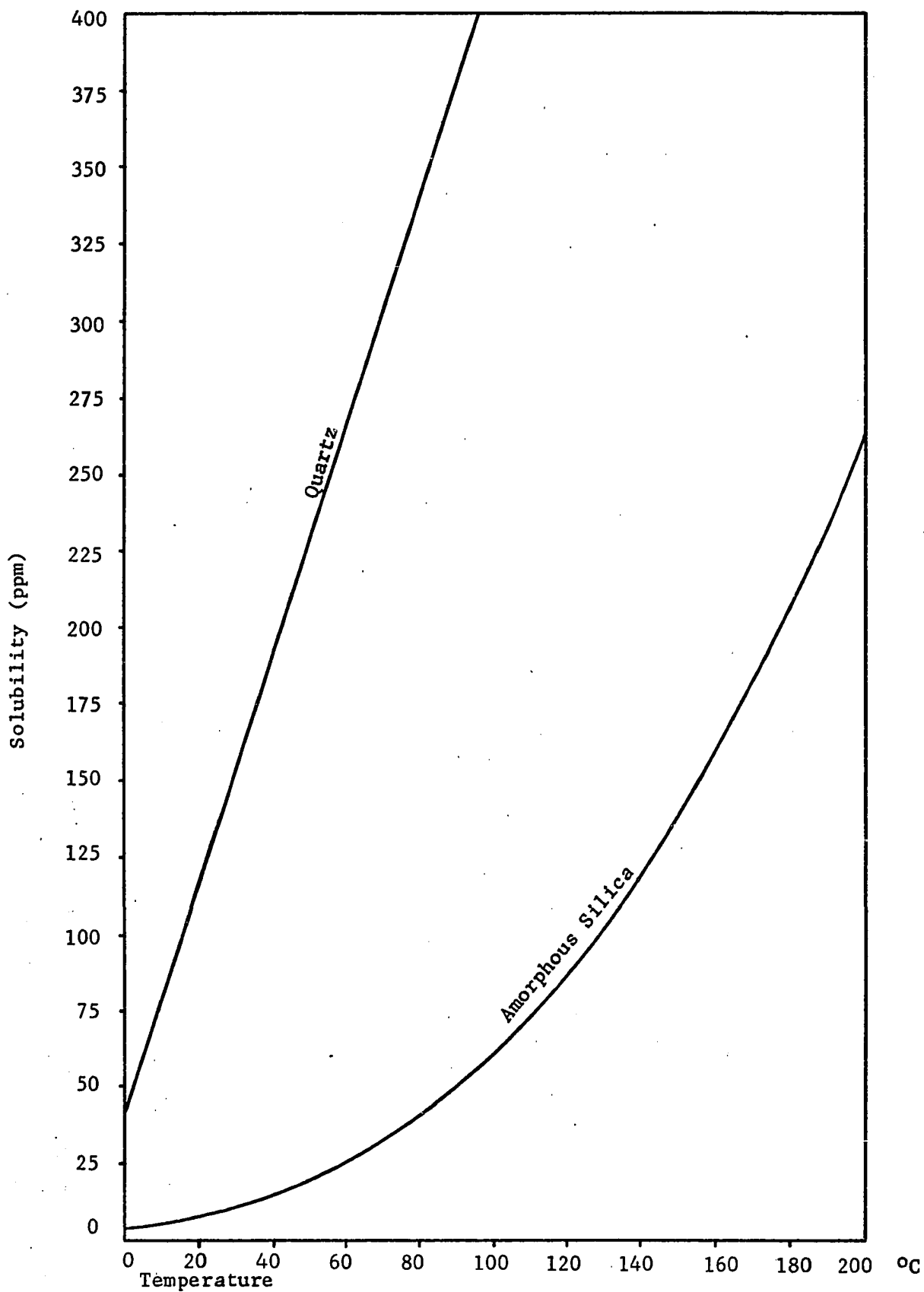


Figure 11  
Solubility of Amorphous Silica and Quartz as a Function  
of Temperature (from data of Krauskopf, 1959, and Siever, 1962)

As the fluid rises rapidly and cools, the undersaturation with respect to amorphous silica decreases, and, at 25° C, the cooled solutions will be slightly supersaturated.

SiO<sub>2</sub>. Recent investigators (Krauskopf, 1956) have shown that the form of silica normally present at surface temperatures and pH values of less than 9 is H<sub>4</sub> SiO<sub>4</sub> in true solution. Above a pH of 9 ionization increases with the formation of H<sub>3</sub> SiO<sub>4</sub><sup>-4</sup> and H<sub>2</sub> SiO<sub>4</sub><sup>-2</sup> accompanied by an increase in silica solubility. The pH of the Pathé solution (9.3) lies on the threshold of this solubility increase.

The variation of silica solubilities as a function of temperature appears to be of primary importance in the operation of geothermal systems and the control of geothermal alteration products. The greatly increased solubility of silica at increasing depths facilitates fluid circulation. As the heated, silica-rich fluids rise and heat is lost they become supersaturated with respect to both amorphous and crystalline forms of silica. The known "sluggishness" in the attainment of equilibrium between solid silica and water may be utilized in the determination of temperatures at depth within a geothermal system. Fournier and Row (1966) have shown that the base temperature of hot springs systems may be accurately estimated from the saturated SiO<sub>2</sub> content of fluid rapidly produced or erupted from depth. The SiO<sub>2</sub> content of the rapidly cooled water reflects the temperature of equilibrium with quartz which existed at depth. Utilizing a SiO<sub>2</sub> content of 142 parts per million, an underground temperature of 150° C is predicted from the curves determined by Fournier and Row (Fig. 12). This measured and predicted base temperature of 150° to 160° C for the Pathé system has been assumed by

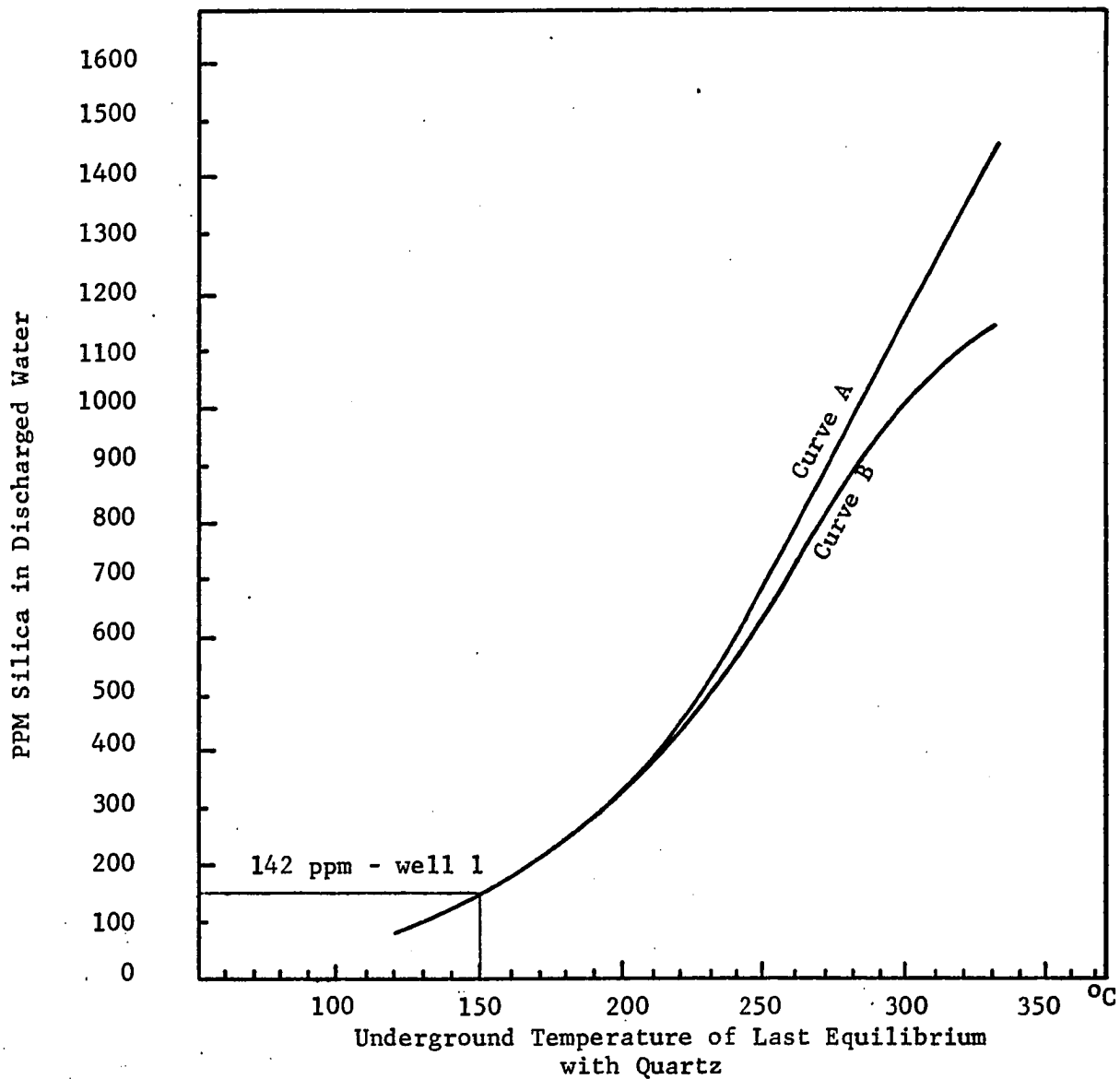


Figure 12

CALCULATED GEOTHERMAL TEMPERATURE BASED ON  $\text{SiO}_2$   
(after Fournier and Rowe, 1960)

White (1968) to be the minimum temperature necessary at depth for the maintenance of circulation in a large geothermal system.

CaCO<sub>3</sub>. The deposition of quartz in the shallow, rapidly cooled portions of a geothermal system is commonly accompanied by a disappearance of vein calcite. In a system closed with respect to  $P_{CO_2}$  Miller (1952) has demonstrated that a decrease in temperature is accompanied by an increase in calcite solubility. The equilibrium control is provided by the variation of the solubility of CO<sub>2</sub> with decreasing temperature. As the solutions rapidly cool following the boiling point curve, the solubility of CO<sub>2</sub> rapidly increases thus increasing the solubility of calcite. A reverse process is sometimes observed in producing steam wells. The flashing of steam liberates CO<sub>2</sub> resulting in the rapid deposition of calcite or aragonite.

Ca, Na and K. Investigations of thermal solution-wallrock alteration by Fenner (1936) and Steiner (1956) established the vertical mobility of Ca, Na and K within the geothermal environment. At depth Ca<sup>++</sup> and Na<sup>+</sup> are removed from plagioclase and replaced by K<sup>+</sup> from solution resulting in the formation of mica and adularia. Higher in the system, the deposition of Ca- and Na-rich minerals such as the zeolites may occur. The Wairakei analyses (Ellis and Wilson, 1960) reveal Na contents averaging approximately 1100 ppm and Na/K atomic ratios generally within a range of 10 to 30. The Pathé analysis indicates a much higher sodium to potassium ratio (sodium 590 ppm and potassium not detected in the analysis). The higher cation content of the Wairakei water is indicative of the higher temperature of the Wairakei system (approximately 255° C). The lack of K<sup>+</sup> in the Pathé water indicates an

initial low potassium content and secondly, the possible retention of  $K^+$  in the zone of mica formation present below 700 m in well 7.

Mg. The only cation that is normally abundant in the Pathé area is  $Mg^{++}$ . Local high  $Mg^{++}$  concentrations were noted by Steiner in the shallow depths of the Wairakei field. He attributed the shallow  $Mg^{++}$  to contamination by downward percolating groundwater. Ellis and Mahon (1964) however, have noted a high  $Mg^{++}$  content in water produced from depth in other wells in the Wairakei system and its source has not been determined.

The abnormally high  $Mg^{++}$  content of the clastic volcanic rocks associated with the olivine basalt unit provides an obvious source for the high Mg content of the Pathé water. An intercommunication between the groundwater and the water and steam in the fissures is known to exist in the Pathé field. Shutting down the steam-producing wells leads immediately to a marked increase in the water level in the deep mines along the fissure (Peter Powers, personal communication, 1968). The MgO content of the vein material (4 to 8 percent) is actually lower than that of the olivine basalt unit (6 to 11 percent MgO). The concentration of Mg in joints and fractures during the alteration of olivine-bearing rock has previously been noted by Wilshire (1958). Loughnan (1969) calculated the solubility of  $Mg(OH)_2$  at 25° C as a function of pH. His calculations show that  $Mg(OH)_2$  may be insoluble at a pH above 10 and he mentions the possibility of this occurring as a result of the high-abrasion pH associated with olivine and augite alteration. The absence of Fe from the vein-filling material and the presence of  $Mg^{++}$  in solution, suggests that Fe, possibly as a soluble hydroxide has been removed and

Mg provided from the surrounding rock has been retained due to its acceptability in the montmorillonite structure.

### Mineral Stabilities

Geothermal systems provide a means of "field-checking" mineral equilibria in a temperature and concentration range in which the attainment of equilibrium is often difficult within the time permitted by laboratory investigation. Investigations of thermal systems have provided confirmation of the silica dissolution and precipitation relationships determined by Krauskopf (1956). The present investigation and that of Muffler and White (1969) provide data points below the 300° C minimum temperatures of phase equilibria studies by Hemley *et al.* (1961) of the systems  $\text{Na}_2\text{O}-\text{Al}_2\text{O}_3-\text{SiO}_2-\text{H}_2\text{O}$  and  $\text{K}_2\text{O}-\text{Al}_2\text{O}_3-\text{SiO}_2-\text{H}_2\text{O}$ .

### Montmorillonite-Illite

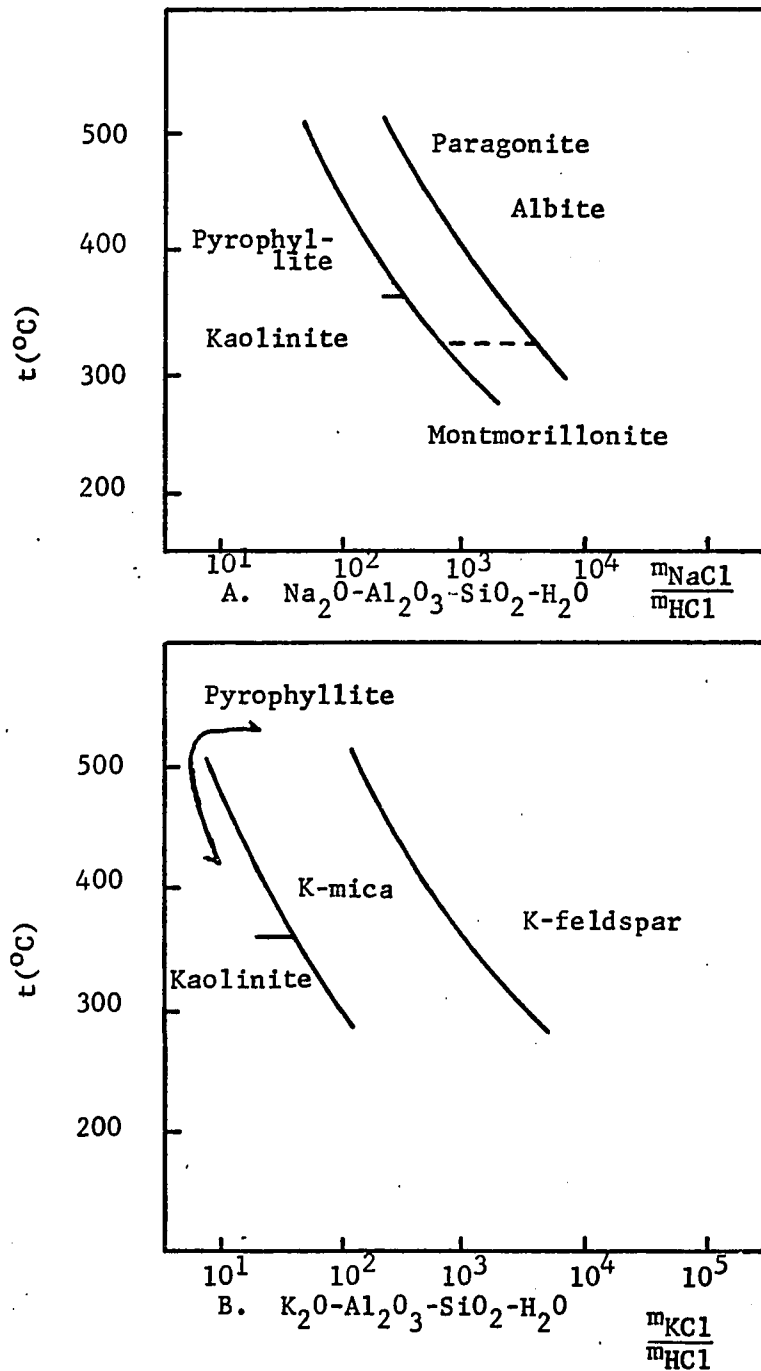
Experiments on montmorillonite stability utilizing the pure components suggests that montmorillonites are stable up to temperatures of 500° to 600° C at one atmosphere total pressure. The conversion of montmorillonite to mixed-layer montmorillonite and illite at temperatures of from 100° to 150° C in apparent conflict with the laboratory stability has been well established. Muffler and White (1969) reported the complete conversion of montmorillonite to mixed-layer clay at a temperature of 100° C in the Salton Sea geothermal system. Steiner (1969) and Burst (1969) noted the conversion to mixed-layer clay at 100° to 120° C. The control of this conversion process is suggested by Khitavov and Pugin (1966) who found that montmorillonite heated in the presence of 0.10 m solution of KCl altered to mixed-layer illite-montmorillonite at a temperature of approximately 150° C. These data

considered with the phase diagrams of Hemley et al. (1961) shown in Figure 13 suggest that the conversion of montmorillonite to mixed-layer clay or illite cannot be discussed meaningfully in terms of temperature alone. The rather limited distribution of montmorillonite as a hydrothermal vein mineral is limited by the same factors which have narrowly bounded the natural occurrences of paragonite, a sodium mica. The natural composition of geothermal solutions is normally more K-rich relative to Na than the K-deficient fluids of the Pathé system. The presence of Mg-rich montmorillonite as an important vein mineral at temperatures to 150° C merely reflects the Mg and Na-rich nature of the thermal solutions.

The alteration developed within the Pathé system contains many examples of the local influence of the source rock's mineral chemistry. In the core of well 8, montmorillonite is present up to temperatures of 150° C within the vein-filling material of the immediate fracture zone. Illitic clay is developed as a sparse alteration product of pumice in the relatively dense rhyolitic ash away from the fractures. The local K-rich environment within the tuff at this temperature is sufficient to produce illite, where the solution composition of the fracture zone provides conditions favoring montmorillonite as a stable phase.

Kaolinite. The alteration within the El Coh mine illustrates that the Eh and pH of the environment may locally be of greater importance than the nature of the source rock in determining the mineralogy of alteration products. The kaolinite is locally produced by sugergene acid leaching of basaltic material. Ten meters distant a montmorillonite

Figure 13  
 STABILITY RELATIONS IN THE SYSTEM  $\text{Na}_2\text{O}-\text{Al}_2\text{O}_3-\text{SiO}_2-\text{H}_2\text{O}$   
 and  $\text{K}_2\text{O}-\text{Al}_2\text{O}_3-\text{SiO}_2-\text{H}_2\text{O}$  AT ELEVATED TEMPERATURES\*



\* After Hemley *et al.*, 1961.

has been derived from the alteration of rhyolitic material under reducing conditions below the water table. The kaolinite produced by the alteration of rhyolite at depths below 700 m and at a temperature of 150° C is associated with calcite and illite. It reflects the stable assemblages predicted by Zen (1961) for alteration at relatively high values of  $P_{CO_2}$ .

Silica minerals. The dominance of chalcedony and quartz within the fissures at Pathé reflect the saturation of the thermal solutions with respect to quartz at 100° C. Its undersaturation with respect to amorphous silica at this temperature is overcome and sinter is deposited as the water further cools to 20°-25° C. The distribution of quartz and sinter along a three kilometer length of the Pathé and La Mesa faults indicates that the former thermal activity in portions of these faults exceeded the present, very localized occurrence.

Calcite. In the mines along the Pathé fault calcite is not a common vein-filling mineral. It was not observed associated with clinoptilolite, montmorillonite and quartz in any of the mines. In the cores of well 8, however, an appearance of calcite and a disappearance of clinoptilolite as an important vein mineral was noted with increasing depth and temperature. The general antipathetic relationship between quartz and calcite in the fault fissures is assumed to be a function of their opposite reactions to increased temperature. Increasing depth and increasing temperature in the system leads to the decreased solubility of  $CO_2$  and encourages calcite precipitation. Increased temperatures increase the solubility of silica and favor its solution rather than deposition.

Zeolites. The zeolites present in the geothermal environment at Pathé generally reflect their low-energy, silica-rich, aqueous environment of formation. Kostov (1960) has grouped the common zeolites in terms of these variables (Fig. 14). Clinoptilolite, mordenite, stilbite and heulandite, the common zeolites at Pathé, are all high-silica, highly-hydrated minerals. Analcite and laumontite are less hydrated, higher-aluminum zeolites, and their occurrence at Pathé is not within the actual fluid-bearing fissures. The presence of analcite rather than montmorillonite at depth in well 5 is accompanied by an absence of any vein development in this core. Stability relations of phases in the system  $\text{Na}_2\text{O}-\text{Al}_2\text{O}_3-\text{SiO}_2-\text{H}_2\text{O}$  at  $25^\circ\text{C}$  and one atmosphere have been extrapolated from higher temperature relations by K. Linn (as reported in Garrels and Christ, 1965, p. 363). Linn's diagram indicates that analcite formation relative to that of Na-montmorillonite occurs at higher pH, higher values of  $\text{Na}^+$  and higher  $\text{H}_4\text{SiO}_4$ .

Chlorite-Montmorillonite. The presence of chlorite in an outer zone of alteration adjacent to montmorillonite is a common feature of wallrock alteration in basic rock. At Pathé the zone of chlorite-saponite represents a marginal alteration zone in which high Mg contents are derived from Mg-rich rocks and preserved in a narrow, highly alkaline, reducing environment.

Pyrite. Pyrite is present throughout the cores except in the main vein of the fissure. It is concentrated in the zone adjacent to the main vein with saponite and/or chlorite. Its presence with kaolinite in the El Coh mine reflects its stability in an acid-reducing environment.

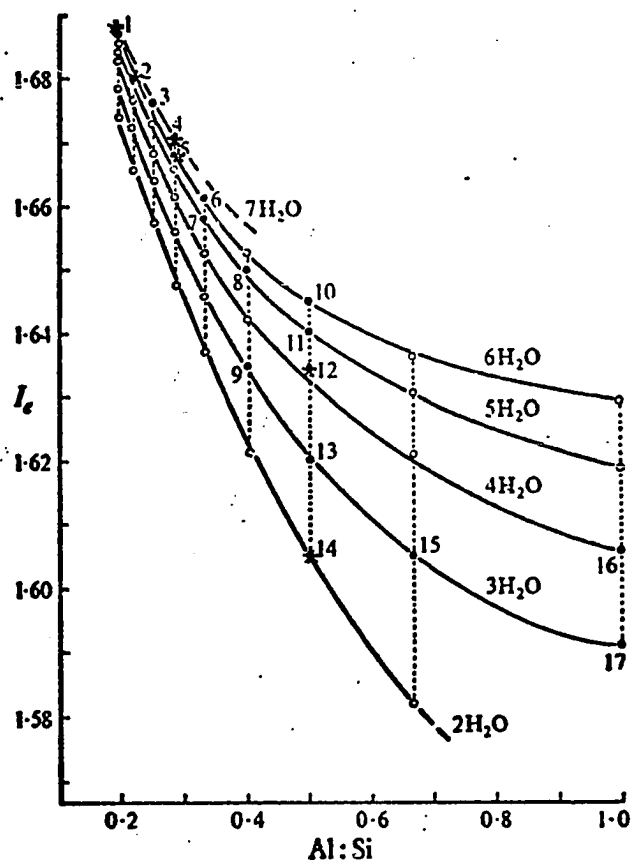


Figure 14

#### ZEOLITES AS A FUNCTION OF $H_2O$ , Al/S: AND THE ENERGY INDEX

Variation of the Al/Si ratio and the energy index (bonding energy) of the calcium zeolites: (1) ptilolite (Si-rich mordenite), (2) mordenite, (3) Ca-dachiardite, (4) stilbite, (5) heulandite, (6) Ca-erionite, (7) epistilbite, (8) Ca-faujasite, (9) yugawaralite, (10) chabazite, (11) levyne, (12) laumontite, (13) leonhardite(?), (14) weirakite, (15) scolecite, (16) gismondine, (17) Ca-thomsonite(?) (after Kostov, 1960). Zeolites recognized at Pathe or closely related species to those recognized are indicated by the symbol \*.

## CONCLUSIONS

Variations in the alteration product mineralogy displayed in the cores and surface exposures of the Pathé geothermal zone reflect the control of three primary factors: temperature, source rock and chemical environment. Within the relatively limited temperature range (100° to 150° C) of the Pathé geothermal system, temperature variations exercise a minor influence on variations in the mineral assemblages. The near surface abundance of chalcedony and quartz in the veins is the result of supersaturation with respect to crystalline quartz which accompanies the lowering of the temperature of ascending thermal solutions.

Temperatures recorded in the wells span the temperature range postulated by Burst (1969) for the conversion of montmorillonite to interstratified illite-montmorillonite. Interstratified illite-montmorillonite is present, but only as an alteration product of rhyolite tuff, and not as a vein mineral. Montmorillonite occurs as a stable hydrothermal vein deposit at the maximum temperatures recorded in the Pathé geothermal zone indicating that temperature increase alone is not sufficient to produce the transformation of montmorillonite to illite.

The unusual alteration product distribution is a reflection of the chemistry of the thermal solutions. The presence of Mg-rich dioctahedral montmorillonite reflects the unusual abundance of Mg and absence of K in the thermal solutions. The abundance of Na with

respect to K places the chemistry of the solutions within the stability field of montmorillonite even at 150° C as predicted by Hemley *et al.* (1961). The presence of the zeolites within the fissure are also indicative of the silica saturation of fluids and secondly, the abundance of Na and Ca relative to K in the system. The absence of K may be attributed to the initial low K content of the rocks in the area, the low temperature of the circulating fluid relative to that of other geothermal systems and the incorporation of K in an acid zone of mica formation at depth.

The chemistry of the thermal solutions is, in turn, partially dependent on a third factor which influences the mineralogy of the alteration products, the chemistry of the wallrock. The high Mg concentration in the thermal solutions reflects the abundance of Mg-rich basaltic tuffs and scoria in the basalt unit which crops out over most of the Pathé zone.

The wallrock alteration provides examples of both the influence of the mineral chemistry of the source rock in determining alteration products and the overriding of this factor by the chemical environment. The development of illite and illite-montmorillonite within the rhyolite unit in well 5 results from the local redistribution of K derived from the alteration of sanidine. In associated veins at the same temperatures within the rhyolite unit montmorillonite is stable as a result of the chemistry of the thermal solutions.

The interplay of temperature, source rock, and chemical environment evident in the Pathé geothermal system is not restricted to hydrothermal alteration associated with geothermal systems. Considerable

research interest within the petroleum industry is at present concerned with the diagenesis of marine sediments, which involves mineral transformations occurring through a temperature range similar to that encountered at Pathé. Much of the present research involves the role of temperature in controlling the transformation of montmorillonite to illite. Caution must be exercised, however, in designating any individual variable as "the controlling factor" in rock alteration or mineral transformation. The present study indicates that a complex interplay of the source rock, temperature and solution chemistry controls the mineral transformation in the Pathé geothermal zone. Similar relationships are to be expected in any other low temperature, rock alteration environment.

#### SELECTED REFERENCES

- Allen, E. T., and Day, A. L., 1935, Hot Springs of the Yellowstone National Park: Carnegie Institute Washington Pub. 466, 525 p.
- Brown, George, ed., 1961, The x-ray identification and crystal structures of clay minerals: London, Mineralog. Soc., 544 p.
- Burst, J. F., 1969, Diagenesis of Gulf Coast clayey sediments and its possible relation to petroleum migration: Amer. Assoc. Petroleum Geologists Bull., v. 53, pp. 73-93.
- Coombs, D. S., 1955, X-ray observations on Wairakite and non-cubic analcime: Mineral Mag. 30, pp. 699-708.
- Craig, Harmon, Boato, Giovanni, and White, D. E., 1956, Isotopic geochemistry of thermal waters chap. 5 of Nuclear processes in geologic settings: Natl. Research Council Comm. Nuclear Sci., Nuclear Sci. Ser. Rept. 19, pp. 29-38.
- de Anda, Luis F., Septien, J. I., Elisondo, J. R., 1961, Geothermal Energy in Mexico: U. N. Conf. on New Sources of Energy, Agenda Item IIA.1, G. 77.
- de Cserna, Zoltan, 1961, Tectonic Map of Mexico: Geol. Soc. of America, scale, 1:2,500,000.
- Deer, W. A., Howie, R. A., and Zussman, J., 1967, Rock Forming Minerals, v. 1: Longmans, Green and Co., Ltd., London, 333 p.
- Ellis, A. J., and Mahon, W. A. J., 1964, Natural hydrothermal systems and experimental hot-water/rock interactions: Geochim. et Cosmochim. Acta, v. 28, pp. 1323-1357.
- \_\_\_\_\_, and Wilson, S. H., 1960, The geochemistry of alkali metal ions in the Wairakei hydrothermal system: N. Z. J. Geol. Geophys., v. 3, pp. 593-617.
- Espinosa, H. A., 1961, La Energia Geothermal en Mexico: Bol. de Federal Comisión de Electricidad, 133 p.

- \_\_\_\_\_, de Anda, L. F., and Mooser, F., 1964, Focos Termales en la Republica Mexicana: Bol. de la Asoc. Mexicana de Geologos Petroleros, v. XVI, pp. 145-152.
- Esquivel, J., and Zamora, S., 1958, Informe Sobre Minerales no Metalicos: Consejo de Recursos Naturales no Renovables, Bol. 44, 226 p.
- Fenner, C. N., 1936, Bore-hole investigations in the Yellowstone Park: Jour. Geology, v. 44, p. 225-315.
- Fournier, R. O., and Rowe, J. J., 1966, Estimation of underground temperatures from the silica content of water from hot springs and wet-steam wells: Amer. Jour. Science, v. 264, pp. 685-697.
- Fyfe, W. S., Turner, F. J., and Verhoogen, J., 1958, Metamorphic reactions and metamorphic facies: Geol. Soc. of America, Mem. 73, p. 175.
- Garrels, Robert M., and Christ, Charles L., 1965, Solutions, minerals, and equilibria: New York, Harper and Row, 450 p.
- Geyne, A. R., Fries, Carl Jr., Segerstrom, Kenneth, Black, R. F., and Wilson, I. F., 1963, Geology and mineral deposits of the Pachuca-Real Del Monte district, state of Hidalgo, Mexico: Consejo de Recursos Naturales no Renovables, Pub. 5 E, 203 p.
- Hemley, J. J., Meyer, Charles, and Richter, D. H., 1961, U. S. Geol. Sur. Prof. Paper 424-D.
- Keller, W. D., and Hanson, Robert F., 1967, Hydrothermal alteration of a rhyolite flow breccia near San Luis Potosi, Mexico, to refractory kaolin: Clays and Clay Minerals, v. 16, pp. 223-229.
- \_\_\_\_\_, 1969, Hydrothermal argillation of volcanic pipes in limestone in Mexico: Clays and Clay Minerals, v. 17, pp. 9-12.
- Khitarov, N. I., and Pugin, V. A., 1966, Behavior of montmorillonite under elevated temperatures and pressures: Geochemistry Internat., v. 3, pp. 621-626.
- Kiss, Klara, and Page, Harold T., 1968, Electron microscopic identification of single crystals of wairakite, a rare component in clays: Clay and Clay Minerals, v. 17, pp. 31-35.
- Kostov, I., 1960, Composition and paragenesis of the zeolitic minerals: Rept. 21st Internat. Geol. Congress, Norden, Part 17, p. 122.
- Krauskopf, Konrad B., 1956, Dissolution and precipitation of silica at low temperatures: Geochim. et Cosmochim. Acta, v. 10, pp. 1-26.

- Lipman, Peter W., 1969, Alkalic and theolitic basaltic volcanism related to the Rio Grande Depression, southern Colorado and northern New Mexico: *Geol. Soc. America Bull.*, v. 80, pp. 1343-1354.
- Loughnan, F. C., 1969, Chemical weathering of the silicate minerals: Elsevier, 154 p.
- Miller, J. P., 1952, A portion of the system calcium carbonate-carbon dioxide-water with geological implications: *Amer. Jour. Science*, v. 250, pp. 161-203.
- Molnar, Peter and Sykes, Lynn R., 1969, Tectonics of the Caribbean and Middle America regions from focal mechanisms and Seismicity: *Geol. Soc. America Bull.*, v. 80, pp. 1639-1684.
- Mooser, F., and Maldonado-Koerdell, M., 1967, Mexican National Report on Volcanology, presented to the XIVth General Assembly of the International Union of Geodesy and Geophysics, Zurich, Sept. 26-Oct. 7, 1967. *Anales del Instituto de Geofisica, UNAM*, v. 12, pp. 99-106.
- \_\_\_\_\_, Nairn, A., and Noltemier, H., 1970, Origen probable de la Faja Volcanica Transmexicana: Programa General Y Resumenes, *Soc. Geol. Mexicana Conv. Nacional*, 12 May, 1970, Oaxaca, Mexico, pp. 64-65.
- Muffler, L. J. Patrick, and White, Donald E., 1969, Active metamorphism of Upper Cenozoic sediments in the Salton Sea Geothermal Field and the Salton Trough, Southeastern California: *Geol. Soc. America Bull.*, v. 80, pp. 157-182.
- Nichols, C. R., and Pomade, B., 1970, Estructura del Campo Geotermico de Pathé, Hgo.: Programa General Y Resumenes, *Soc. Geol. Mexicana Conv. Nacional*, 12 May, 1970, Oaxaca, Mexico, pp. 70-71.
- Nockolds, S. R., 1954, Average chemical compositions of some igneous rocks: *Geol. Soc. America Bull.*, v. 80, pp. 1007-1032.
- Ross, C. S., and Hendricks, S. B., 1945, Minerals of the montmorillonite group: *U. S. Geol. Sur. Prof. Paper 205B*, 79 p.
- \_\_\_\_\_, and Smith, R. L., 1961, Ash-flow tuffs; their origin, geologic relations, and identification: *U. S. Geol. Sur. Prof. Paper 366*, 81 p.
- Rowland, R. A., Weiss, E. J., and Bradley, W. F., 1956, Dehydration of monoionic montmorillonites: *Clays and Clay Minerals*, v. 4, pp. 85-95, *Natl. Acad. Science-Natl. Research Council Pub.*

- Segerstrom, Kenneth, 1961, Geologia del suroeste del Estado de Hidalgo y del noreste del Estado de Mexico: Asoc. Mexicana Geologos Petrol., Bol., v. 13, pp. 147-168.
- \_\_\_\_\_, 1962, Geology of south-central Hidalgo and northeastern Mexico, Mexico: U. S. Geol. Sur. Bull. 1104C, pp. 87-162.
- Siever, Raymond, 1962, Silica solubility 0° - 200° C, and the diagenesis of siliceous sediments: Jour. Geol., v. 70, pp. 127-150.
- Simons, F. S., and Mapes-Vazquez, Eduardo, 1956, Geology and ore deposits of the Zimpan mining district, State of Hidalgo, Mexico: U. S. Geol. Sur. Prof. Paper 284, 128 p.
- Steiner, A., 1967, Clay minerals in hydrothermally altered rocks at Wairakei, New Zealand: Clays and Clay Minerals, 1968, v. 16, pp. 193-213.
- Stirling, Matthew W., 1969, Solving the mystery of Mexico's great stone spheres: National Geographic, v. 136, No. 2, 1969, pp. 295-300.
- Turner, F. J., and Verhoogen, Jean, 1951, Igneous and metamorphic petrology: New York, McGraw-Hill Book Co., 602 p.
- White, Donald E., 1968, Hydrology, activity and heat flow of the Steamboat Springs thermal system, Washoe County, Nevada: U. S. Geol. Sur. Prof. Paper 458C, 109 p.
- \_\_\_\_\_, Brannock, W. W., and Murata, K. J., 1956, Silica in hot-spring waters: Geochim. et Cosmochim. Acta, v. 10, pp. 27-59.
- Wilshire, H. G., 1958. Alteration of olivine and orthopyroxenes in basic lavas and shallow intrusions: Amer. Min., v. 43, p. 120.
- Wilson, B. W., Hernandez, J. P., and Meave-Torrescano, Eduardo, 1955, Un banco calizo del Cretacico en la parte oriental del Estado de Queretaro, Mexico: Soc. Geol. Mexicana, Bol., v. 18, pp. 1-10.
- Wise, Wm. S., Geology and petrology of the Mt. Hood area: A study of High Cascade volcanism: Geol. Soc. America Bull., v. 80, pp. 969-1006.
- Zen, E-An, 1961, The zeolite facies; an interpretation: Amer. Jour. Science, v. 259, pp. 401-409.

## APPENDIX A

### ANALYTICAL TECHNIQUES

#### Sample Preparation

A total of 210 samples collected from outcrops, mines and cores were examined utilizing equipment of the X-ray Laboratory, School of Geology and Geophysics, University of Oklahoma. Sample locations are shown in Figure 2 and sample descriptions are included as Appendix B. All argillized samples were routinely prepared for analysis by x-ray diffraction.

Ten gram portions of the samples were first hand ground in an agate mortar and pestle to pass a 200 mesh screen. The ground sample was then homogenized and sprinkled through an 80 mesh screen onto a glass slide smeared with a thin coating of petroleum jelly. These powder-coated glass slides were then utilized as sample holders for obtaining bulk, randomly oriented x-ray diffraction patterns.

If phyllosilicate phases were indicated by the bulk powder patterns (00) oriented slides were prepared by sedimentation. A split of the sample was first dispersed in distilled water by a Powertron Ultrasonic autasonic generator. The less-than-four-micron fraction for each sample was removed by fluid withdrawal based upon Stokes' Law

(Folk, 1965, p. 40). Suspensions of the clay fractions were evaporated onto glass slides at a temperature of 65° C.

Samples which yielded 14 Å reflections or reflections intermediate between 10 and 14 Å were exposed to ethylene glycol vapor at a temperature of 65° C for eight hours as a test for expansion.

Splits of 33 samples were prepared for quantitative chemical analysis by x-ray fluorescence. Four-gram portions of the samples which had been ground to pass 200 mesh screens were combined with one gram of polyvinyl alcohol binder to yield a mixture containing 80 percent sample. These mixtures were pressed into briquettes at approximately 15 tons/in<sup>2</sup> pressure. Standard samples obtained from the United States Geological Survey and Bureau of Standards were prepared in the same fashion for use as standards.

#### X-ray Diffraction

A North American Phillips (Norelco) diffraction unit operated at 40 KV and 20 ma was employed in the routine examination of the bulk powder patterns. A Siemens-Halske diffraction unit operated at 35 KV and 18 ma was utilized in the examination of sedimented and solvated slides. The nickel-filtered Cu (K-alpha) radiation generated by both units was detected with scintillation counters. A scanning rate of 1° 20 per minute was used with both units. Constant scale factor and multiplier settings (1 x 8 x 1) were used on the Norelco unit in the examination of the bulk powder pattern to facilitate the comparison of mineral abundance in a semi-quantitative manner.

X-ray Fluorescence

Nine core samples and 24 samples from the surface and mines were selected for chemical analysis by x-ray fluorescence. Analyses were obtained utilizing a Siemens-Halske sequential x-ray fluorescence spectrometer, model SRS-1. A Cr tube, gas flow proportional counter and vacuum path of less-than-100 microns was utilized for the analyses of calcium and lighter elements. A Tungsten tube and scintillation counter were utilized for the excitation and detecting Ti, Mn and Fe.

Acceptable totals (98.5-101.0 percent) were obtained for the 14 relatively unaltered samples. The 19 samples which contained appreciable amounts of hydrated clays or zeolites yielded totals over 101 percent, with the average approximately proportional to their degree of hydration. Wise (1969) has noted the "dewatering" which occurs when hydrated samples are subjected to the vacuum conditions utilized in x-ray fluorescence. He assumes that analyses performed with a vacuum yield totals equivalent to samples in a "dried" state without their  $H_2O^-$ , or low temperature ( $110^\circ-115^\circ$  C) water loss. If the  $H_2O^-$  values for the hydrated samples are subtracted from the totals for samples over 101 percent acceptable totals are obtained. Hydrated samples in the present investigation were recalculated to total 100 percent with the  $H_2O^-$  value obtained by heating at  $110^\circ$  C for 8 hours included in the total. Ignition loss was obtained by firing samples to  $1000^\circ$  C after determining  $H_2O^-$  values by heating at  $100^\circ$  C for 8 hours.

## APPENDIX B

### SAMPLE DESCRIPTIONS AND LOCATIONS

The location of 116 samples collected from the mines and outcrops at Pathé are shown in Figure 2. The locations of the five diamond cored exploration wells (4, 5, 8, 9, and 11) are given in Figure 2. Surface and mine samples have "M" designations and core samples are designated by a well number followed by a depth in meters.

#### Sample Descriptions, Federal Comisión de Electricidad Cores

All core samples were collected from 5.5 and 2.5 cm diameter cores provided by the Federal Comisión de Electricidad. Cores are 5.5 cm unless noted otherwise. The cores were obtained during the period 1956-1959 and are presently stored at the Pathé camp where they were described and sampled by the author during February, 1968. Well locations are shown in Figure 2. Logs of the lithology and alteration product mineralogy are shown in Plate XIV.

#### Sample Description Format

Well number and sample depth (thin section number, if different from well and depth notation)

- I. Rock name
  
- II. Hand specimen description
  - A. Color
  - B. Fabric
  - C. Mineralogy

- III. Thin section description
  - A. Fabric
  - B. Mineralogy: (Minerals described in order of decreasing abundance)
- IV. Remarks: supplemental x-ray diffraction, chemical and electron microscope data, recorded temperature, etc.

## Well 4

4-9

- I. Bentonite
- II. A. Tan with red-brown hematite staining.
- B. Clastic volcanic texture. Relic ash shards averaging 1 mm in diameter in a finer clay groundmass. Hematite-staining localized on bedding surfaces, other primary features obscured by argillation.
- C. Montmorillonite with minor hematite.
- IV. XRD indicates a pure montmorillonite. Oxidization is restricted to the top 19 m of the core. Argillation of the ash decreases downward, indicating alteration probably controlled by the present weathering surface.

4-18

- I. Lithic tuff
- II. A. Red, grey, and purple clasts in a tan groundmass.
- B. Clastic volcanic texture. Angular basalt and subrounded scoria clasts averaging 1 cm in diameter. Within poorly-bedded ash. Blocks and bombs locally present.
- C. Montmorillonite: Argillized ash. Calcite and zeolite: veins.
- III. A. Poorly sorted volcanic clastic texture. Hypocrystalline basalt clasts with plagioclase microlites in a hematite-rich glass.
- B. Clinoptilolite: Sheath-like aggregates in the matrix, amygdular filling in the scoria clasts, and an alteration product of basaltic glass. Montmorillonite: alteration product of plagioclase and ash. Calcite: veinlets within clasts concentrated around the margins of clasts. Plagioclase: microlites, twinning obscured by alteration. Chalcedonic quartz: hematite-staining of basalt and scoria.

- IV. XRD indicates clinoptilolite and montmorillonite as the major phases. Texture of hand specimen is shown in Plate III.

## 4-21.25

- I. Bentonite
- II. A. Tan to light brown.
- B. Fine clastic volcanic texture. Argillized volcanic ash with relic glass shards. Sparse, subrounded, olive-colored clay clasts averaging 2 mm in diameter in a fine argillized matrix.
- C. Montmorillonite as major alteration product of glass shards. Clinoptilolite as cement between clasts. Pyrite present throughout sample as minute, disseminated grains.

## 4-47

- I. Fine lapilli tuff
- II. A. Mottled olive-green and cream.
- B. Clastic volcanic texture. Lapilli average 4 mm in diameter, maximum diameter 10 mm. Lapilli subrounded to rounded, primary textures obscured by argillation.
- C. Montmorillonite: major alteration product of lapilli. Clinoptilolite and calcite: cement. Pyrite: disseminated fine grains.

## 4-65

- I. Fine lapilli tuff
- II. A. Mottled olive-grey.
- B. Clastic volcanic texture. Subrounded to angular lapilli averaging 4 mm in diameter. Moderately well sorted. Matrix of clay and secondary cementing agents. Alteration of lapilli variable, some completely argillized. Some relatively fresh basalt clasts displaying white microphenocrysts in a dark (glass?) matrix.
- C. Montmorillonite: alteration product of lapilli. Yellow-green clay (nontronite?). Calcite and clinoptilolite: cement. Pyrite: euhedral grains.
- IV. Sample is generally similar to 4-47. Argillation is less extensive, and lapilli appear to be well sorted basalt and possibly scoria clasts. Differential reactivity of scoria and basalt may result

in completely argillized and relatively fresh "lapilli".  
Sample is poorly consolidated.

4-87

- I. Fine lithic tuff
- II. A. Purple to yellow-brown clasts in a buff matrix.
- B. Clastic volcanic texture. Subrounded scoria fragments averaging 4 to 5 mm in diameter closely packed in a fine matrix. Fracture surface coated with drusey clinoptilolite and bladed calcite aggregates.
- C. Clinoptilolite and montmorillonite: alteration products of the scoria.

4-94

- I. Basalt breccia
- II. A. Dark grey coarser fragments. Matrix and finer clasts are purple.
- B. Altered basalt (?) lapilli and blocks set in a dense porcelaneous matrix. Poorly sorted. Basalt displays elongated amygdules and near vertical fracturing. Strongly porphyritic with abundant altered mafic phenocrysts averaging 1 to 2 mm in diameter.
- C. Calcite and montmorillonite: amygdule fillings. Iddingsite: alteration product of olivine (?) phenocrysts.
- III. A. Basalt displays intersertal texture with plagioclase microlites averaging 0.1x0.015 mm set in dark glass. Abundant amygdules. Poor fluidal orientation of microlites.
- B. Calcite and zeolite (clinoptilolite?): fracture and cavity fillings. Montmorillonite: hematite-stained.

4-96.2

- I. Argillized basalt breccia
- II. A. Light purple; fractured areas white with yellow staining.
- B. Aphanitic texture obscured by extensive alteration. Sparse mafic phenocrysts averaging 2 mm in diameter. Numerous small fractures and veinlets.
- C. Calcite: in veins. "Iddingsite": alteration of microphenocrysts.

- III. A. Relic intersertal texture.
- B. Plagioclase: laths locally altered to clay and calcite. Clinoptilolite: dominant alteration product of glass and as vein filling.

## 4-125

- I. Lithic tuff
- II. A. Red-brown, orange, grey and purple.
- B. Clastic volcanic texture: graded bedding. Basalt and scoria clasts 2 to 6 mm in diameter.
- C. Calcite and zeolite: fracture coating and cement.
- III. A. Graded volcanic clastic texture. Scoriaceous and hyaloophitic, amygdular basalt clasts in calcite and zeolite cement.
- B. Feldspar: microlites in basalt and scoria. Zeolite (clinoptilolite?) and calcite: veins and cement. Montmorillonite: amygdular filling and an alteration product of glass. Quartz: several 0.3 mm diameter angular grains.
- C. XRD indicates montmorillonite and clinoptilolite. Sample is relatively unaltered and is similar to lapilli tuff collected at several surface locations.

## 4-140.5

- I. Vesicular basalt
- II. A. Grey-purple.
- B. Aphanitic, finely vesicular-zeolite-lined vesicles. average 1 mm diameter. Vertical 2 mm wide calcite veins.
- C. Calcite veins: zeolite vesicle coating. Pyrite associated with fractures.
- IV. Texture of the sample appears similar to the hyaloophitic basalt lapilli common throughout the overlying clastic volcanic section. Vesicular basalt flow is 5 m thick. Montmorillonite and clinoptilolite indicated by XRD.

## 4-149.2

- I. Fractured basalt
- II. A. Grey with green fracture surface.

- B. Aphanitic, exceptionally dense. Slightly porphyritic, with sparse altered olivine (?) phenocrysts averaging 1 mm diameter. Calcite-filled vertical veinlets and "soapy" smooth fracture surfaces.
- C. Calcite and talc: coating on fracture surfaces. "Iddingsite": alteration product of olivine (?) phenocrysts.

IV. Basalt similar to samples described in detail below (4-183).

4-183

- I. Basalt
- II. A. Grey.
  - B. Aphanitic. Talc-coated fracture surfaces with horizontal slickensides.
  - C. Talc and calcite.
- IV. A. Pilotaxitic to intergranular. Plagioclase.
  - B. Plagioclase: microlites average 0.3 mm by 0.03 mm. Locally altered to montmorillonite. Clinopyroxene: abundant subhedral grains averaging 0.02 mm in diameter. Magnetite: abundant, subhedral to anhedral grains averaging 0.15 mm in diameter. Altered to hematite.

4-212

- I. Fractured basalt
- II. A. Mottled red-grey. Green fracture coatings.
  - B. Aphanitic, splotchy iron concentrations.
  - C. Calcite and talc: fracture surfaces. Hematite: horizontal concentrations. "Iddingsite": sparse microphenocrysts averaging 0.8 mm in diameter.
- III. A. Intergranular to glomeroporphyritic.
  - B. Clinopyroxene: anhedral grains with optical continuity averaging 0.03 mm diameter concentrated in aggregates averaging 1.2 mm to 1.4 mm in diameter. Surrounded by anhedral magnetite grains. Plagioclase: microlites and sparse tabular laths averaging 0.4 mm by 0.3 mm. Montmorillonite, with hematite: alteration product ("Iddingsite") of olivine microphenocrysts. Montmorillonite: pleochroic green veinlets.

- IV. Similar basalts are present in the thick basalt unit cored in well 5.

## 4-224

- I. Amygdular basalt
- II. A. Light purple with green amygdular fillings.  
B. Aphanitic, amygdular, average diameter 2 mm, nonporphyritic.  
C. Clay and calcite.
- III. A. Amygdular intergranular to intersertal microporphyritic.  
B. Plagioclase: sparse, zoned phenocrysts averaging 0.3 mm by 0.4 mm and abundant microlites. Clinopyroxene: anhedral grains in groundmass. Magnetite: extensive hematite staining and abundant anhedral grains. Montmorillonite: weakly pleochroic, green to yellow. Clay replaces interior of zoned feldspar. Montmorillonite and chalcedony: amygdular fillings.  
C. XRD indicates clay is a trioctahedral montmorillonite (saponite?).

## 4-230.55

- I. Argillized lapilli tuff
- II. A. Mottled shades of buff to red.  
B. Relic clastic volcanic texture. Subrounded, scoria and basalt lapilli. Compact.  
C. Clay and zeolite: cavity filling in scoria and replacement of finer matrix.
- IV. XRD indicates montmorillonite and clinoptilolite. Sample is from baked contact zone between overlying basalt and underlying clastic volcanic deposit and scoria.

## 4-231

- I. Scoria agglomerate
- II. A. Red-brown, purple and orange clasts.  
B. Lapilli and bombs ranging from 2 cm to greater than core diameter (6 cm). Finely amygdular scoriaceous clasts apparently compressed together in a semi-molten state.
- IV. Coarseness of the bombs indicates a local source.

4-254

- I. Tuff
- II. A. Mottled, light green with cream relic clasts.
- B. Relic clastic volcanic texture. Clasts average 3 mm in diameter.
- C. Pyrite: light green blocky clay with disseminated grains. Quartz: subhedral grains averaging 0.5 mm.
- IV. XRD indicates montmorillonite and quartz. Alteration is quite extensive and sample is crumbly.

4-255

- I. Vitric tuff
- II. A. Cream to light green.
- B. Hypocrystalline, porphyritic.
- C. Quartz: euhedral to subhedral grains averaging 2 mm in diameter. Pyrite: disseminated. Calcite: partially devitrified glass groundmass.
- III. A. Clastic volcanic texture.
- B. Quartz: bipyramidal embayed phenocrysts averaging 2 to 3 mm.

4-261

- I. Basalt
- II. A. Purple-grey.
- B. Aphanitic, nonporphyritic. Fracture zone with fracture planes inclined at an angle of  $45^{\circ}$ .
- C. Calcite and montmorillonite: coating on fracture-surfaces. "Iddingsite": sparse alteration product of mafic grains less than 1 mm in diameter.
- III. A. Intergranular to intersertal texture.
- B. Plagioclase: microlites with poor flow orientation in brown glass. Pyroxene: intergranular anhedral grains .03 by .05 mm in groundmass. Titaniferous magnetite: anhedral grains.

## 4-269

- I. Rhyolite porphyry
- II. A. Mottled light green and pink.
  - B. Relic volcanic clastic texture. 1 to 3 mm clasts of pumice in an aphanitic groundmass. Abundant phenocrysts.
  - C. Quartz: phenocrysts averaging 1 to 3 mm in diameter.
- III. A. Vitrophyric. Glass groundmass with perlitic fractures. Abundant pumice clasts and phenocrysts.
  - B. Quartz: abundant subhedral fractured bipyramidal phenocrysts and minor chalcedony. Sanidine: subhedral fractured phenocrysts.
- IV. This sample represents the upper, partially welded portion of the rhyolite unit.

## 4-296

- I. Rhyolite tuff
- II. A. Light grey-green.
  - B. Volcanic clastic texture. Extensively altered, indistinct lapilli-sized pumice and quartz phenocrysts in a fine matrix.
  - C. Quartz: abundant phenocrysts averaging 1 mm in diameter. Pyrite: fractures and disseminated euhedral grains.

## 4-308

- I. Lapilli tuff
- II. A. Light green with grey clasts.
  - B. Lapilli clasts (pumice?) in fine groundmass.
  - C. Clay and pyrite: green matrix. Calcite: veinlets.
- IV. XRD indicates abundant montmorillonite; argillation is extensive. Core diameter is 2.5 cm.

## 4-309

- I. Andesite (?)
- II. A. Purple.

- B. Amygdular basalt or andesite lava with flow banding.
  - C. Clay and zeolite: amygdular fillings.
- IV. XRD indicates abundant montmorillonite and clinoptilolite.

## 4-327

- I. Lapilli tuff
- II. A. Tan with green to grey clasts.
- B. Clastic volcanic. Angular to subrounded lapilli clasts.
- C. Pyrite and clay: associated with vertical fractures.
- III. A. Clastic volcanic texture. Spherulitic rhyolite clasts total 60 - 70% of slide. Several basalt lapilli.
- B. Montmorillonite and clinoptilolite: alteration products of groundmass and basalt clasts. Quartz: grains averaging 0.2 mm with altered grain-boundaries in rhyolite. Pyrite: cubes and irregular grains.

## 4-377

- I. Lapilli tuff
- II. A. Light green, grey and tan lapilli in white groundmass.
- B. Volcanic clastic. Aphanitic basalt or andesite clasts averaging 6 mm in diameter.
- C. Disseminated pyrite.
- IV. Core diameter is 2.5 cm.

## 4-383

- I. Vesicular basaltic andesite
- II. A. Light grey.
- B. Aphanitic, nonporphyritic, vesicular.
- C. Drusey coating on vesicule surfaces, opal?
- III. A. Pilotaxitic, vesicular.
- B. Chalcedony: vesicules and veinlets. Plagioclase: laths average 0.12 by 0.015 mm. Hematite: concentrated around vesicules. Clinopyroxene: sparse microphenocrysts.
- IV. The maximum recorded temperature was 90° C.

## Well 5

5-45

- I. Basalt
- II. A. Olive grey.
  - B. Aphanitic, nonporphyritic. Horizontal hematite banding.
  - C. Hematite.
- III. A. Intergranular.
  - B. Plagioclase: microlites averaging 0.3 by 0.05 mm. Minor alteration of plagioclase to calcite. Clinopyroxene: anhedral grains averaging 0.03 mm in diameter. Titaniferous magnetite: grains averaging 0.15 mm in diameter and disseminated hematite staining. Minor interstitial calcite.

5-51

- I. Scoriaceous agglomerate
- II. A. Red.
  - B. Pyroclastic. Indistinct scoria clasts in zeolitized matrix.
  - C. Zeolite.
- IV. XRD indicates abundant montmorillonite and clinoptilolite.

5-58

- I. Basalt
- II. A. Grey to purple with green amygdular filling.
  - B. Aphanitic, nonporphyritic, amygdular basalt.
  - C. Clay: greenish amygdular filling.
- III. A. Intergranular, microporphyritic, amygdular.
  - B. Plagioclase: microlites averaging 0.3 by 0.05 mm and sparse microphenocrysts. Clinopyroxene: fine anhedral grains. Hematite: abundant as a replacement of mafic (?) microphenocrysts and as fine anhedral grains. Montmorillonite: amygdular.

5-84

- I. Scoriaceous agglomerate
- II. A. Grey to purple clasts in an orange groundmass.
- B. Coarse clastic texture. Rounded clasts average 3 to 4 cm in diameter. Crowded lapilli in matrix. Clasts are finely amygdular.
- C. Clay and zeolite.

5-123

- I. Basalt
- II. A. Light grey.
- B. Aphanitic, nonporphyritic with banded hematite staining.
- III. A. Intergranular, microporphyritic.
- B. Plagioclase: microphenocrysts with normal zoning average 0.4 by 0.3 mm. Abundant microlites with albite twinning. Clinopyroxene: euhedral grains average 0.03 mm in diameter. Titaniferous magnetite: anhedral grains.

5-135.45

- I. Scoriaceous agglomerate
- II. A. Red-brown.
- B. Coarse clastic texture. Individual clasts almost indistinguishable. Clasts vary from compact to finely vesicular.
- C. Zeolite veins and vesicule linings.

5-144 (#2292)

- I. Lithic tuff
- II. A. Buff.
- B. Pyroclastic. Clasts include pumice, basalt and rhyolite.
- C. Quartz.
- III. A. Clastic texture. Partially welded? Glass shards bent around quartz crystals. Partially collapsed pumice.

- B. Quartz: abundant bipyramidal, embayed phenocrysts averaging 1 mm in diameter. Abundant euhedral to subhedral sanidine and sparse plagioclase. Zeolite and calcite grains in matrix. Hematite-stained basalt clasts.

IV. XRD indicates abundant clinoptilolite.

5-186

- I. Basalt.
- II. A. Grey.
  - B. Aphanitic, nonporphyritic. Vertical veinlets.
  - C. Calcite.
- III. A. Intergranular, microporphyritic.
  - B. Plagioclase: microphenocrysts and microlites. Clinopyroxene: abundant fine anhedral grains. Illmenite: acicular microlites averaging 0.3 mm in length. Montmorillonite: greenish yellow. Abundant as an alteration product of plagioclase.

5-246

- I. Basalt.
- II. A. Grey.
  - B. Aphanitic, nonporphyritic. Slickensided fracture surface.
  - C. Hematite.
- III. A. Microporphyritic, intergranular to intersertal. Poor parallel orientation of acicular illmenite crystallites.
  - B. Plagioclase: altered microphenocrysts averaging 0.7 by 0.2 mm. Pyroxene: abundant fine anhedral grains. Illmenite: acicular crystallites 0.15 mm in length.
- IV. Whole rock K/Ar dates of 6.3<sup>±</sup>0.2 m.y.

5-279

- I. Basalt.
- II. A. Grey.
  - B. Aphanitic, weakly porphyritic.

- III. A. Intergranular? Poor fluidal orientation.
- B. Stubby plagioclase laths averaging 0.4 mm by 0.1 mm. Plagioclase: sparse phenocrysts to 1.3 mm in length. Clinopyroxene: abundant subhedral to anhedral intergranular grains averaging 0.1 mm in diameter. Olivine phenocrysts: 1.3 mm in diameter extensively altered to "Iddingsite" composed of hematite and mica. Magnetite grains.

5-287

- I. Rhyolite tuff.
- II. A. Light purple-grey.
- B. Indurated fine clastic volcanic texture.
- III. A. Clastic volcanic texture. No apparent welding. Indistinct glass shards and accidental clasts of basalt to rhyolite composition. Maximum size of clasts approximately 4 mm.
- B. Quartz: partially resorbed, bipyramidal phenocrysts. Sanidine: fractured and argillized crystals averaging 0.25 mm in diameter.

5-294 (#2293)

- I. Volcanic breccia.
- II. A. Purple clasts in green groundmass.
- B. Coarse volcanic clastic texture. Composition of clasts variable. Andesite and basalt most common. Block-sized clasts present.
- III. A. Poorly sorted volcanic clasts including basalt or andesite, pumice, spherulitic rhyolite, and scoria.
- B. Quartz: common euhedral to subhedral crystals concentrated in rhyolite. Sanidine: euhedral laths 0.7 mm in length common in pumice clasts. Plagioclase: microlites restricted to basalt and andesite clasts. Sparse larger plagioclase laths (An<sub>32</sub> to An<sub>54</sub>) dispersed in matrix. Calcite: amygdular filling in basalt clasts and as alteration product of pumice. Pyrite and magnetite.

5-302

- I. Lapilli tuff.
- II. A. Light and dark green.

- B. Volcanic clastic texture. Pumice lapilli averaging 4mm in diameter.
  - C. Subhedral pyrite grains averaging 5 mm in diameter.
- III. A. Volcanic clastic texture. Glass shards obscured by alteration. Spherulitic rhyolite, siltstone and basalt clasts present in addition to pumice.
- B. Quartz: abundant euhedral to subhedral, embayed, averaging 0.3 mm in diameter. Sanidine: euhedral laths average 0.7 by 0.5 mm in diameter. Calcite: common alteration product of pumice. Zeolite: sparse euhedral crystals. Pyrite: disseminated grains.
- IV. XRD indicates analcite and minor illite (?).

## 5-350.55

- I. Lapilli tuff.
- II. A. Light and dark green with purple clasts.
- B. Poorly sorted clastic volcanic texture. Collapsed lapilli-sized pumice clasts and block-sized angular basalt or andesite clasts.
  - C. Quartz.
- IV. XRD indicates abundant analcite or wairakite and minor amounts of illite-montmorillonite. Scanning electron microscopy indicates altered euhedral zeolite crystals associated with quartz and clay (Plate

## 5-377

- I. Lapilli tuff.
- II. A. Light pink groundmass and green clasts.
- B. Volcanic clastic texture. Pumice clasts and sparse basalt or andesite clasts average 1 cm in diameter.
  - C. Zeolites and quartz crystals.
- IV. XRD indicates abundant analcite or wairakite, abundant quartz and minor feldspar.

## 5-392

- I. Olivine basalt.

- II. A. Mottled grey and red-brown.
- B. Aphanitic, weakly amygdular, nonporphyritic.
- III. A. Glomeroporphyritic texture with associated clusters of pyroxene, plagioclase and magnetite.
- B. Olivine: abundant euhedral phenocrysts of altered to "Iddingsite". Plagioclase: microlites and sparse microphenocrysts. Clinopyroxene: grains average 0.03 mm in diameter. Clusters of grains in glomeroporphyritic masses display common extinction. Titaniferous magnetite: surrounds clinopyroxene concentrations. Calcite and montmorillonite: amygdular fillings.

5-415

- I. Welded tuff.
- II. A. Mottled light and darker green.
- B. Welded clastic volcanic texture. Collapsed pumice fragments averaging 1 cm in length flattened parallel to the bedding plane. Vitric groundmass.
- III. A. Welded texture. Collapsed pumice fragments wrapped around lithic and crystal inclusions.
- B. Quartz: euhedral, embayed phenocrysts averaging 1.5 mm in diameter. Calcite: patches developed as alteration of glass. Sanidine: euhedral microphenocrysts to 1 mm. Interior alteration to clay. Illite(?): green to yellow birefringent clay developed from pumice.
- IV. Texture of rock shown in Plate III (H).

5-430

- I. Basalt.
- II. A. Grey.
- B. Aphanitic, finely vesicular. Vertical fractures.
- III. A. Pilotaxitic to trachytic. Poor fluidal orientation of microlites.
- B. Plagioclase: crowded microlites with subparallel alignment. Pyroxene: anhedral grains. Magnetite: abundant fine grains. Quartz, chalcedony and calcite: fracture filling. Clay: minor illite?

5-448

- I. Felsite.
- II. A. Light green.
- B. Vitric (?) amygduler.
- III. A. Vitric (?). Perlitic fractures in vitric groundmass. Fluidal banding of sparse microlites.
- B. Feldspar: microlites with flow orientation. Quartz: disseminated anhedral grains and chalcedony. Clay and calcite: fracture and amygduler filling.

5-461

- I. Flow breccia.
- II. A. Purple and green.
- B. Brecciated flow-banded.
- III. A. Spherulitic development in flow-banded microcrystalline clasts. Andesite clasts present. Minor perlitic fracturing.
- B. Chalcedony: matrix of flow-rock and vein filling. Feldspar: sparse, extensively altered microlites. Calcite: vein filling and alteration product of microlites. Montmorillonite: associated with chalcedony in spherulites. Chlorite: occurs in matrix of green clasts. Pyrite: disseminated grains.

5-495

- I. Partially welded pumice tuff.
- II. A. Light and dark green.
- B. Welded texture. Pumice, rhyolite and sparse andesite clasts averaging 0.8 mm in diameter in a vitric groundmass. Extensive collapse of pumice.
- IV. Texture is shown in Plate III (E).

5-498

- I. Zeolitized scoria.
- II. A. Purple with white alteration.
- B. Aphanitic, finely vesicular. Alteration extensive.

- C. Zeolite: acicular aggregates developing in scoria.
- IV. XRD indicates Laumontite (Plate XI) and quartz.

## Well 8

## 8-4

- I. Argillized porphyritic basalt.
- II. A. Grey with extensive white alteration.
- B. Porphyritic texture. Slickensides, fracturing, and extensive argillation.
- C. Clay, calcite and zeolite: fracture filling. Plagioclase: phenocrysts in tachylyte.
- IV. XRD indicates major calcite and clinoptilolite, minor montmorillonite and quartz. Calcite is present at shallow depth along the Pathé fault north of the Rio San Juan but absent at the surface.

## 8-7

- I. Argillized porphyritic basalt.
- II. A. Olive grey.
- B. Porphyritic texture. White laths 1 mm in length in tachylyte, extensive fractures and vein development.
- C. Plagioclase: phenocrysts. Quartz and montmorillonite: vein deposit.
- IV. XRD indicates montmorillonite and quartz vein filling.

## 8-9

- I. Basalt.
- II. A. Grey.
- B. Aphanitic, nonporphyritic. Extensive fractures and veins.
- C. Calcite: cellular vein filling.

## 8-13

- I. Basalt.

- II. A. Grey.
- B. Amygdules averaging 1 mm in diameter. White plagioclase phenocrysts to 1 mm.
- C. Clay: amygdules. Plagioclase: phenocrysts.
- III. A. Hyaloophitic, porphyritic. Phenocrysts in black glass.
- B. Plagioclase: stubby laths averaging 0.35 by 0.1 mm with extensive alteration. Calcite and clay: alteration of plagioclase and veinlets. Clay is green-yellow montmorillonite.

8-17

- I. Argillized porphyritic basalt.
- II. A. Light brown.
- B. Aphanitic. Relic phenocrysts 1 mm in length. Extensive vein development with porous, cellular structure. Pyrite: abundant anhedral fracture filling.
- IV. XRD indicates calcite and minor quartz are vein minerals.

8-23

- I. Altered amygdular basalt.
- II. A. Olive-brown.
- B. Argillized porphyritic, amygdular basalt.
- C. Pyrite: abundant anhedral vein filling. Calcite, zeolite and montmorillonite: veins and amygdules.
- III. A. Hyaloophitic, porphyritic amygdular basalt.
- B. Plagioclase: stubby laths 0.75 by 0.4 mm in black glass. Montmorillonite, calcite and zeolite: amygdular filling.

8-32

- I. Argillized basalt.
- II. A. Light green.
- B. Aphanitic basalt. Fracturing extensive.
- C. Clay: vein filling. Pyrite: disseminated grains.
- IV. XRD indicates the clay is dioctahedral montmorillonite.

8-69

- I. Fractured basalt.
- II. A. Olive grey.
  - B. Aphanitic, nonporphyritic. Extensive, near vertical fracturing.
- III. A. Altered hyaloophitic texture.
  - B. Plagioclase: stubby laths locally preserved in less altered areas. Chalcedony: present in larger veins. Mordenite: aggregates of brown, fibrous crystals occur as fracture filling. Clinoptilolite: broad, twinned laths associated with mordenite. Montmorillonite: minor aggregates with chalcedony.

8-97.3

- I. Basalt.
- II. A. Grey.
  - B. Aphanitic, sparsely porphyritic.
  - C. "Iddingsite": sparse phenocrysts averaging 1 mm in diameter.

8-120

- I. Basalt and vein deposit.
- II. A. Tan to grey basalt and pure white vein.
  - B. Aphanitic basalt. Vein is 2 cm thick.
  - C. Chalcedony and clay.
- III. A. Felty texture of basalt obscured by alteration.
  - B. Montmorillonite: spherulitic aggregates replacing basalt and vein filling. Iron-staining of montmorillonite variable depending on proximity to larger veins where it is absent. Quartz: microcrystalline aggregates lining veinlets. Subhedral quartz gradational to chalcedony. Zeolite and calcite: patchy calcite and aggregates of zeolite sheaths present in veins. Plagioclase: relic microlites. Pyrite: vein deposit.
- IV. XRD indicates montmorillonite with exceptionally intense diffraction maxima similar to samples from the Tizpathe mine.

8-136

- I. Rhyolitic tuff.
- II. A. Pink and white.
  - B. Clastic volcanic texture. Partially welded? Pumice clasts average 1 cm in diameter.
- III. A. Clastic volcanic. Abundant spherulites 1 mm in diameter.
  - B. Quartz: subhedral phenocrysts 0.7 mm in diameter and chalcedony in groundmass. Rim alteration of phenocrysts noted. Sanidine: euhedral phenocrysts averaging 0.5 mm. Pyrite: sparse 0.5 mm cubes.

8-140.8

- I. Lapilli tuff.
- II. A. Green with purple lapilli.
  - B. Clastic volcanic texture. Clasts average 1 cm in diameter.
- IV. XRD indicates abundant quartz, common calcite and mixed-layer illite-montmorillonite, and minor clinoptilolite.

8-168

- I. Lapilli tuff.
- II. A. Green and white.
  - B. Clastic volcanic texture. Extensive veining.
  - C. Calcite and chalcedony: vein filling. Pyrite: abundant cubes.
- III. A. Clastic volcanic texture flow-banded rhyolite and pumice clasts.
  - B. Quartz: abundant bipyramidal phenocrysts to 1 mm. Sanidine: euhedral laths 0.7 mm in length. Illite (?): alteration of pumice clasts. Pyrite: cubes 0.1 mm in diameter.

8-178

- I. Rhyolite porphyry.
- II. A. Green and white.
  - B. Aphanitic, porphyritic spherulitic. Vertical clay veins 1.5 cm in width

C. Quartz: phenocrysts to 1 mm. Abundant chalcedony.

IV. XRD indicates clay in veins is montmorillonite.

8-181.5

I. Spherulitic porphyritic rhyolite.

II. A. Grey.

B. Porphyritic, spherulitic.

C. Quartz: phenocrysts to 1 mm in diameter. Pyrite: fracture surface coating.

III. A. Spherulitic.

B. Quartz: embayed, euhedral phenocrysts to 1 mm. Sanidine: sparse euhedral crystals to 1.5 mm. Pyrite: cubes.

8-182.5

I. Basalt.

II. A. Grey.

B. Nonporphyritic.

III. A. Intergranular to glomeroporphyritic. Concentrations of clinopyroxene in plagioclase-free areas.

B. Plagioclase: flow-oriented microlites. Clinopyroxene: disseminated grains and concentrations. Iron ore: anhedral magnetite (?) grains extensively altered to hematite.

Well 9

9-8

I. Spherulitic rhyolite.

II. A. Grey to grey-green.

B. Spherulitic, brecciated. Larger clasts of spherulitic rhyolite in dense chalcedonic matrix.

III. A. Spherulitic.

B. Quartz: subhedral phenocrysts to 1 mm in diameter and chalcedonic matrix. Sanidine: euhedral fractured crystals to 1.5 mm.

- IV. The presence of this rock at the surface within suggests that it is a locally preserved remnant of a younger rhyolitic flow-rock.

9-20

- I. Amygdloidal porphyritic basalt.
- II. A. Purple-grey.
- B. Amygdloidal, porphyritic. Clay and zeolite-filled cavities, tabular feldspar phenocrysts.
- III. A. Hyaloophitic, porphyritic basalt.
- B. Plagioclase: argillized uncrowded laths averaging 2 by 0.5 mm in black glass. Clinoptilolite: interlocking laths in amygdules associated with montmorillonite. Biotite: alteration of mafic minerals.

9-47

- I. Vesicular porphyritic basalt.
- II. A. Grey.
- B. Vesicular, porphyritic texture. Slightly elongate vesicles averaging 1 cm in diameter. Cavities contain bundles of fibrous zeolites (Plate III A).
- C. Feldspar: laths in black glass. Zeolite: vesicular. Pyrite: fine, subhedral grains.
- III. A. Hyaloophitic, porphyritic.
- B. Plagioclase: laths averaging 1.5 mm in length. Alteration of laths not extensive. Mordenite: brown, acicular aggregates in vesicles.

9-59.6

- I. Vesicular basalt.
- II. A. Grey and white.
- B. Vesicular, porphyritic. Vesicles to 2 cm in diameter. Vertical fractures.
- C. Clay, calcite and quartz: vein filling.

- III. A. Hyaloophitic, vesicular, porphyritic.
- B. Plagioclase: lath-shaped phenocrysts to 2 mm in black glass. Relatively fresh.
- IV. XRD indicates calcite, quartz and montmorillonite in veins.

9-63

- I. Fractured vesicular basalt.
- II. A. Grey and white.
- B. Vesicular, porphyritic basalt. White laths 2 mm in length in vesicular black glass. Extensive fracturing and alteration.
- C. Calcite: coarse bladed crystals on fracture surface.

9-75

- I. Lapilli tuff.
- II. A. Red, orange, purple and grey.
- B. Clastic volcanic texture. Angular scoriaceous clasts averaging 5 mm in diameter in calcite matrix.

9-88

- I. Basalt.
- II. A. Grey.
- B. Aphanitic, nonporphyritic. Slickensided fracture surface.
- C. Talc: coating on fracture.

9-100

- I. Scoria.
- II. A. Red.
- B. Finely vesicular. Nonporphyritic. Extensive alteration.
- C. Calcite: veinlets.
- III. A. Holohayline, vesicular. Vesicles 0.1 mm in diameter. Fractured.

B. Zeolite: stubby laths in hematite-stained glass and vesicles. Montmorillonite: patchy alteration of glass. Calcite: vein filling.

IV. XRD indicates trioctahedral montmorillonite, calcite and clinoptilolite.

9-135

I. Basalt.

II. A. Tan.

B. Aphanitic, nonporphyritic. Extensive argillation.

C. Montmorillonite. Pyrite: subhedral grains to 1 cm in diameter.

IV. XRD indicates montmorillonite and clinoptilolite.

9-141

I. Basalt.

II. A. Olive-grey.

B. Aphanitic, nonporphyritic.

III. A. Felt textures. Glomeroporphyritic concentrations of clinopyroxenes. Texture is locally gradational to intergranular.

B. Plagioclase: flow-oriented microlites. Pyroxene: concentrated in areas relatively free of plagioclase microlites. Illite (?): micaceous alteration of plagioclase. Magnetite: euhedral to subhedral grains.

9-167

I. Lithic tuff.

II. A. Grey and white.

B. Clastic volcanic texture. Angular clasts to 3 cm and quartz crystals. Indurated, rock fracture across clasts.

III. A. Clastic volcanic. Clasts of spherulitic rhyolite and pumice tuff.

B. Quartz: euhedral embayed grains averaging 1 mm and small anhedral grains in matrix. Sanidine: subrounded laths averaging

0.7 by 0.3 mm. Magnetite and pyrite: small grains concentrated in rhyolite clasts.

9-175

- I. Altered lapilli tuff.
- II. A. Light green.  
B. Clastic volcanic texture obscured by argillation. Pumice clasts to 1 cm in diameter.
- IV. XRD indicates quartz, clinoptilolite and montmorillonite.

9-184

- I. Tuff.
- II. A. Light green.  
B. Fine clastic volcanic texture. Average is ash-sized.
- IV. XRD indicates quartz, clinoptilolite and montmorillonite.

9-211

- I. Spherulitic rhyolite.
- II. A. Grey.  
B. Spherulitic, porphyritic, aphanitic.  
C. Quartz: phenocrysts.
- III. A. Porphyritic, spherulitic.  
B. Quartz: bipyramidal embayed crystals to 2.5 mm. Sanidine: subhedral laths to 0.75 mm displaying some rim alteration. Albite: altered laths.

9-232

- I. Lapilli tuff.
- II. A. Green.  
B. Altered clastic volcanic texture. Clasts average 6 mm.
- IV. XRD indicates montmorillonite and quartz.

9-260

- I. Lapilli tuff.
- II. A. Mottled, tan, red and green lapilli.  
B. Clastic volcanic texture. Poorly sorted.
- III. A. (Thin section of finer, ash-sized material.) Fine clastic volcanic texture; clasts of rhyolite, pumice and basalt.  
B. Calcite: patchy cement and alteration product. Quartz: subhedral, corroded grains. Plagioclase: microlites in basalt clasts. Montmorillonite: yellow-green.
- IV. XRD indicates montmorillonite, quartz and calcite. Diameter of small core is 2.5 cm.

9-271

- I. Lapilli tuff and vein deposit.
- II. A. White to pink.  
B. Clastic volcanic texture. Vein has coarse cellular structure. Rounded clasts to 2 cm in diameter.
- IV. XRD indicates quartz, montmorillonite and calcite vein filling. Diameter of core is 2.5 cm.

9-274

- I. Scoriaceous agglomerate.
- II. A. Red and purple.  
B. Coarse clastic volcanic texture. Bomb-sized, rounded scoria. Finely vesicular.
- IV. XRD indicates montmorillonite and clinoptilolite.

Well 11

11-2

- I. Basalt.
- II. A. Grey.  
B. Aphanitic, nonporphyritic. Relatively fresh.
- IV. This dense basalt is similar to basalt in well 5.

11-40

- I. Basalt.
- II. A. Grey.
  - B. Aphanitic, nonporphyritic.
- III. A. Intergranular texture.
  - B. Clinopyroxene: abundant fine grains 0.02 mm in diameter.  
Plagioclase: microlites and stubby laths 0.2 mm in length.  
Montmorillonite: patchy fine-grained alteration. Hematite: disseminated throughout slide.

11-78

- I. Scoria.
- II. A. Red and purple.
  - B. Finely vesicular. Rounded bomb-sized fragments.
- III. A. Vesicular, holohyaline, zeolite-filled vesicles average 0.2 mm in diameter.
  - B. Clinoptilolite: sheath-like aggregates with sector twinning.  
Montmorillonite: vesicular filling and vermicular aggregates.  
Calcite: vesicular filling. Hematite: ubiquitous staining.
- IV. XRD confirms abundant montmorillonite and clinoptilolite.

11-83.5

- I. Fractured, veined basalt.
- II. A. Tan basalt and white veins.
  - B. Aphanitic, nonporphyritic texture. Cellular vein rock.
- III. A. Intergranular texture. Bladed vein deposits.
  - B. Calcite: bladed aggregates. Zeolite: laths averaging 0.2 mm in length.
- IV. XRD indicates laumontite and calcite in veins.

11-84

- I. Basalt.
- II. A. Dark grey.

- B. Aphanitic, nonporphyritic texture. Relatively fresh sample. Vertical fracturing.
- III. A. Intergranular with local flow orientation.
- B. Plagioclase: microlites with poor flow orientation. Clinopyroxene: abundant fine grains. Magnetite: abundant subhedral grains.

## 11-114

- I. Felsite.
- II. A. Grey.
- B. Aphanitic. Vertical veinlets.
- C. Calcite and pyrite: vein filling.
- III. A. Flow banded acicular crystallites.
- B. Feldspar: oriented crystallites in iron-stained glass.

## 11-133

- I. Bentonite.
- II. A. Yellow-grey.
- B. Fine clastic volcanic texture. Relic ash shards and clasts to 1 mm. Conchoidal fracture.
- C. Montmorillonite and pyrite.

## 11-134

- I. Vitric lapilli tuff.
- II. A. Pink, with light and dark clasts.
- B. Welded (?) clastic volcanic texture. Collapsed pumice and spherulitic rhyolite clasts to 3 cm in fine ash matrix.
- C. Pyrite: concentrated in individual clasts.
- III. A. Clastic volcanic texture. Collapsed pumice clasts. Rhyolite strongly spherulitic.
- B. Quartz: embayed, subrounded phenocrysts averaging 0.8 mm in diameter. Abundant chalcedony in groundmass. Sanidine:

euohedral to subhedral phenocrysts in pumice clasts. Clay: micaceous alteration product of pumice. Pyrite: localized in individual felsite clasts.

11-140

- I. Lithic vitric tuff.
- II. A. Pink.
  - B. Clastic volcanic texture. Clasts of rhyolite to 3 cm and pumice to 1 cm in dense chalcedonic matrix.
  - C. Quartz: phenocrysts in rhyolite clasts.
- III. A. Clastic volcanic texture. Microporphyrritic rhyolite clasts.
  - B. Quartz: embayed phenocrysts and chalcedony. Sanidine: euohedral phenocrysts to 1 mm in rhyolite and pumice clasts.

11-147

- I. Lapilli tuff.
- II. A. Green.
  - B. Clastic volcanic texture. Lapilli-sized pumice clasts obscured by alteration.
- IV. XRD indicates montmorillonite and quartz.

11-188

- I. Lapilli tuff.
- II. A. Mottled green.
  - B. Relic clastic volcanic texture. Extremely indurated.
- IV. XRD indicates montmorillonite and quartz. Sample is similar to 11-147 (above) and is representative of green tuff zone of the rhyolite unit.

11-198

- I. Rhyolite flow breccia.
- II. A. Green.
  - B. Aphanitic, vitric, brecciated.

- III. A. Vitric, brecciated. Spherulitic groundmass in rhyolite.
- B. Quartz: fractured, embayed, euhedral microphenocrysts to 1 mm. Abundant chalcedony in groundmass. Sanidine: euhedral, relatively fresh phenocrysts to 2 mm.
- IV. This sample is characteristic of the rhyolite flow breccia zone at the base of the rhyolite unit.

Surface and Mine Sample Locations and Descriptions

Sample number (thin section number, if different).

- I. Rock name: location.
- II. Hand specimen description.
  - A. Color.
  - B. Fabric.
  - C. Mineralogy.
- III. Thin section description.
  - A. Fabric.
  - B. Mineralogy.
- IV. Remarks: x-ray diffraction and chemical data.

M-1

- I. Porphyritic basalt: south side of Pathé road, 100 m west of Rio San Juan crossing.
- II. A. Dark grey.
- B. Porphyritic.
- C. Plagioclase phenocrysts averaging 1.5 mm in length.
- III. A. Intersertal texture gradational to hyaloophitic.
- B. Plagioclase: phenocrysts in dark glass. "Iddingsite": sparse phenocrysts after olivine. Clinopyroxene: sparse microphenocrysts and grains in base.

## M-2

- I. Basalt: south side of Pathé road at Rio San Juan crossing.
- II. A. Grey with red-brown staining.
- B. Aphanitic, nonporphyritic.
- C. Hematite: blotchy staining.
- III. A. Intergranular texture: subparallel orientation of microlites.
- B. Plagioclase: microlites with subparallel orientation. Clinopyroxene: fine grains distributed between plagioclase laths. Magnetite: subhedral grains.

## M-3 (same as M-48)

- I. "Blue" montmorillonite: samples "hand-picked" from first 10 m of Santa Rosa entrance shaft.
- II. A. Turquoise or "Robin's egg" blue.
- B. Pure, waxy clay. Derived from altered basalt. Associated with hematite. Clay occurs as 1 cm-thick pods and veinlets within hematite-rich areas.
- IV. XRD indicates a dioctahedral montmorillonite. Chemical analysis shows a higher  $\text{Fe}_2\text{O}_3$  content (0.53%) than "Pathé montmorillonite".

## M-4

- I. Basalt: west side of cobble-stone Pathé road directly west of Pathé cliff.
- II. A. Grey.
- B. Aphanitic, porphyritic.
- III. A. Intersertal to hyaloophitic texture. Porphyritic, plagioclase laths to 2 mm in length.
- B. Plagioclase: zoned phenocrysts and sparse microlites. Clinopyroxene: sparse phenocrysts and fine grains. Tachylyte base.

## M-5

- I. Argillized lapilli tuff. Underlies basalt, M-4.
- II. A. Dark bluish grey.

B. Argillized clastic volcanic texture: lapilli average 8 mm in diameter.

IV. XRD indicates montmorillonite. Sample similar to M-14, El Coh mine.

M-6

I. Porphyritic basalt: see description of M-1. Sample from same lava flow 100 m west of M-1 location at turn in Pathé road.

M-7

I. Vein filling: sample from mine dump, Tizpathe mine.

II. A. White.

B. Bladed vein filling. Porous.

III. A. Cellular structure.

B. Quartz: chalcedony "walls", linear structures of chalcedony bounding triangular, open spaces lined with euhedral quartz crystals perpendicular to the walls. Montmorillonite: fine aggregates as void-filling and replacement of chalcedony and zeolite. Stilbite associated with euhedral quartz.

IV. XRD indicates more abundant stilbite and montmorillonite than was apparent in thin section. Scanning electron microscopy indicates chalcedony probably contains microcrystalline stilbite and montmorillonite.

M-8

I. "Pure" clay: sample from mine dump, Tizpathe mine.

II. A. Pure white.

B. Soapy when damp, breaks with conchoidal fracture when dry.

IV. XRD and scanning electron microscopy indicate the contamination of clay by stilbite and quartz. The montmorillonite is dioctahedral with a high MgO content (Table 3, Cols. 1-4). The intensity of the basal reflections is exceptional and 7 or 8 orders are obtained from oriented slides.

M-9

I. Argillized basalt: sample from the right wall of entrance cut 3 m west of portal, Tizpathe mine.

- II. A. Mottled tan and brown.
- B. Aphanitic, argillized basalt.

## M-10

- I. Argillized basalt: roof of entrance shaft at mine portal, Tizpathe mine.
- II. A. Brown, yellow and white.
- B. Waxy, argillized basalt.
- III. A. Relic pilotaxitic or intergranular texture.
- B. Plagioclase: microlites present in small, less altered areas. Montmorillonite: ubiquitous replacement of basalt. Large areas display parallel extinction.
- IV. XRD indicates abundant montmorillonite, minor feldspar.

## M-11

- I. Kaolinite: north wall, El Coh mine. See sample M-109.

## M-12

- I. Pink kaolinite: active, south face shaft, El Coh mine. Samples M-35 and M-46 are from the same cut.
- II. A. Pink when damp. Faded to a lighter shade when dried.
- B. Slickensided, waxy clay.
- C. Kaolinite: quartz phenocrysts to 2 mm.
- IV. XRD indicates quartz, kaolinite and feldspar. The pink clay from the east face of the cut M-75 is a mixture of kaolinite and montmorillonite.

## M-13

- I. Kaolinite: north face of central, unmined pillar, El Coh mine.
- II. A. White with iron-stained areas.
- B. Porphyritic clay, quartz phenocrysts to 2 mm. Waxy on slickensided surfaces. Clay "gritty" due to quartz content.
- III. A. Argillized clastic volcanic texture similar to M-25.

- B. Quartz: euhedral embayed bipyramidal to subrounded phenocrysts in kaolinized groundmass. Sanidine: fractured, subhedral laths. Kaolinite: extensively developed in matrix.

## M-14

- I. Argillized lapilli tuff: bedded deposits exposed in drainage ditch, south side of south entrance road to El Coh.
- II. A. Dark blue-grey.
- B. Relic clastic volcanic texture.
- IV. XRD indicates a relatively crystalline dioctahedral montmorillonite.

## M-15, M-16

- I. Pathé montmorillonite: Tizpathe mine dump.
- II. A. White.
- B. "Pure" clay.

## M-17

- I. Montmorillonite: mine dump, El Carmen north.
- II. A. White.
- B. Pure, waxy.
- IV. XRD indicates montmorillonite, stilbite and quartz.

## M-18

- I. Chalcedony: mine dump El Carmen north.
- II. A. Light green exterior, white interior.
- B. Dense, aphanitic vein rock.
- IV. XRD indicates pure quartz.

## M-19A and M-19B

- I. Olivine basalt (M-19B) and basalt-derived clay (M-19A). Samples from lava flow 11 m east of Pathé fault at Cerro Grande.
- II. A. Grey basalt and yellow clay.
- B. Porphyritic.

- C. "Iddingsite" phenocrysts to 2 mm in diameter.
- III. A. Porphyritic, pilotaxitic texture: flow-oriented microlites.
- B. Plagioclase: flow-oriented microlites and sparse microphenocrysts. Olivine: phenocrysts completely altered to "Iddingsite". Magnetite: disseminated fine, subhedral grains. Clinopyroxene: fine grains and sparse microphenocrysts.
- IV. Textures of the basalt and clay are shown in Plate X (A and B). Chemical analyses of the rocks are shown in Table 3, Cols. 17 and 18.

## M-20

- I. Silicified tuff: sample from entrance to old mine above Tizpathe.
- II. A. Yellow and white.
- B. Relic clastic texture?
- IV. XRD indicates only crystalline constituent is quartz.

## M-21

- I. Basalt: lava flow on north flank of Cerro Peligroso; sample from highest point of knoll.
- II. A. Dark grey.
- B. Aphanitic, weakly porphyritic.
- C. "Iddingsite" phenocrysts averaging 2 mm in diameter.
- III. A. Intergranular, porphyritic.
- B. Plagioclase: microlites with poor flow orientation and sparse laths. Olivine: phenocrysts with rim alteration to "iddingsite". Clinopyroxene: fine anhedral grains. Magnetite: fine subhedral grains.
- IV. Olivine alteration shown in Plate V (A).

## M-22

- I. Lapilli tuff: sample from top clastic bed in arroyo, north slope of Cerro Peligroso. The bed underlies the basalt, sample M-21.
- II. A. Red.
- B. Clastic volcanic texture. Coarse scoria and basalt lapilli.
- IV. XRD indicates montmorillonite and clinoptilolite.

## M-23

- I. Lapilli tuff: sample from lower clastic bed, north slope of Cerro Peligroso.
- II. A. Yellow.
- B. Clastic volcanic texture: fine basaltic lapilli. Relatively fresh.
- IV. XRD indicates montmorillonite and clinoptilolite.

## M-24

- I. Argillized rhyolite porphyry: north slope of Cerro Peligroso. Underlies volcanic section represented by M-21, 22 and 23.
- II. A. Cream to grey.
- B. Spherulitic, porphyritic with quartz phenocrysts to 2.5 mm.
- IV. Exterior of large sample is silicified. The interior is argillized. XRD indicates montmorillonite as the alteration product.

## M-25

- I. Rhyolite porphyry: southwest flank of Cerro Peligroso.
- II. A. Pink to cream.
- B. Spherulitic, porphyritic textures. Sparse, relatively fresh lithic clasts.
- C. Quartz: phenocrysts and chalcedony in matrix. Feldspar: fine microlites and sanidine phenocrysts.
- IV. Texture of M-25 is similar to sample from El Coh mine, M-13. Contorted, near vertical flow-banding and argillized surfaces of Cerro Peligroso indicate the intrusive nature of the rhyolite, its subsequent erosion, and later silicification. K/Ar dates from sanidine separations of 6.6 and 6.7 ± 0.1 m. y. were the oldest obtained from the Pathé zone.

## M-26

- I. Yellow lapilli tuff: sample from badlands 100 m north of Rancho San Juanita. See sample description for sample M-23.

## M-27

- I. Red lapilli tuff: sample from badlands 100 m north of Rancho San Juanita. See sample M-22 for description.

## M-28

- I. Vein filling: sample from small vertical fracture 100 m north of Rancho San Juanita.
- II. A. Purple and green.  
B. Aphanitic.
- IV. XRD indicates only quartz.

## M-29

- I. Lapilli tuff: lower unit of "The Knob", an erosional remnant overlying the basalt unit 1 km west of El Coh mine. Sample from basal unit on east flank.
- II. A. Tan.  
B. Clastic volcanic texture. Bedded impure pumice and silty ash.
- IV. XRD indicates minor montmorillonite.

## M-30

- I. Silty tuff: sample from top unit of "The Knoll" sampled at south end of hill.
- II. A. Dark brown.  
B. Clastic volcanic texture. Lacustrine deposit? Poorly sorted clasts of pumice and ash (?) in an organic-rich, silty matrix.

## M-31

- I. Basalt: sample from top of 5 m fault scarp, 100 m south of the knoll.
- II. A. Light grey.  
B. Aphanitic, nonporphyritic. Pillow lava present near base of scarp.

## M-32

- I. Basalt: sample from lava capping bluff, north bank of Rio San Francisco, due south of the knoll.
- II. A. Grey.

- B. Aphanitic, nonporphyritic.
- C. "Iddingsite": sparse microphenocrysts to 1 mm.

## M-33

- I. Lapilli tuff: sample from head of arroyo, 100 m southwest of El Coh mine.
- II. A. Red, brown and tan.  
B. Clastic volcanic texture: well sorted scoria and basalt clasts averaging 1 cm in diameter in clay-zeolite cement. Graded bedding.
- IV. XRD indicates abundant montmorillonite and minor calcite and clinoptilolite.

## M-34

- I. Argillized lapilli tuff: sample from east wall of El Coh mine. See M-73 for description.

## M-35

- I. Pink kaolin: sample from south wall of El Coh mine: see M-12 for description.

## M-36

- I. Kaolin and pyrite: sample from fault zone, north wall of El Coh. See sample M-109 for description.

## M-37

- I. Argillized coarse lapilli tuff: west wall of El Coh #2.
- II. A. Tan and cream.  
B. Relic coarse clastic volcanic texture. Clasts differentially altered. Sample 2 m below present surface.
- IV. XRD indicates subequal montmorillonite and kaolinite.

## M-38

- I. Altered amygdular basalt: sample from prospect pit 50 m southeast of south end of generator plant.

- IV. A. Light green.
- B. Altered amygdular basalt. Abundant spherical amygdules averaging 1 to 2 mm in diameter with larger cavities to 6 mm.
- III. A. Relic hyaloophitic texture?
- B. Montmorillonite: alteration of plagioclase laths and amygdular filling. Zeolite: aggregates of laths in centers of amygdules. Calcite: patchy alteration of plagioclase. Chalcedony: associated with zeolite in interiors of amygdules.
- IV. Scanning electron micrographs reveal arcuate montmorillonite flakes surrounded by stilbite in an amygdule (Plate XI, B).

## M-39

- I. Altered basalt: depth of 7 m in vertical entrance shaft, Tizpathe west.
- II. A. Pure white and light green.
- B. Extensively argillized, original texture destroyed.
- IV. XRD indicates clinoptilolite, montmorillonite and plagioclase.

## M-40

- I. Bentonite: sample from bed capping hill west of well 3.
- II. A. Tan.
- B. Altered. Blocky texture. Original texture of clastic volcanic rock obscured by weathering and/or hydrothermal alteration.
- IV. XRD indicates relatively pure montmorillonite with minor quartz.

## M-41

- I. Clay: depth of 8 m in vertical entrance shaft, Tizpathe-west.
- II. A. White and green.
- B. Boxwork of clay and chalcedony.
- C. Montmorillonite: pure fist-sized pieces. Chalcedony: porous vein deposit. Pyrite: minor disseminated grains in green portions of sample.

- IV. XRD of pure clay indicates montmorillonite with exceptionally strong diffraction maxima and minor quartz and chalcedony.

## M-42

- I. Rhyolite felsite: sample from vertical north-south trending, 1 m wide dike in windgap at north end of main valley, Campo de Pathé.
- II. A. Banded shades of red, cream, and grey.  
B. Flow-banded, aphanitic, vitric.
- IV. XRD indicates quartz and minor feldspar. Sample is similar to T2-1 above well 3 on same fault.

## M-43

- I. Vein deposit: sample from the entrance portal of first mine north of the ford of the Rio San Juan. Mine is southernmost of series of mines working the Pathé fault north of the river.
- II. A. Pink to white clay and white vein rock.  
B. Cellular vein deposits, blocky clay.
- IV. XRD indicates dioctahedral montmorillonite and quartz. Fluorite has been reported from this shaft (de Pablo, personal communication, 1968).

## M-44

- I. Vein deposit: sample from main shaft of "Bat cave" 20 m east of mine entrance at first intersection with north-south drifts. Overhead sample. "Bat cave" is second mine north of Rio San Juan on Pathé fault.
- II. A. White.  
B. Cellular vein filling.
- IV. XRD indicates calcite with minor gypsum, montmorillonite and quartz.

## M-45

- I. Alum crystals: entrance portal to Tizpathe-west. See description of sample M-51.

## M-46

- I. Pink kaolin: south face of El Coh mine. See M-12 for description.

## M-47

- I. Brown montmorillonite: sample from older filled mine shaft cut by present working of south face, El Coh mine. Montmorillonite derived from overlying argillized basaltic lavas and ash. See sample M-14.

## M-48

- I. "Blue" montmorillonite: larger sample from Santa Rosa mine identical with M-3.

## M-49

- I. Clay and vein deposits: "hot" sample from steam-bearing fissure in Tizpathe mine. Temperature of sample when collected, 95° C.
- II. A. White.  
B. Porous, cellular vein rock.  
C. Chalcedony: chief constituent of cellular structure. Montmorillonite: associated with chalcedony and in small pure lenses.
- IV. XRD indicates montmorillonite with abnormally intense basal reflections. See sample M-7 for description of similar vein filling.

## M-50

- I. Clay: "hot" sample from 3 cm vein in Tizpathe-west mine. Collected from intersection of east-west trending entrance shaft with vertical fissure.
- II. A. White.  
B. Featureless, plastic clay.
- IV. XRD indicates dioctahedral montmorillonite and minor quartz. Sample similar to M-8.

## M-51

- I. Alum crystals: handpicked from entrance portal to Tizpathe-west mine. Crystals growing on damp, altered-basalt surface.

- II. A. White.
- B. Acicular crystals to 1 cm in length.
- IV. XRD indicates a sulfate of the intermediate jarosite-natrojarosite type.

## M-52

- I. Wallrock: sample from west wall of north-south fissure being mined in Tizpathe-west mine.
- II. A. Black outer coating on white to tan vein rock.
- B. Zoned or banded vein rock with cellular structure.
- III. A. Banded. Cellular.
- B. Towards center of fissure montmorillonite and chalcedony grade into stilbite and then to gypsum. Chalcedony and montmorillonite: intimately associated in dense aggregates. Stilbite: 1 cm thick band of fine laths. Gypsum: coarse bladed aggregates most recently formed. Fluorite: veinlet 1 mm in width.

## M-53

- I. Wallrock: east wall of north-south fissure at point of intersection with entrance shaft, Tizpathe-west mine.
- II. A. Green and white.
- B. Coarsely cellular.
- C. Gypsum: bladed aggregates, relatively pure.

## M-54

- I. Clay: mine dump, Tizpathe-west mine.
- II. A. White.
- B. Fist-sized lump of pure clay.
- IV. XRD indicates minor quartz.

## M-55

- I. Basalt and derived clay: mine dump, Tizpathe-west mine.

- II. A. Grey basalt and white clay.
- B. Spheroidal alteration of fist-sized basalt clast. Grey basalt surrounded by concentrically banded clay.

## M-56

- I. Basalt and derived clay: mine dump, Tizpathe-west mine.
- II. A. Grey basalt and white clay.
- B. Spheroidal alteration similar to M-55, but pyrite and bornite coat one fractured surface of the basalt.

## M-57

- I. Vein rock: surface sample from collapsed mine entrance, vertically above intersection of present inclined Tizpathe-west shaft with north-south fissure.
- II. A. Banded light green, yellow and white.
- B. Banded vein deposit. Vertical, 5 mm wide veinlets.
- IV. XRD indicates gypsum, fluorite, and minor chalcedony.

## M-58

- I. Basalt: Tecozautla-Huichipan road. Lava capping high hill, 3 km east of Pablada de San Francisco.
- II. A. Black.
- B. Aphanitic, nonporphyritic.
- C. No alteration observed.
- IV. Sample is fresher than any at Pathé. Lavas of probable Pliocene age.

## M-59

- I. Basalt: top of fault scarp, southern edge of El Coh mine claim.
- II. A. Grey.
- B. Aphanitic, nonporphyritic.
- C. Iddingsite: sparse microphenocrysts to 1 mm.

## M-60

- I. Lapilli tuff: bedded exposure at head of arroyo on south flank of hill west of well 3.
- II. A. Mottled pink and cream.
- B. Clastic volcanic texture. Lapilli-sized clasts of basalt and andesite. Zeolite cement.
- IV. XRD indicates abundant clinoptilolite. Sample is relatively fresh.

## M-61

- I. Lapilli tuff: El Carmen mine entrance. Overhead sample from soil zone.
- II. A. Mottled red and brown.
- B. Clastic volcanic texture: angular basalt and scoria lapilli to 1.5 cm, closely packed.
- IV. XRD indicates dioctahedral montmorillonite and calcite.

## M-62

- I. Lapilli tuff: El Carmen mine shaft, horizontal distance of 19 m west of mine entrance.
- II. A. Tan.
- B. Clastic volcanic texture partially obscured by alteration. Clasts clearly visible.
- IV. XRD indicates dioctahedral montmorillonite and minor clinoptilolite.

## M-63

- I. Argillized tuff: El Carmen mine shaft, horizontal distance from entrance 38 m. 10 m east of fissure.
- II. A. Light green.
- B. Compact. Alteration has obscured texture.
- C. Pyrite: disseminated grains.
- IV. XRD indicates mixed dioctahedral and trioctahedral montmorillonite.

## M-64

- I. Wallrock: 5 m east of Pathé fault, El Carmen mine.
- II. A. Green.
- B. Argillized. Original texture masked.
- C. Pyrite: disseminated grains.
- IV. XRD indicates dioctahedral montmorillonite and chalcedony.

## M-65 and M-66

- I. Pure clay (M-66) and associated vein rock (M-65): Samples from west wall of mine at intersection of entrance shaft with fissure.
- II. A. Banded white to reddish brown.
- B. Zoned wallrock. Parallel 1 cm thick alternating bands of porous and dense vein rock.
- IV. XRD indicates pure clay (M-66) and chalcedony (M-65). Clay development here is not extensive. Vein widens to the north.

## M-67

- I. Silicified tuff: road cut 40 m west of El Carmen entrance. Directly above Pathé fault.
- II. A. Light pink.
- B. Aphanitic. Texture obscured by alteration.
- IV. Silicification of tuff complete: chemical analysis (Table 3, Col. 14) indicates 83.6% SiO<sub>2</sub>.

## M-68

- I. Basaltic lapilli tuff: sample from slope 30 m east of well 12. Exposure of tuff is 28 m thick.
- II. A. Red and red-brown.
- B. Clastic volcanic texture: relatively fresh, angular basalt and scoria lapilli with graded bedding. Clasts grade from 2 mm to 2 cm in vertical distance of 8 cm. Dip of beds is 35° W. Strike is north-south paralleling the Pathé fault.
- IV. XRD indicates montmorillonite, calcite and clinoptilolite.

## M-69

- I. Vesicular basalt: caps 28 m section of lapilli tuff described for M-68.
- II. A. Dark grey.
- B. Coarsely vesicular, porphyritic basalt. Elongate cavities averaging 1 cm in length.
- C. Plagioclase: laths averaging 1 mm in length.
- IV. Lava flow grades upward into non-vesicular basalt.

## M-70

- I. Altered basalt: west wall of drainage ditch at north end of main valley. Point where rhyolite felsite dike parallels the ditch.
- II. A. Grey and white.
- B. Texture of basalt obscured.
- IV. XRD indicates calcite and dioctahedral montmorillonite.

## M-71

- I. Argillized tuff: east face El Coh mine. 25 cm below surface, above hanging wall of fault.
- II. A. White.
- B. Extensive argillation. Texture obscured.
- IV. XRD indicates kaolinite.

## M-72

- I. Argillized tuff: east face El Coh mine. Depth below surface 75 cm.
- II. A. Orange.
- B. Relic lapilli-sized basalt or scoria clasts.
- IV. XRD indicates kaolinite, trace of montmorillonite.

## M-73

- I. Bedded lapilli tuff: east face El Coh mine, 1.5 m below surface.

- II. A. Banded white and red.
- B. Altered volcanic clastic texture. Alternating hematite-rich and hematite-free areas paralleling bedding surfaces.

IV. XRD indicates montmorillonite and kaolinite.

M-74

I. Lapilli tuff: east face, El Coh mine. Sample from mottled zone 1.75 m below surface.

II. A. Mottled white and red.

B. Clastic volcanic texture. Borders of clasts obscured.

IV. XRD indicates montmorillonite.

M-75

I. "Pink" kaolin: east wall of El Coh. Sample from depth of 3 m, below hanging wall of fault.

II. A. Light pink. Turns white when dried.

B. Aphanitic. Soapy clay.

IV. XRD indicates kaolinite and quartz.

M-76 and M-77

I. Argillized lapilli tuff: north El Coh entrance road. Samples from east side of road cut 30 m north of bridge.

II. A. Dark red (M-76) and mottled yellow (M-77).

B. Clastic volcanic texture. Argillation more extensive in sample M-77 collected above intersection of north-south and east-west trending faults.

IV. XRD indicates M-76 contains montmorillonite, and M-77 contains montmorillonite and clinoptilolite.

M-78

I. Pyrite-rich kaolinite: north wall of El Coh. Same as sample M-109.

M-79

I. Tuffaceous sandstone: sample from 100 m southwest of Rio San Francisco ford on La Mesa Trail.

- II. A. Tan.
- B. Poorly sorted clastic texture. Pumice-rich. Relatively free of basaltic clasts.

## M-80

- I. Felsite: sample from 3 m high scarp 75 m east of La Mesa Trail crossing of Rio San Francisco.
- II. A. Banded red, cream and grey.
- B. Aphanitic, nonporphyritic, vitric.
- IV. Sample is similar to T1-1 and M-42.

## M-81

- I. Pumice tuff: sample 20 m south of Rio San Francisco ford, La Mesa Trail.
- II. A. Tan.
- B. Clastic volcanic texture. Bedded fine pumice and siltstone.

## M-82

- I. Pumice tuff: sample from 3 m thick section of dark pumice tuff which caps "La Mesa" sampled on north slope.
- II. A. Dark brown.
- B. Coarse clastic volcanic texture. Poorly sorted. Bomb-sized clasts in silty matrix.
- IV. The tuff is resistant to erosion.

## M-84 and M-84

- I. Clay (M-83) and associated sulfur vein (M-84): sample from mine dump, Tizpathe mine.
- II. A. Yellow and white.
- B. Cellular vein deposit with 1 mm thick coating of sulfur and clay-rich sample.

## M-85

- I. Wallrock: 10 m east of the fissure, El Carmen #2 mine.

- II. A. Dark green.
- B. Completely argillized wallrock.
- IV. XRD (Figure 5 and Table 4) indicates a regularly interstratified chlorite-saponite. Chemical data is included in Table 3 (Col. 12).

## M-86

- I. Wallrock: 1 m east of the fissure, El Carmen #2 mine.
- II. A. Light green.
- B. Argillized, veined wallrock.
- IV. XRD indicates abundant quartz and dioctahedral montmorillonite.

## M-87

- I. Clay sample: El Carmen north mine dump.
- II. A. White.
- B. Pure clay.
- IV. XRD indicates exceptional (00 ) intensities characteristic of Pathé montmorillonite.

## M-88

- I. Silicified wood: east bank of Rio San Juan, 150 m west of well 12.
- II. A. Tan.
- B. Well preserved wood and cactus (or other relatively porous plant) preserved in silica-cemented volcanic sandstone.

## M-89

- I. Lapilli tuff: bedded tuff below basalt, 20 m northwest of well 3.
- II. A. Purple and red.
- B. Clastic volcanic texture. Basalt and scoria lapilli averaging 1.5 cm in diameter.
- IV. XRD indicates montmorillonite and quartz.

## M-90

- I. Argillized lapilli tuff: sample from depth of 0.5 m, 3 m southwest of well 3.

- II. A. Mottled brown.
- B. Clastic volcanic texture. Extensively altered.

## M-91

- I. Argillized lapilli tuff: sample from west wall of arroyo, 30 m southwest of well 3.
- II. A. Dark purple and red.
- B. Clastic volcanic texture: basalt and scoria lapilli.
- IV. XRD indicates mixed dioctahedral and trioctahedral montmorillonite.

## M-92

- I. Argillized basalt: intersection of east-west and north-south trending faults on "La Mesa" Trail. 40 m southwest of well 3.
- II. A. Olive-grey.
- B. Spheroidal argillation of basalt producing rounded boulders 1 m in diameter. Relic porphyritic texture. "Iddingsite" phenocrysts.
- IV. XRD indicates abundant clinoptilolite and minor montmorillonite.

## M-93

- I. Lapilli tuff: west side of "La Mesa" Trail at high point. Elevation 50 m above well 3. Sample obtained by digging 0.5 m into bank.
- II. A. Dark-brown clasts.
- B. Clastic volcanic texture: mixed basalt and scoria lapilli to 1.5 cm in diameter.
- IV. XRD indicates mixed dioctahedral and trioctahedral montmorillonite.

## M-94

- I. Gypsum and bentonite: collected 7 m above M-93.
- II. A. Yellow to tan.
- B. Horizontal gypsum bed and argillized clastic volcanic bed. Extremely indurated. Bed is 1 m thick.

## M-95.

- I. Lapilli tuff: collected 12 m above "La Mesa" Trail, vertically above M-93 and M-94.
- II. A. Brown.
- B. Clastic volcanic texture: basalt and scoria clasts.
- IV. XRD indicates dioctahedral montmorillonite and clinoptilolite. Note: the 7 samples described above were obtained by digging to depths of approximately 0.5 m. Relatively fresh samples were obtained in spite of the altered, bentonitic nature of the surface material. These samples demonstrate that the entire upper half of the hill southwest of well 3 is composed of basaltic lapilli tuff.

## M-96 and M-97

- I. Scoria (M-97) and associated hydrothermal deposit (M-96): from the "Mines de Metal", an abandoned mine shaft near the crest of Cerro Colorado.
- II. A. Red scoria and white hot water deposits.
- B. Texture of scoria is finely vesicular. Fist-sized scoria bombs in finer scoria groundmass. White coating is finely cellular.
- C. Magnetite: euhedral crystals. Calcite: vein-like porous coating may be traced down slope for 50 m marking path of past thermal waters.
- IV. Analysis of M-97 listed in Table 3 (Col. 4).

## M-98

- I. Olivine basalt: beneath office, Campo de Pathé, east bank of Rio San Juan.
- II. A. Olive grey.
- B. Porphyritic texture. "Iddingsite" phenocrysts to 2 mm maximum diameter.
- IV. Basalt is similar to olivine basalt which crops out over much of area (M-19 and M-21).

## M-99

- I. Volcanic sandstone: east bank of Rio San Juan below mess hall, Campo de Pathé.
- II. A. Tan.
- B. Clastic texture. Sand-sized volcanic clasts in opaline cement.
- IV. See sample M-110 for thin section description.

## M-100

- I. Argillized vesicular basalt: intersection of road to well 5 and Pathé fault.
- II. A. Red with white vesicular coating.
- B. Argillized vesicular texture. Vesicles average 7 mm in diameter.
- IV. XRD indicates montmorillonite is major alteration product. M-100 is similar to M-38 but M-100 is oxidized, whereas M-38 is reduced.

## M-101

- I. Rhyolite felsite: additional sample from dike at north end of main valley. See M-42 for description.

## M-102 and M-103

- I. Clay: from floor of arroyo, 50 m south of well 1A.
- II. A. White.
- B. Porcelaneous vein deposit. Near vertical, 2 cm wide clay vein in argillized basalt.
- IV. XRD indicates montmorillonite. The presence of hydrothermal montmorillonite here is possibly related to the fissure system feeding well 1A.

## M-104

- I. Argillized volcanic breccia (?): El Coh #2, large sample from west wall.
- II. A. Yellow-white and local waxy blue areas.
- B. Coarse clastic volcanic texture? Some block-sized white areas.

- IV. Separations of white areas yield mixed montmorillonite and kaolinite XRD reflections. Blue areas are pure montmorillonite.

## M-105

- I. Argillized volcanic breccia (?): El Coh #2, east wall.
- II. A. Light purple.
  - B. Relic clastic volcanic texture. Argillation extensive, entire sample is waxy clay.
- IV. XRD indicates pure montmorillonite.

## M-106 and M-107

- I. Argillized (M-106) and relatively fresh basalt (M-107): Associated samples from above abandoned main shaft shown in Plate IX (B) on south face of El Coh mine.
- II. A. Grey basalt and greenish basalt-derived clay.
  - B. Aphanitic texture. Extensive vein development and iron concentrations associated with faulting.
- IV. XRD of green clay indicates a dioctahedral montmorillonite (non-tronite(?)).

## M-108

- I. Argillized wallrock: sample from small shaft, north wall of El Coh mine near north end of shaft.
- II. A. Green.
  - B. Plastic clay: extensive slickensides related to east-west trending fault.
- IV. XRD indicates dioctahedral montmorillonite. Chemical analysis given in Table 3, Col. 6.

## M-109

- I. Argillized wallrock: sample from small shaft in north face of El Coh mine, 1.5 m south of sample M-108.
- II. A. White.
  - B. Dense, soapy clay.

C. Pyrite: cubic crystals to 1 cm in diameter enclosed in kaolinite. Very minor, yellow iron-staining surrounding pyrite crystals.

IV. Chemical analyses of sample listed in Table 3, Col. 7. Analysis shows marked decrease in Fe as compared with sample M-108 and increase in  $Al_2O_3$ .

## M-110

I. Volcanic sandstone: sample from silicified wood occurrence on east bank of Rio San Juan due west of well 12.

II. A. Tan.

B. Clastic texture. Sand-sized clasts in opaline matrix.

III. A. Moderately sorted, clastic texture. Lithic and crystal clasts of variable composition in opaline cement. Clasts include plagioclase laths, quartz crystals, angular basalt, scoria, and spherulitic rhyolite lithic fragments.

IV. Photomicrograph of sample shown in Table V (H).

## M-111

I. Altered lapilli tuff: north wall of creek bed, 10 m south of well 1E.

II. A. Mottled cream to red.

B. Coarse clastic volcanic texture. Elongate relic, light clasts averaging 1.5 cm in length in a dense matrix.

IV. Sample is similar to argillized tuff sample T1-4.

## M-112

I. Vesicular basalt: sample from base of trail up north wall of the canyon of the Rio San Juan from Rancho El Chilar.

II. A. Dark grey.

B. Coarsely vesicular, microporphyritic basalt. Slightly elongate vesicles average 1 cm in length.

C. Olivine microphenocrysts.

IV. Vesicles are free of coating or zeolites.

## M-113

- I. Altered tuff (?): from intersection of foot path and south entrance road above well 7.
- II. A. Cream to yellow.  
B. Texture completely obscured.
- IV. XRD indicates quartz and montmorillonite.

## M-114, M-115, M-116 and M-117

- I. Four samples of identical scoria collected from the following locations:
  - M-114: northwest slope of Cerro Grande.
  - M-115: red section above well 18.
  - M-116: red section north of well 5.
  - M-117: uppermost red section beneath lava cap of high east-west trending hill east of generator plant.
- II. A. Red to reddish purple.  
B. Finely vesicular coarse lapilli-to bomb-sized subrounded scoria clasts.
- IV. Montmorillonite and clinoptilolite indicated by XRD of all 4 samples, independent of proximity to faulting.

## M-118

- I. Don Guinyo welded tuff: east end of high bridge over arroyo de Don Guinyo, Huichipan-Ixmiquilpan highway (locality described by Segerstrom, 1962).
- II. A. Dark banded red. Locally solid black.  
B. Eutaxitic texture. Elongate lenses of black and red glass.
- III. A. Eutaxitic structure. Glass lenses, abundant crystals in glass.  
B. Plagioclase: resorbed euhedral zoned laths. Pyroxene: subhedral crystals. Quartz: sparse subhedral phenocrysts.
- IV. Analysis (Table 2, Col. 6) indicates dacite composition (Nockolds, 1954).

## Traverse Tl-1

Samples Tl-1 through Tl-8 were collected on a traverse beginning at a cement claim marker in the rhyolite caprock of the hill southwest of well 3 (Fig. 2). The traverse extends a horizontal distance of 55 m northwest to a point south of well 3. The traverse was intended to examine the lithologic and mineralogical variation in what appeared to be an extensively argillized area to the southeast of well 3. Samples M-89 through M-95 were collected on a similar traverse southwest of well 3. These samples failed to reveal any extensive argillation beneath the 0.5 m thick surface soil zone. Extensive alteration, particularly silicification, was revealed by traverse Tl-1 which is described below.

## Tl-1

- I. Rhyolite felsite: caprock, northwest corner of "rhyolite" hill 11 m N47°W from cement claim marker.
- II. A. Banded pink, yellow, tan and cream.  
B. Aphanitic, nonporphyritic, vitric flow banded.
- III. A. Aphanitic: sparse microphenocrysts and microlites in ground-mass.  
B. Quartz: sparse microphenocrysts and chalcedony.
- IV. Chemical analysis of this rock (Table 2, Col. 11) indicates extensive silicification. Similar "flow rock" is present near the intersection of La Mesa Trail and Rio San Francisco and at the north end of the main valley. All these occurrences lie along the same northeast trending fault.

## Tl-2

- I. Silicified tuff: sample of resistant bed 11 m below sample Tl-1.
- II. A. Mottled tan to brown.  
B. Relic clastic volcanic texture. Outlines of angular clasts averaging 1 cm in diameter.  
C. Quartz: "microphenocrysts" 1 mm in diameter in extensively silicified areas of specimen.

## Tl-3

- I. Argillized lapilli tuff: sample collected inside shaft entrance 14 m below sample Tl-1.

- II. A. Tan.
  - B. Relic clastic texture. Fine lapilli-sized light areas in darker matrix. Blocky fracture.
- IV. XRD indicates montmorillonite. This clay was once mined from numerous vertical shafts sunk in the surface of the hill.

## Tl-4

- I. Argillized lapilli tuff: resistant bed 12.5 m below sample Tl-2, 4 m below level of mine entrance.
- II. A. Light clasts in pink matrix.
  - B. Clastic volcanic texture. Subround clasts of scoria and pumice (?) averaging 1 cm in diameter. Silicification extensive. Individual beds average 6 cm in thickness.
- IV. This sample is of similar nature to sample from floor of main valley. XRD indicates minor montmorillonite and quartz.

## Tl-5

- I. Massive bedded silica: top of resistant bed which forms ledge around arroyo south of well 3. Sample 7 m below Tl-4.
- II. A. Mottled cream and pink.
  - B. Pitted, silicified rock: original texture not determined. Numerous large and small cavities which could represent clasts removed by solutions or primary vesicular structures. Thickness of bed is 0.65 m.
- IV. XRD indicates montmorillonite and quartz.

## Tl-6

- I. Argillized basalt (?): resistant unit 1 m in thickness, 5 m below Tl-5.
- II. A. White to grey.
  - B. Argillized, texture obscured. Same pink areas have a relic, finely vesicular texture.
  - C. Quartz: microphenocrysts present throughout sample.

## Tl-7

- I. Argillized basalt: sample 2 m below Tl-6.
- II. A. Pink to white.  
B. Relic vesicular texture. Variable degree of alteration, pods of pure clay and clay filled fine vesicles.
- IV. XRD indicates montmorillonite. Sample collected from east-west trending fault zone which parallels north flank of "rhyolite" hill.

## Tl-8

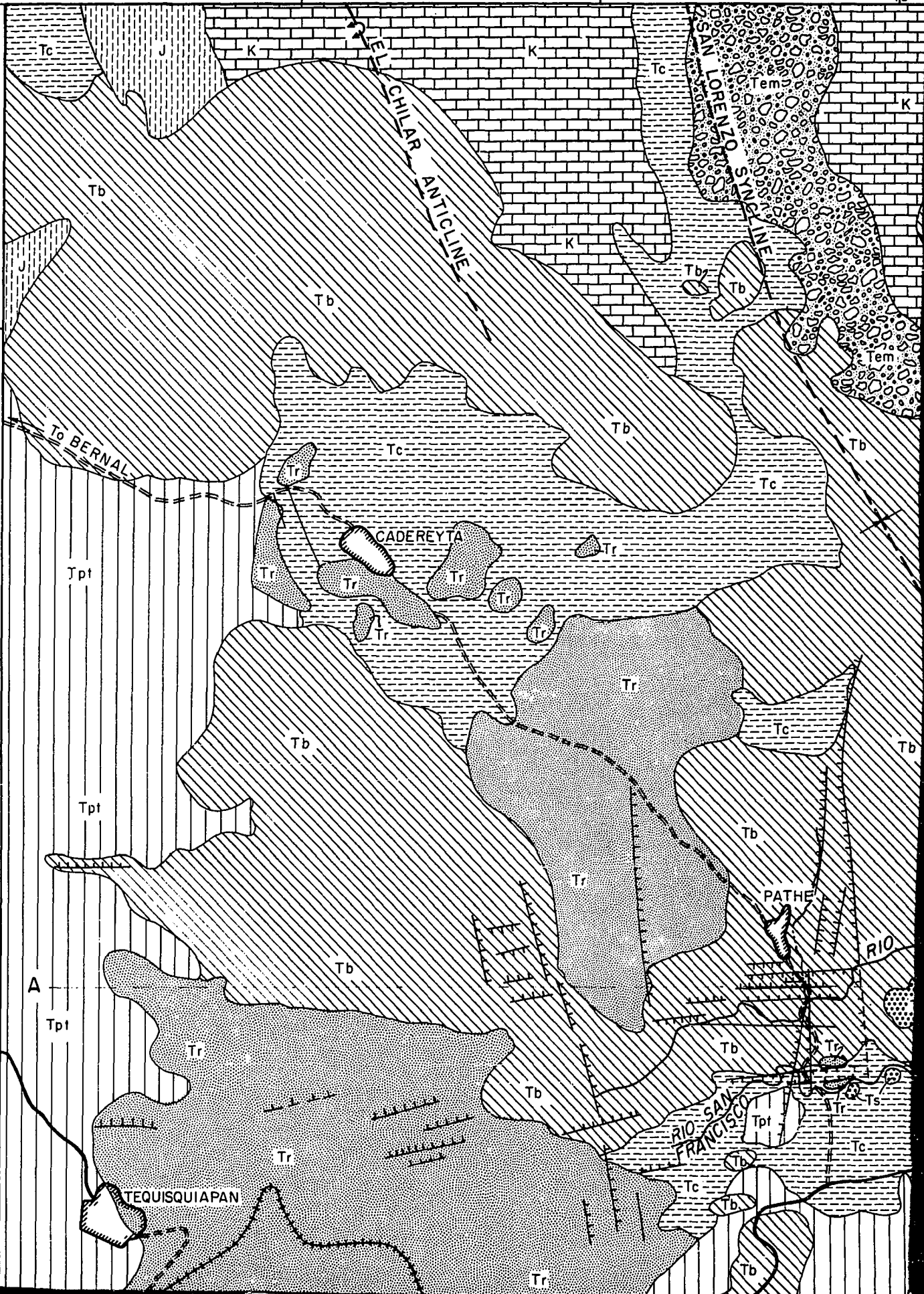
- I. Olivine basalt: sample from creek bed 5 m below Tl-7 and due south of well 3.
- II. A. Olive grey.  
B. Porphyritic, dense, basalt. Abundant "iddingsite" phenocrysts in dense aphanitic groundmass.  
C. "Iddingsite": exceptionally abundant red euhedral phenocrysts averaging 1 mm in diameter. Alteration of olivine.
- IV. This olivine basalt is similar to samples M-19A, M-21 and samples of lava south of the Rio San Juan.

20°50'

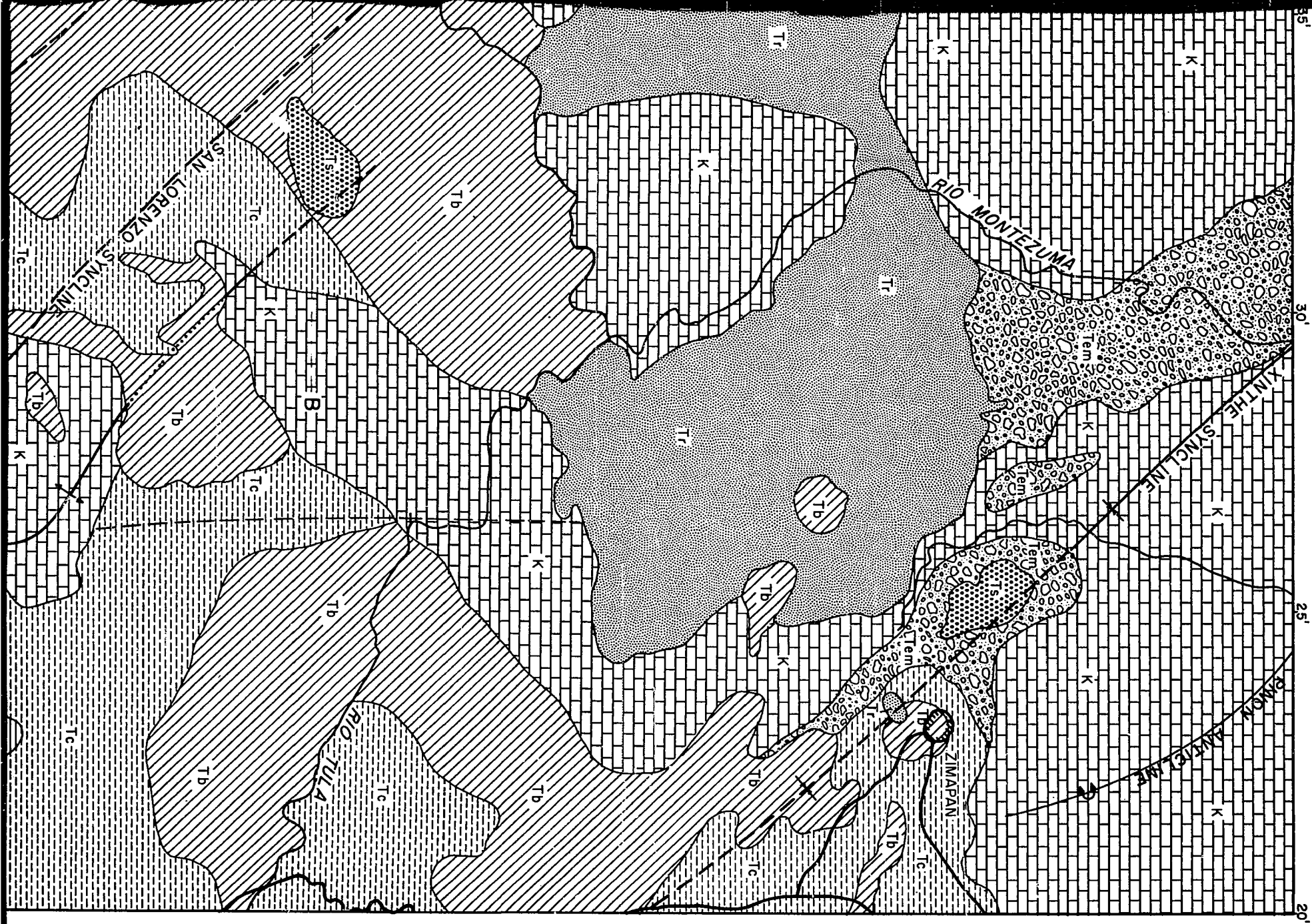
99° 50'

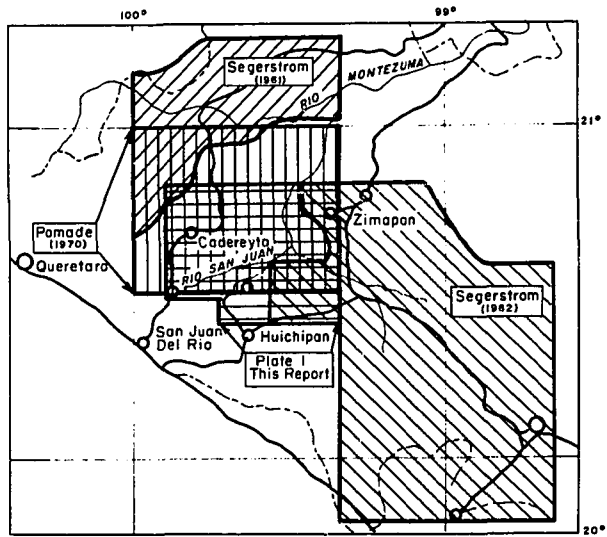
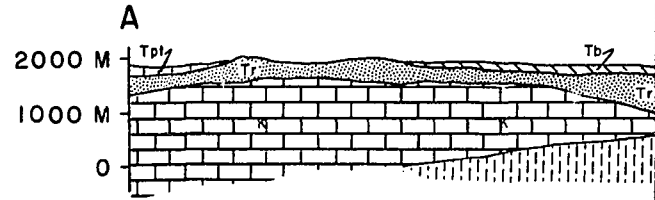
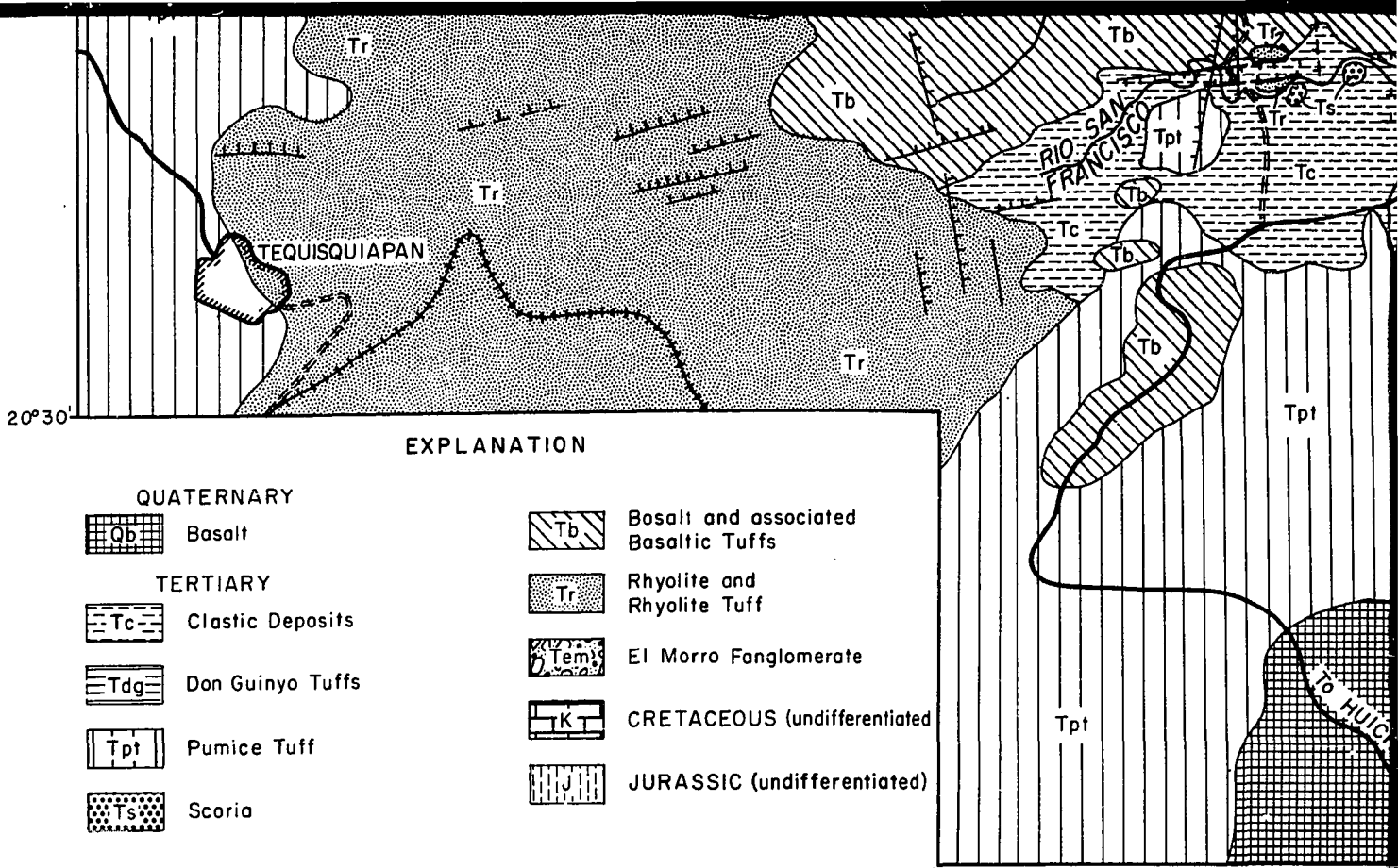
45'

40'







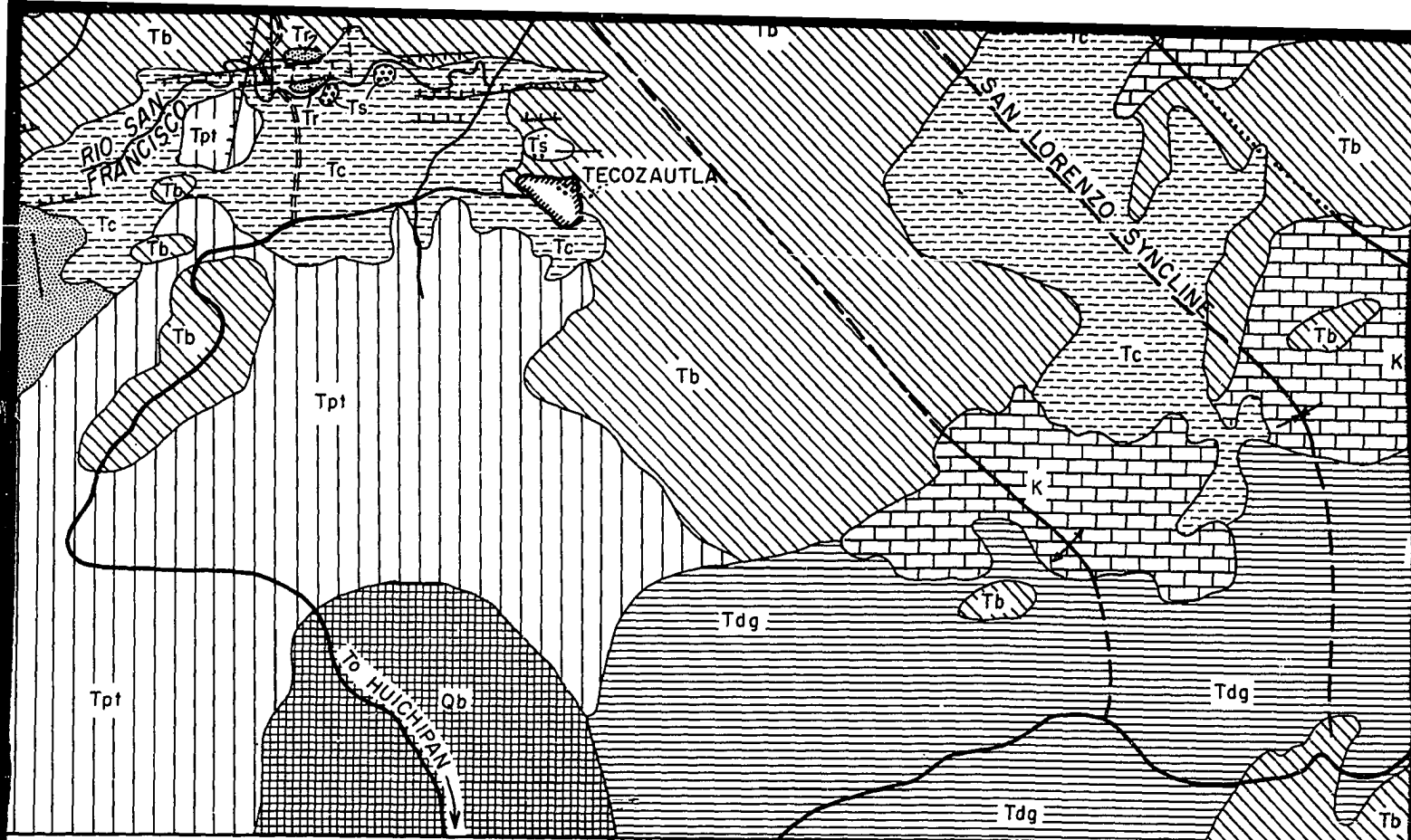


LOCATION MAP AND PREVIOUS MAPPING

C. R. Nichols — Ph.D. Thesis — University of Oklahoma  
— 1970 —

Compiled from Segerstrom (1961, 1962), and Pomade (1970)

RECO



0 1 2 3  
 SCALE IN KILLOMETERS

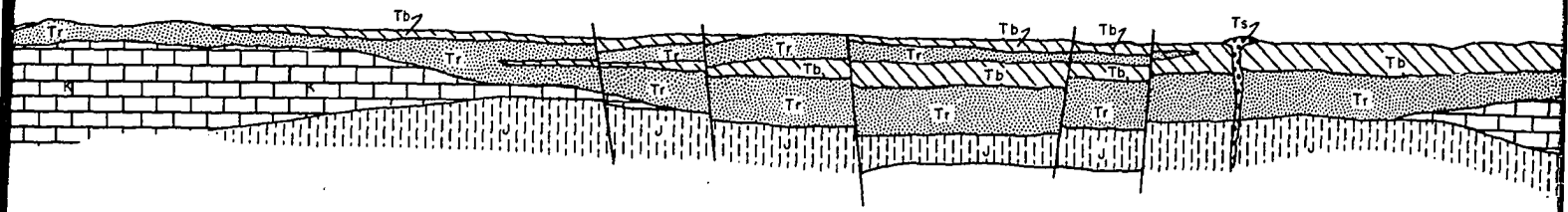


PLATE I

RECONNAISSANCE GEOLOGIC MAP OF THE TECOZAUTLA - CA  
 HIDALGO AND QUERETARO, MEXICO

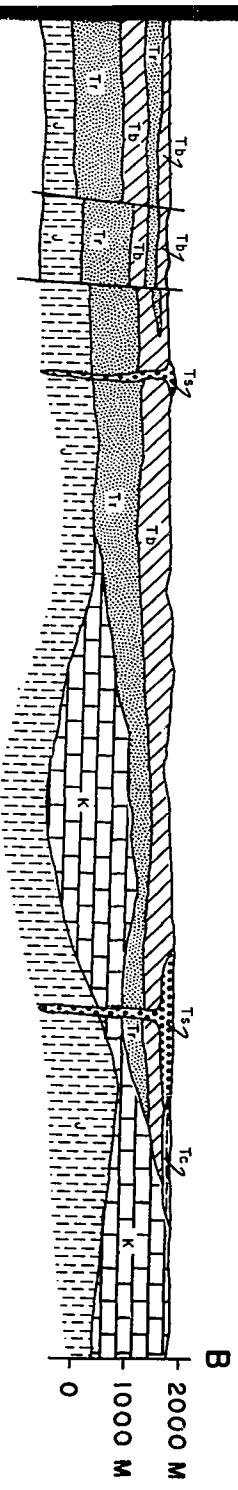
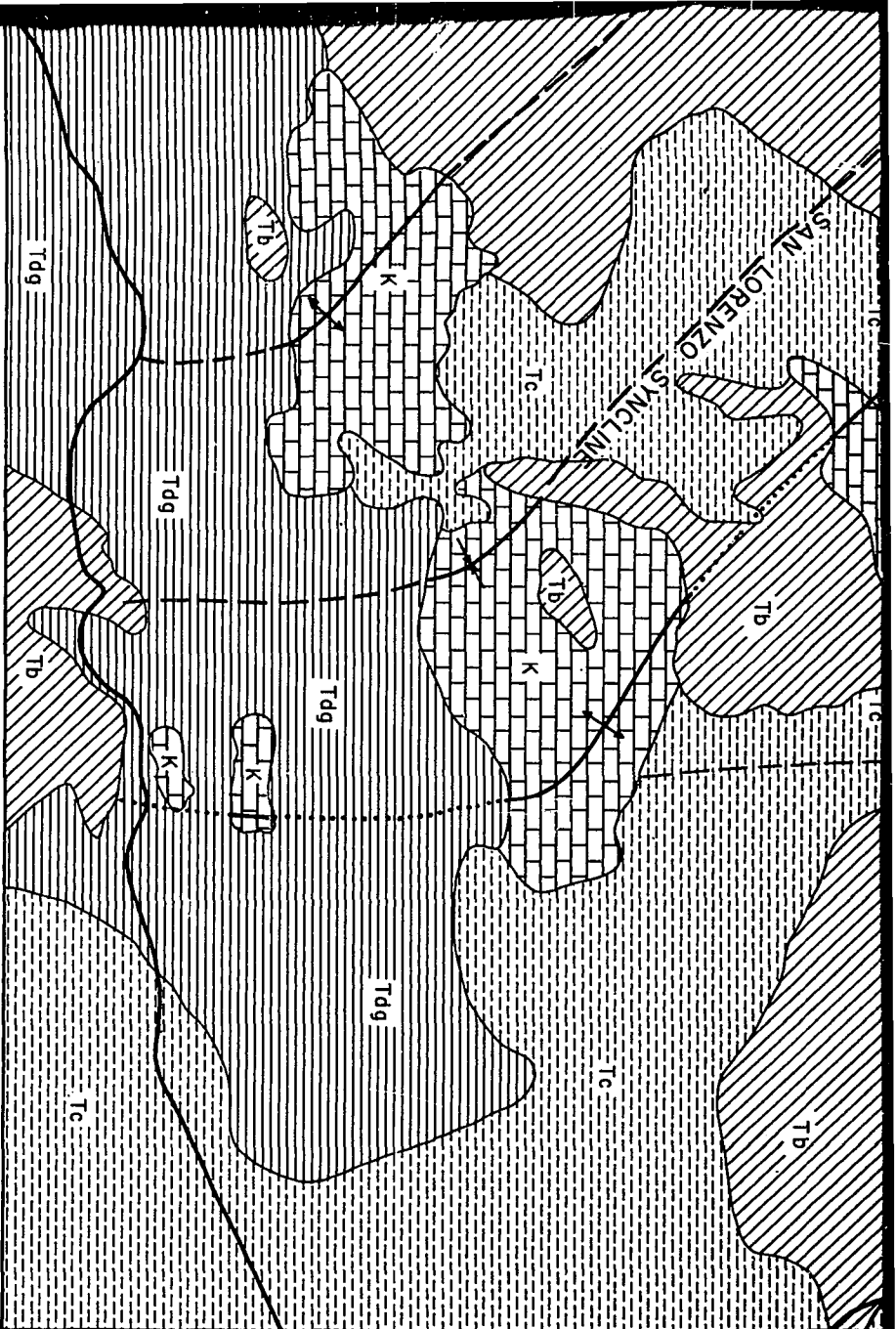
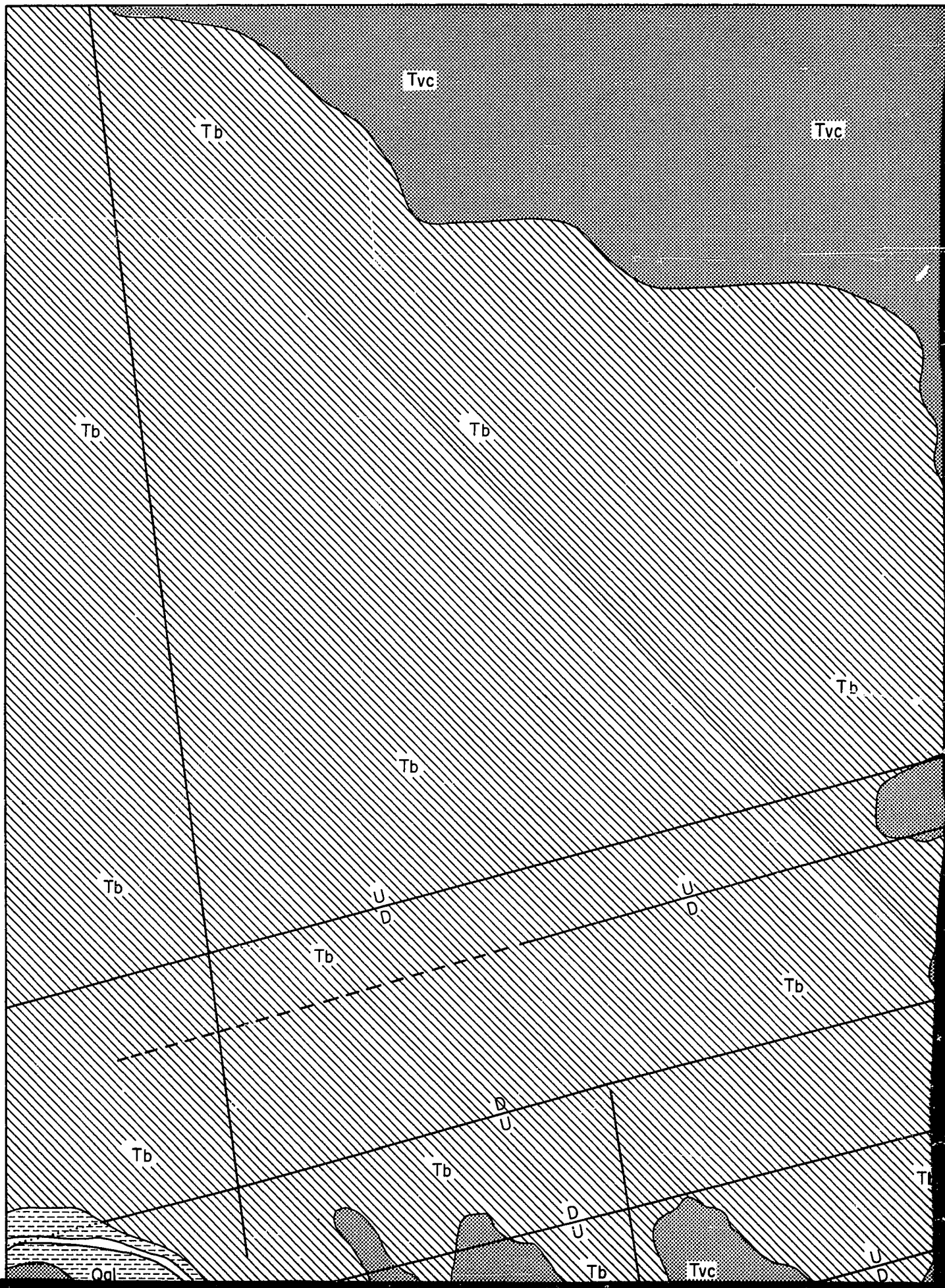
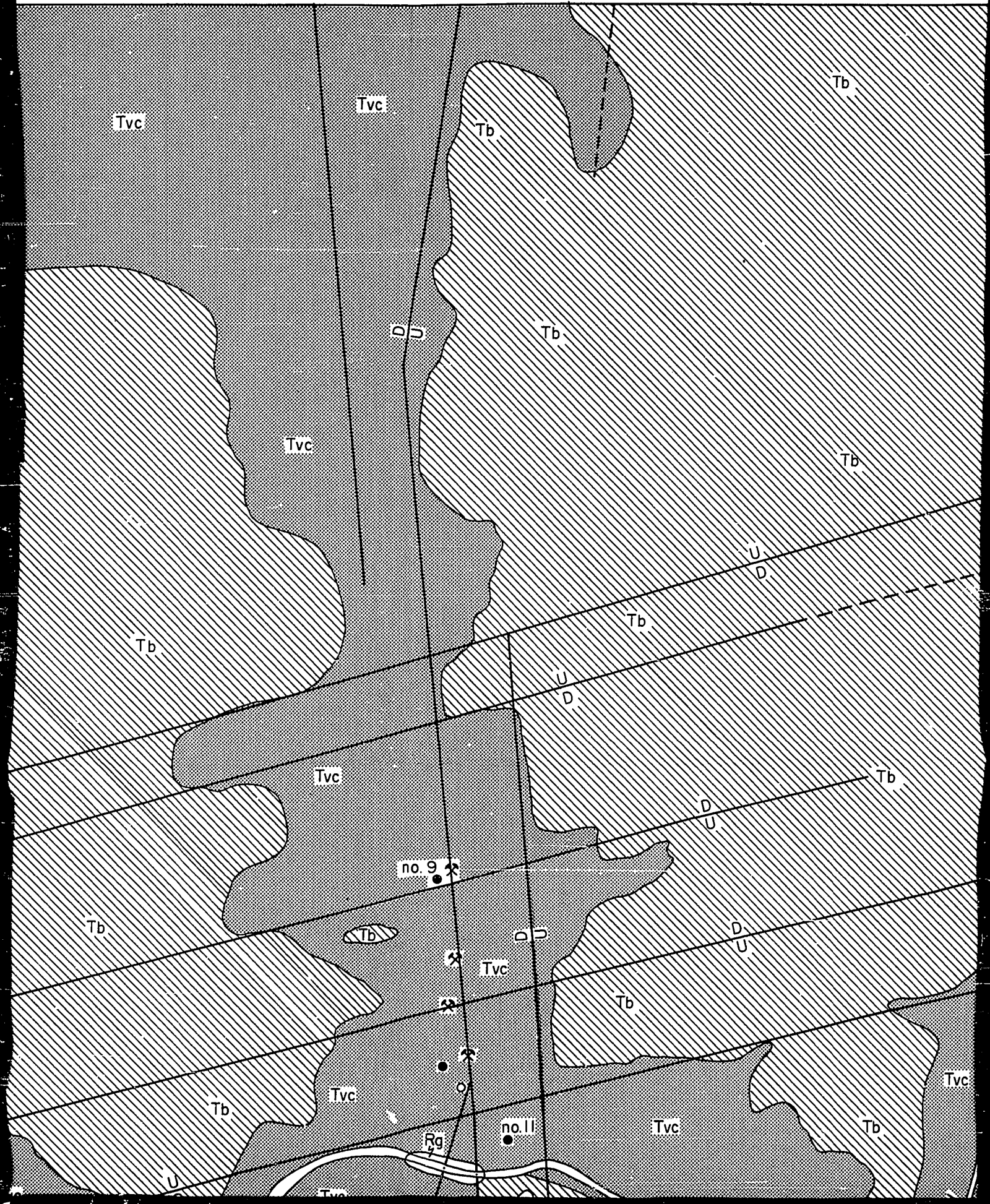
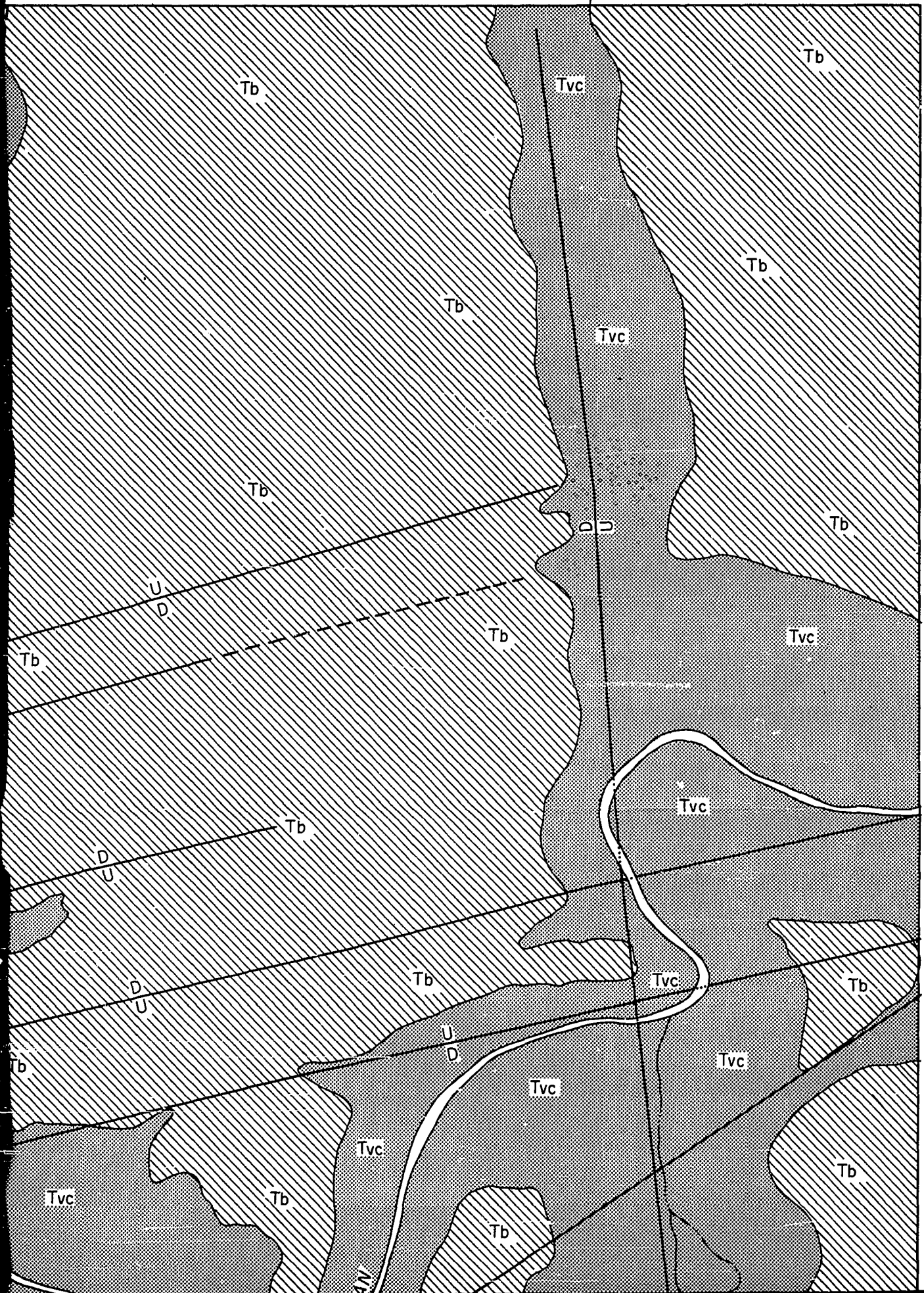
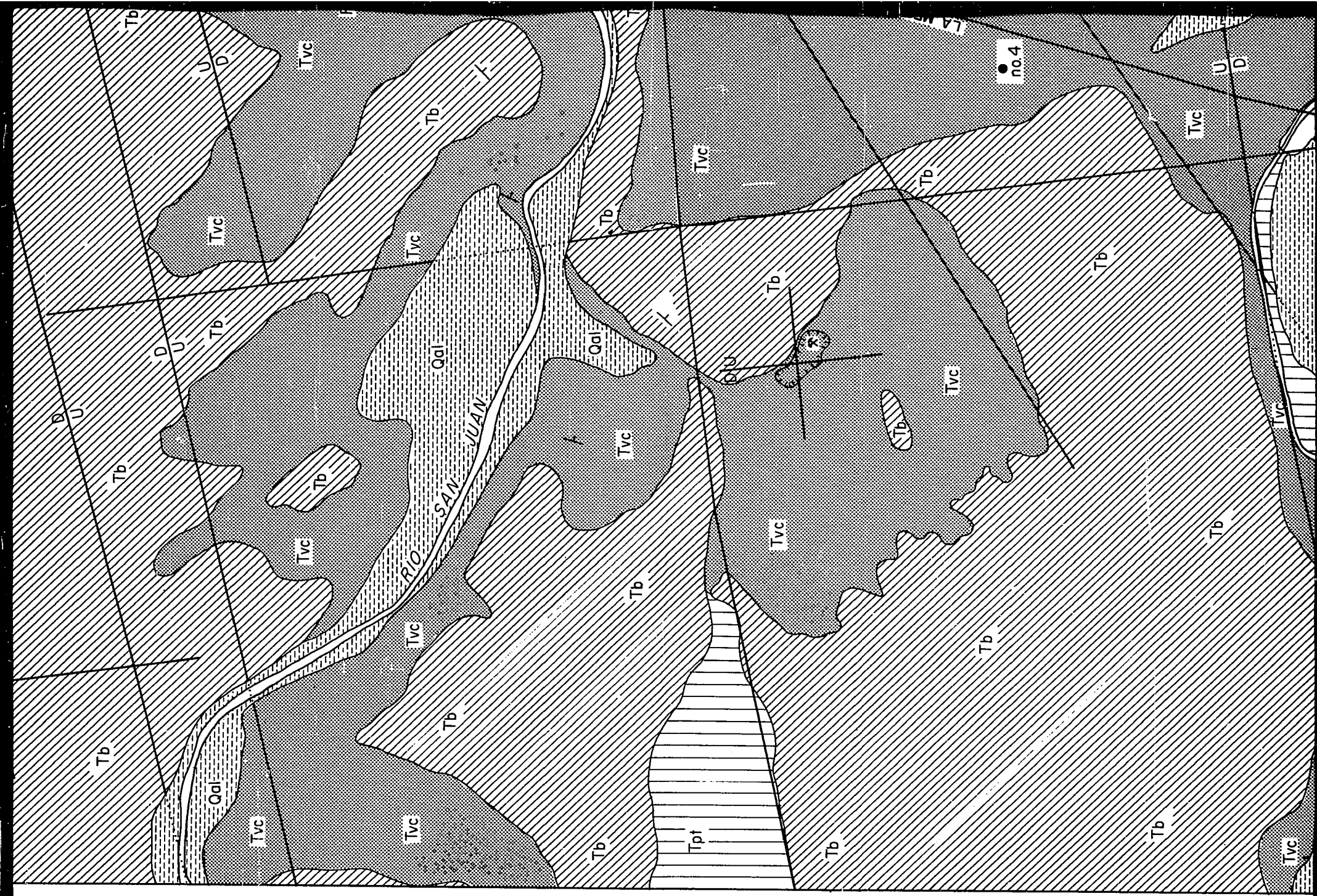


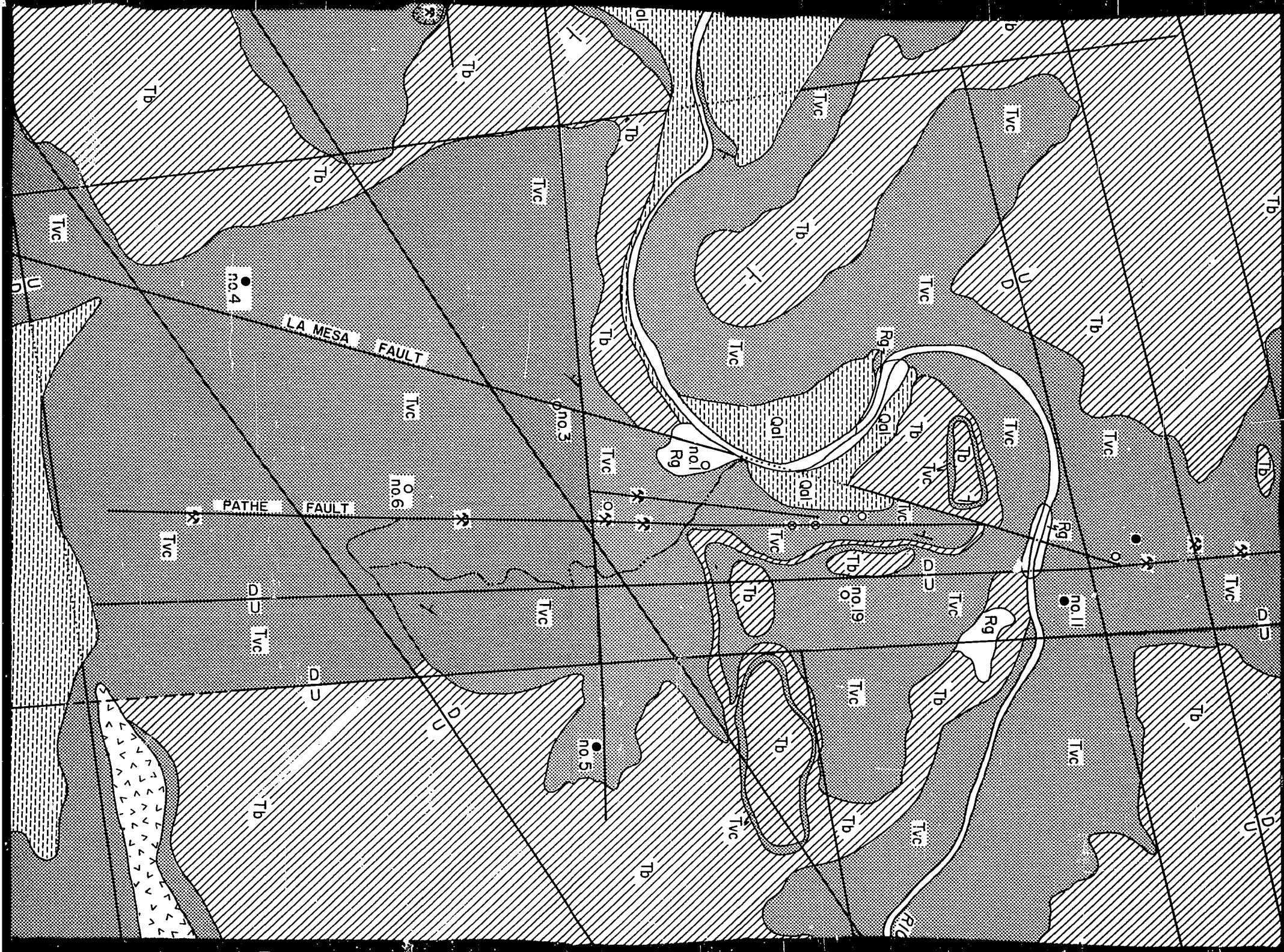
PLATE I  
 GEOLOGICAL MAP OF THE TECOZAUTLA — CADEREYTA AREA  
 TOLUCA AND QUERETARO, MEXICO

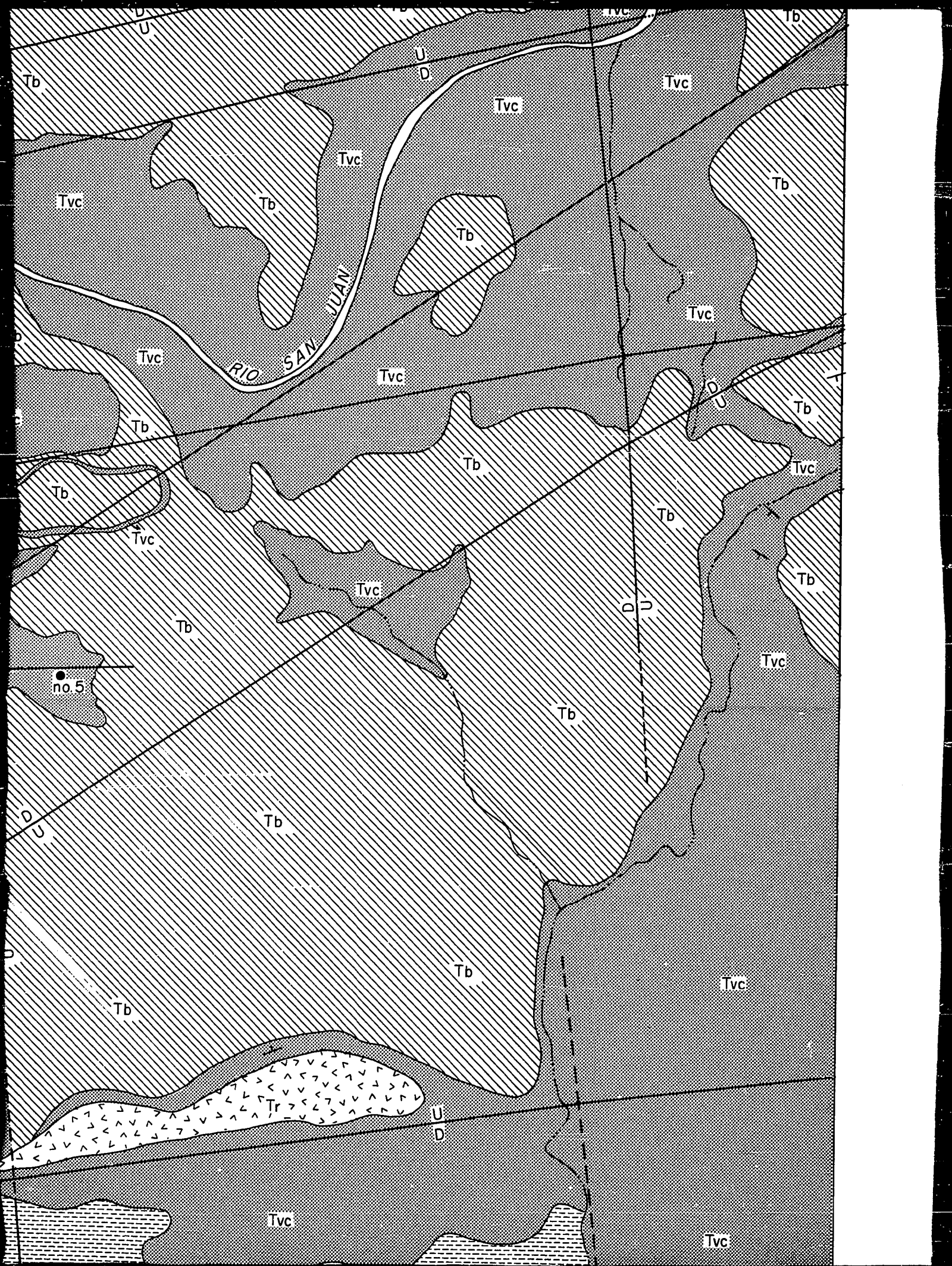














EXPLANATION

- Diamond Cored Exploration Wells
- ⊗ Producing Steam Wells
- Dry Wells

QUATERNARY and RECENT

- Rg Geysrite
- Qal Alluvium

TERTIARY

- Tpt Pumice Tuff
- Ts Scoria
- Tb Basalt
- Tvc Clastics Volcanic
- Tr Rhyolite Porphyry

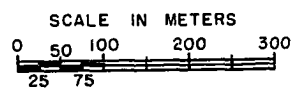
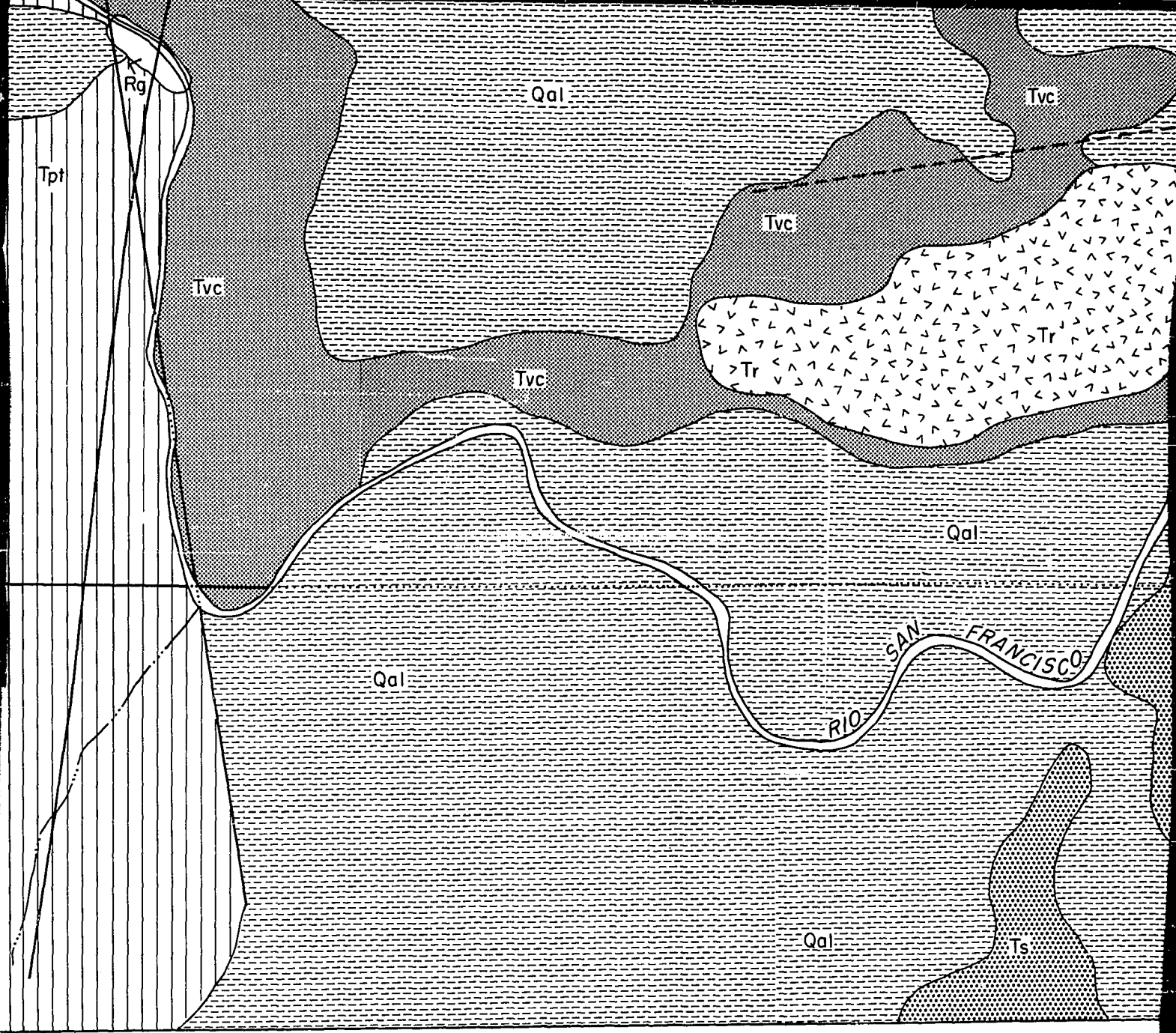
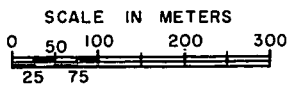


PLATE II

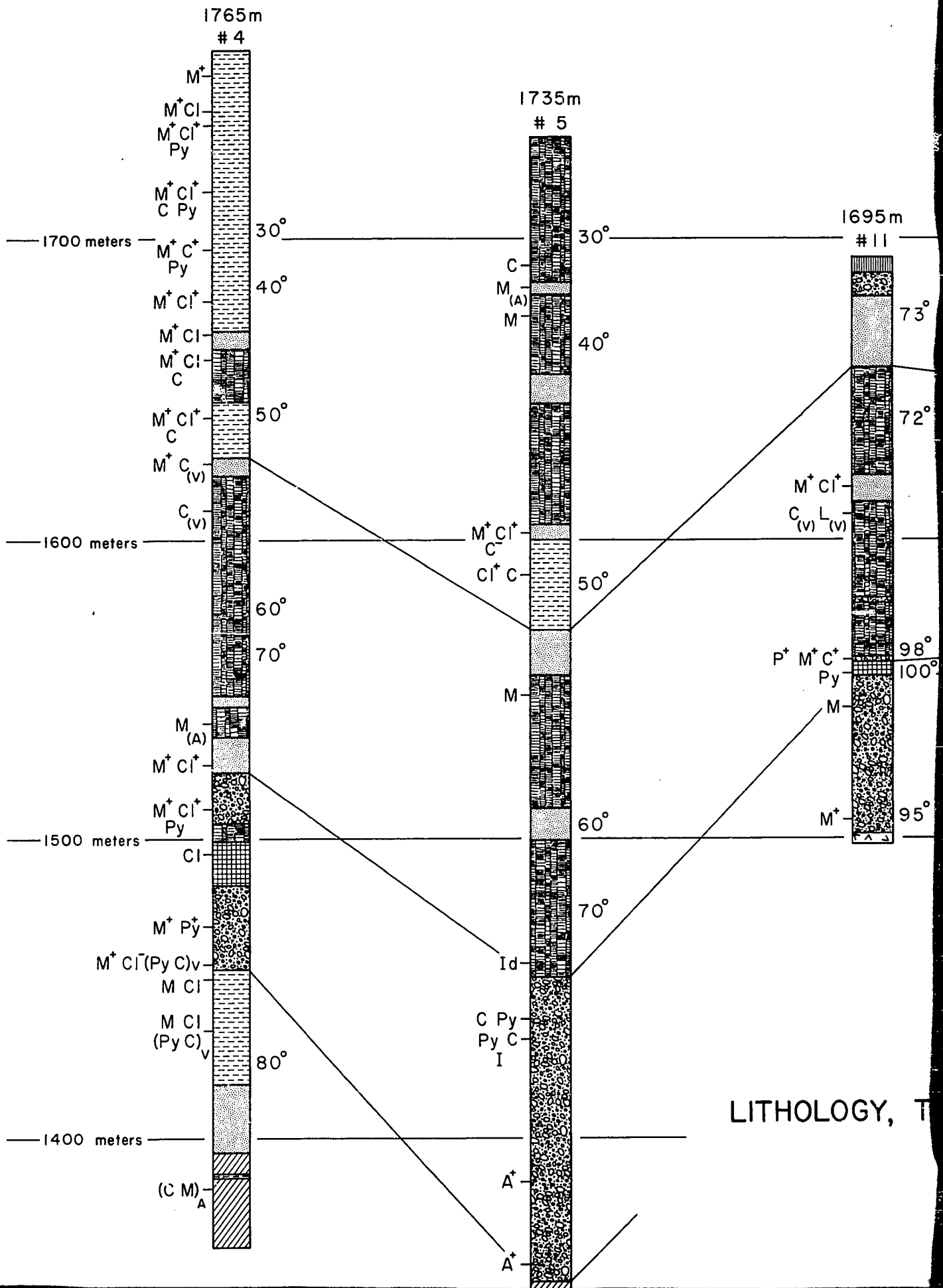
GEOLOGIC MAP OF THE PATHE GEOTHE  
 HIDALGO AND QUERETARO, MEXI

uff  
 Volcanic  
 Porphyry



Mapping by C.R. Nichols, January and February, 1968

PLATE II  
 OF THE PATHE GEOTHERMAL ZONE  
 AND QUERETARO, MEXICO



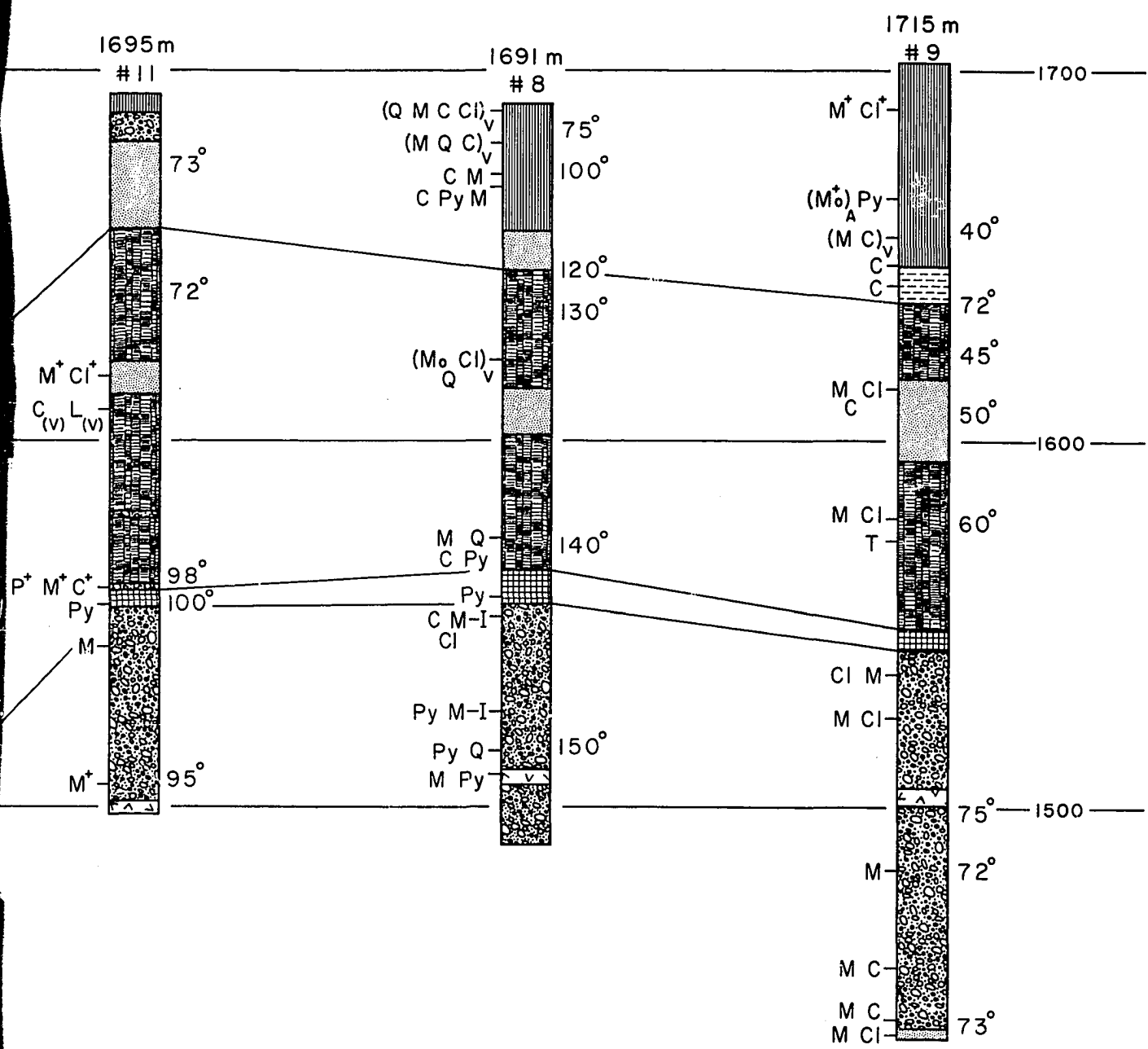
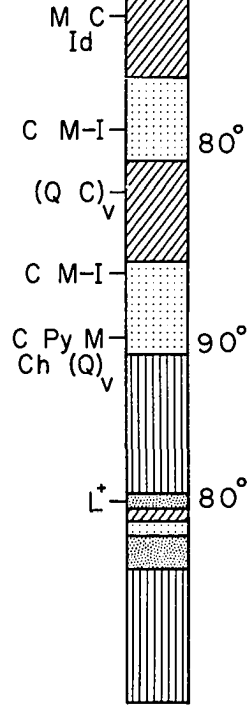
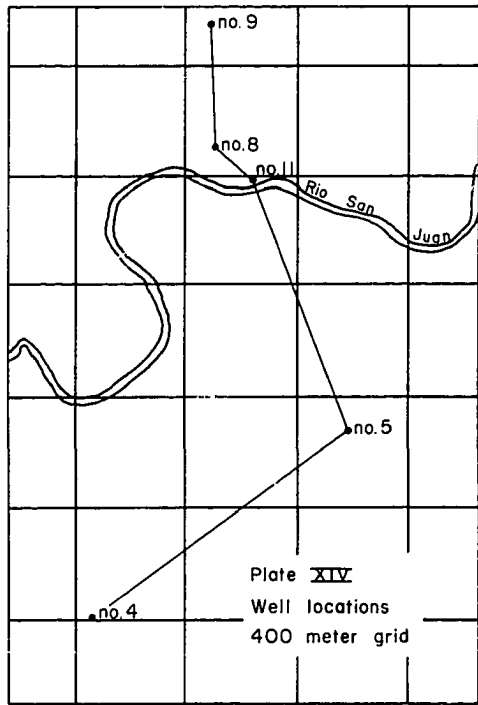
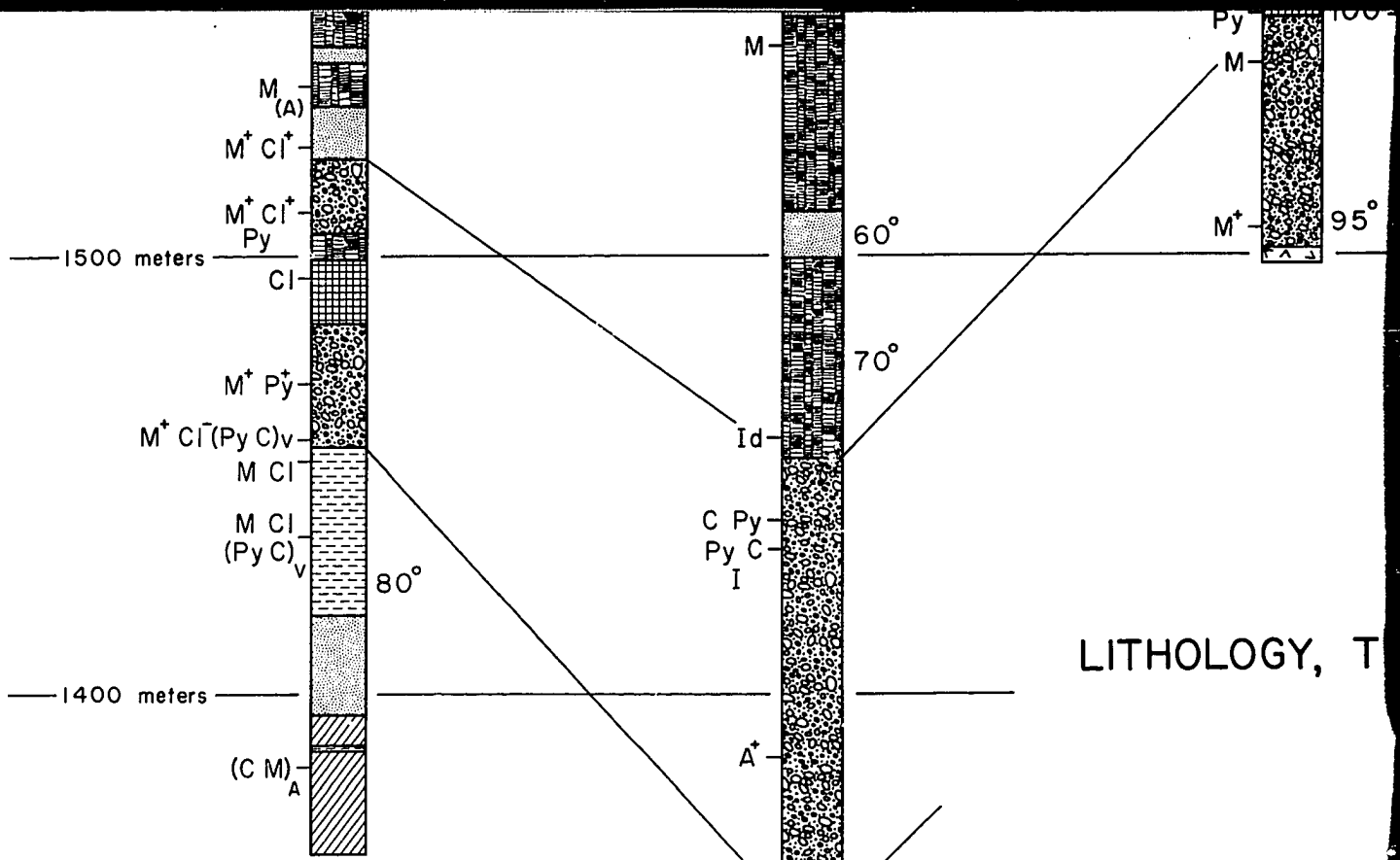


PLATE XIV

MINERALOGY, TEMPERATURE AND ALTERATION MINERALOGY  
 PATHE CORES

PATHE GEOTHERMAL ZONE  
 HIDALGO, MEXICO  
 C. R. NICHOLS, 1970



- BASALT UN**
- Lapilli Tuff
  - Hyaloophitic
  - Intergranular
  - Scoria
- RHYOLITE**
- Rhyolitic Vit
  - Rhyolite Tuff
  - Rhyolite Flow
- INTERSTRA**
- Basalt
  - Pumice Tuff
  - Scoria
  - Basaltic Ar

Wellhead elev  
Temperature  
at depth recd

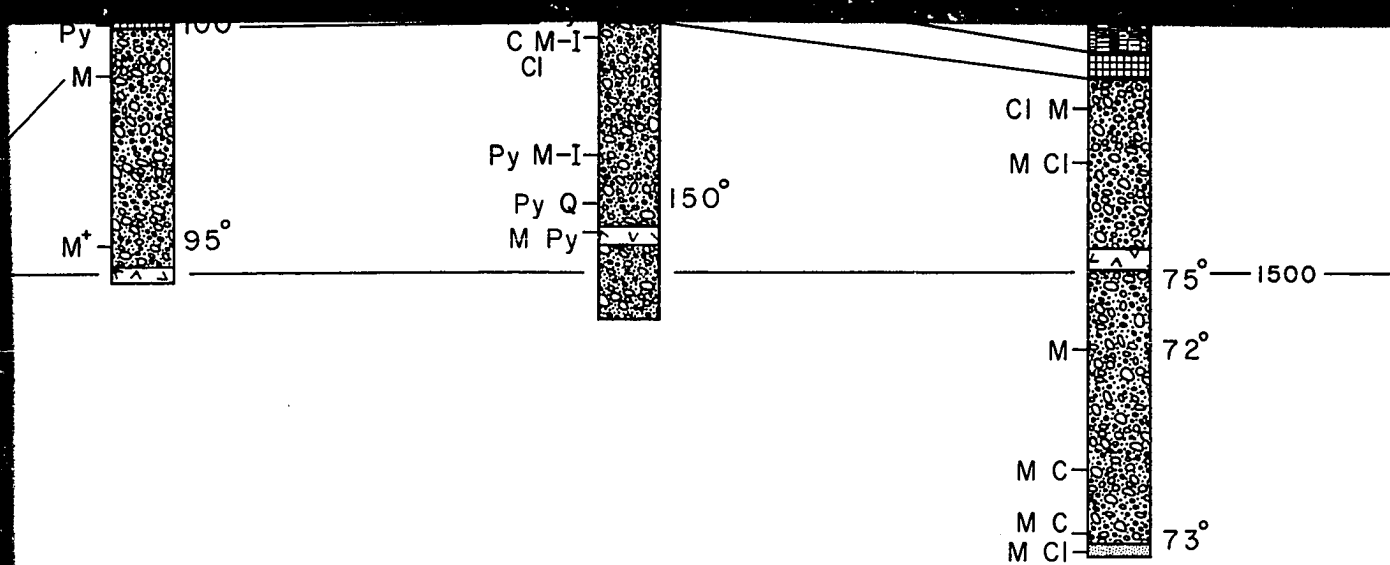


PLATE XIV

GEOLOGY, TEMPERATURE AND ALTERATION MINERALOGY  
PATHE CORES

PATHE GEOTHERMAL ZONE  
HIDALGO, MEXICO  
C. R. NICHOLS, 1970

EXPLANATION

BASALT UNIT

-  Lapilli Tuff \_\_\_\_\_ Basalt and scoria lapilli averaging 1 cm in diameter. Scattered, bomb-sized basalt clasts.
-  Hyaloophitic Basalt \_\_\_\_\_ Porphyritic basalt with abundant white feldspar laths averaging 1 mm in length in a black glass.
-  Intergranular Basalt \_\_\_\_\_ Dense, grey, nonporphyritic basalt. Plagioclase laths with intergranular clinopyroxene and magnetite.
-  Scoria \_\_\_\_\_ Lapilli to bomb-sized red and purple scoria fragments in a clinoptilolite-rich groundmass.

RHYOLITE UNIT

-  Rhyolitic Vitric Tuff \_\_\_\_\_ Collapsed pumice, lithic clasts, and embayed quartz in a vitric groundmass. Partially welded.
-  Rhyolite Tuff \_\_\_\_\_ Green, indurated tuff. Abundant quartz and sanidine phenocrysts in an altered, fine ash groundmass.
-  Rhyolite Flow Breccia \_\_\_\_\_ Grey, angular, cobble-sized clasts of spherulitic rhyolite in a dense, flow-banded, vitric matrix.

INTERSTRATIFIED VOLCANIC UNIT

-  Basalt \_\_\_\_\_ Finely vesicular, nonporphyritic basalt with intergranular texture. Poor flow orientation.
-  Pumice Tuff \_\_\_\_\_ Green, collapsed, lapilli-sized pumice and quartz in a light green, perlitic groundmass.
-  Scoria \_\_\_\_\_ Coarse red and purple scoria lapilli and bombs. Extensive zeolitization and argillation.
-  Basaltic Andesite \_\_\_\_\_ Grey to purple, finely vesicular lava with well developed flow orientation. Nonporphyritic.

ALTERATION PRODUCTS

- M - Montmorillonite
- C - Calcite
- S - Saponite
- Q - Quartz
- Ch - Chlorite
- Cl - Clinoptilolite
- S - Stilbite
- A - Analcite
- Mo - Mordenite
- L - Laumontite
- G - Gypsum
- M-I - Montmorillonite-Illite
- I - Illite
- Py - Pyrite
- Id - Iddingsite
- T - Talc
- (Q,C)<sub>V</sub> - Indicates minerals occurring as vein filling
- (Q,C)<sub>A</sub> - Indicates minerals occurring as amygdular filling

Wellhead elevations indicated in meters  
Temperature is indicated to the right of the log  
at depth recorded in °C